Fall 1-31-1999

A theoretical study of bubble motion in surfactant solutions

Yanping Wang
New Jersey Institute of Technology

Copyright Warning & Restrictions

The copyright law of the United States (Title 17, United States Code) governs the making of photocopies or other reproductions of copyrighted material.

Under certain conditions specified in the law, libraries and archives are authorized to furnish a photocopy or other reproduction. One of these specified conditions is that the photocopy or reproduction is not to be "used for any purpose other than private study, scholarship, or research." If a, user makes a request for, or later uses, a photocopy or reproduction for purposes in excess of "fair use" that user may be liable for copyright infringement,

This institution reserves the right to refuse to accept a copying order if, in its judgment, fulfillment of the order would involve violation of copyright law.

Please Note: The author retains the copyright while the New Jersey Institute of Technology reserves the right to distribute this thesis or dissertation

Printing note: If you do not wish to print this page, then select "Pages from: first page # to: last page #" on the print dialog screen

ABSTRACT

A THEORETICAL STUDY OF BUBBLE MOTION IN SURFACTANT SOLUTIONS

by
Yanping Wang

We examine the effect of surfactants on a spherical gas bubble rising steadily in an infinite fluid at low and order one Reynolds number with order one and larger Peclet numbers. Our mathematical model is based on the Navier-Stokes equations coupled with a convection-diffusion equation together with appropriate interfacial conditions. The nonlinearity of the equations and boundary conditions, and the coupling between hydrodynamics and surfactant transport make the problem very challenging.

When a bubble rises in a fluid containing surface-active agents, surfactant adsorbs onto the bubble surface at the leading edge, convects to the trailing edge by the surface flow and desorbs into the bulk along the interface. This adsorption develops a surface concentration gradient on the interface that makes the surface tension at the back end relatively lower than that at the front end, and thus retards the bubble velocity. Because of surfactant impurities unavoidably present in materials, this retardation can cause a problem in materials processing in space and glass processing when bubbles are created during chemical reactions. Thus the study of how to remobilize (remove the surfactant gradient on the surface) the bubble surface becomes necessary. Many studies have been done on this retarding effects of the surfactant on a moving bubble. However, most were focused on the retarding effect due to a trace amount of surfactant, in which case the bubble velocity monotonically decreases as the bulk concentration increases. The question of how to remobilize the bubble surface remains unanswered. In this work, we will show

that the bubble velocity can be controlled by remobilizing the bubble interface using the surfactant concentration. This technique not only can be used to maximize the bubble velocity, but also can be used to maximize mass transfer on purifying materials and extracting materials from mixtures.

In the first part of the work, we illustrate numerically that the bubble interface can be remobilized by increasing the bulk concentration of surfactant, for any fixed Peclet number, at low Reynolds number. For any fixed bulk concentration, the bubble velocity decreases with increasing Peclet number. The larger the Peclet number is the larger the required bulk concentration needed to bring the velocity back to the clean surface value. In the second part of the work, we will show that the remobilization still remains effective for order one Reynolds numbers. Moreover, when the rate of convection on the surface is much larger than the rate of diffusion at the back end, a stagnant cap develops near the back stagnation point that makes the bubble surface there act like a solid boundary. Wakes form at higher Reynolds numbers that drastically reduce the terminal velocity, and disappear as the bubble interface remobilizes. Finally, we consider the problem analytically for asymptotically large Peclet numbers. When the Peclet number is very large, a stagnant cap forms at the back end which makes one part of the bubble surface clean of surfactant, and the other part completely immobile. Also boundary layers develop along the bubble surface with different thicknesses on the clean part of the surface and on the stagnant cap. The asymptotic structures are obtained and the governing equations posed and partly addressed numerically and analytically.

A THEORETICAL STUDY OF BUBBLE MOTION IN SURFACTANT SOLUTIONS

by
Yanping Wang

A Dissertation
Submitted to the Faculty of
New Jersey Institute of Technology
in Partial Fulfillment of the Requirements for the Degree of
Doctor of Philosophy

Department of Mathematical Sciences

January 1999

BIOGRAPHICAL SKETCH

Author: Yanping Wang

Degree: Doctor of Philosophy

Date: January 1999

Undergraduate and Graduate Education:

- Doctor of Philosophy in Mathematical Sciences,
  New Jersey Institute of Technology, Newark, NJ, 1999
- Master of Science in Applied Mathematics,
  New Jersey Institute of Technology, NJ, 1995
- Bachelor of Science in Engineering,
  Northwestern Institute of Textile Technology, Xian, China, 1986

Major: Applied Mathematics

Presentations and Publications:

Maldarelli, C., Papageorgiou, D. and Wang, Y., "Surfactant Control of Wake Formation at the Back End of a Rising Bubble at Order One Reynolds Number", *American Chemical Society Colloid and Interface Science Symposium*, Penn State, PA, June 1998.

Wang, Y., Papageorgiou, D. and Maldarelli, C., "Increased Mobility of a Surfactant Retarded Bubble at High Bulk Concentrations", *J. Fluid Mech.*, Submitted.

Wang, Y., Papageorgiou, D. and Maldarelli, C., "Theoretical Study of Surfactant Effects on Rising Gas Bubbles", *Association for Women in Mathematics (AWM) Workshop in Conjunction with the SIAM Annual Meeting*, Kansas City, MO, July 1996.

Wang, Y., Papageorgiou, D. and Maldarelli, C., "Controlling the Mobility of a Fluid Particle in Space by Using Remobilizing Surfactants", *Third Microgravity Fluid Physics Conference*, Cleveland, OH, June 1996.

Wang, Y., Papageorgiou, D. and Maldarelli, C., "Theoretical Study of Surfactant Effects on Rising Gas Bubbles", *SIAM Student Conference and Annual Meeting of the Southeastern Atlantic Section*, Clemson, SC, March 1996.

APPROVAL PAGE

A THEORETICAL STUDY OF BUBBLE MOTION IN SURFACTANT SOLUTIONS

Yanping Wang

Demetrius Papageorgiou, Ph. D., Dissertation Advisor Associate Professor, Department of Mathematical Sciences, NJIT	Date
Gregory A. Kriegsmann, Ph. D., Committee Member Professor and Sponsored Chair in Applied Mathematics, Department of Mathematical Sciences, NJIT	Date
Jonathan Luke, Ph. D., Committee Member Associate Professor, Department of Mathematical Sciences, NJIT	Date
Charles Maldrelli, Ph. D., Committee Member Professor, Department of Chemical Engineering, CUNY	Date
Michael Siegel, Ph. D., Committee Member Associate Professor, Department of Mathematical Sciences, NJIT	Date

Wang, Y., Papageorgiou, D. and Maldarelli, C., "Theoretical Study of Surfactant Adsorption onto Rising Spherical Gas Bubbles at Low and Order One Reynolds Numbers," *Annual Meeting of the American Institute of Chemical Engineers*, Miami, FL, November 1995.

To my beloved family

ACKNOWLEDGMENT

I would like to take this opportunity to express my deepest appreciation to my advisor, Dr. Demetrius Papageorgiou, who not only provided me with generous resources and shared with me his valuable insight and intuition for my research, but also gave me support and encouragement constantly over the last several years. I was very fortunate to have a patient and selfless advisor who was willing to spend countless hours working with me. Without the guidance of his sharp mind and mathematical sophistication I would not have been able to overcome many of the obstacles. He also went well above and beyond what an advisor normally does for his students and helped greatly in more mundane matters such as defraying the cost of summer courses to lighten my financial burden.

My thanks also goes to Dr. Charles Maldrelli for helping me understand the nature of my research problems and applications of the results from an applied scientist's point of view, and to Drs. Gregory A. Kriegsmann, Jonathan Luke and Michael Siegel for actively participating in my dissertation committee.

Many of my friends helped me directly or indirectly during my entire course of graduate study and are deserving of recognition for their support. Although their names are too many to list here, they have my sincere gratitude.

Finally I would also like to thank my husband's support for my pursuit of mathematical research at a time when studying mathematics was neither fashionable nor practical. He understands that a true scholar obtains pleasure from learning itself.

TABLE OF CONTENTS

Chapter Page

LIST OF FIGURES

CHAPTER 1

INTRODUCTION

The effect of soluble surface active agents on the motion of drops and bubbles has attracted much interest for many years. It is motivated primarily by its relevance to the understanding of the performance of dropwise and aeration processes (see, for example, [Huang & Kintner (1969)] and [Beitel & Heideger (1971)]), where the existence of surface active species reduces the mass transfer. The problem has applications in material processing in space for making superconductive materials, optical fibers and better crystals for the semiconductor and bio-medical industry, and also in pollution cleansing systems, purification of materials and extraction of materials from mixtures, gap solidification, glass processing and composite preparation. An interesting aspect of this problem is the significant retardation on the particle (bubble or drop) motion due to the existence of surface active impurities in the fluid phases. Since it is impractical to remove the impurities from the material, the study of how the Marangoni force can be reduced (remobilization) becomes a question of technological significance.

Employing both numerical and asymptotic methods, we will investigate how the bubble motion is affected by the bulk concentration in general, and show that the retardation can be reduced by increasing the bulk concentration. Although we model the problem for buoyancy driven motion, the technique applies to thermocapillary migration as well.

In Section 1.1, a description of the Levich framework will be followed by a discussion of some of the subsequent works and questions that remain open. In Section 1.2 we will outline the results of our study.

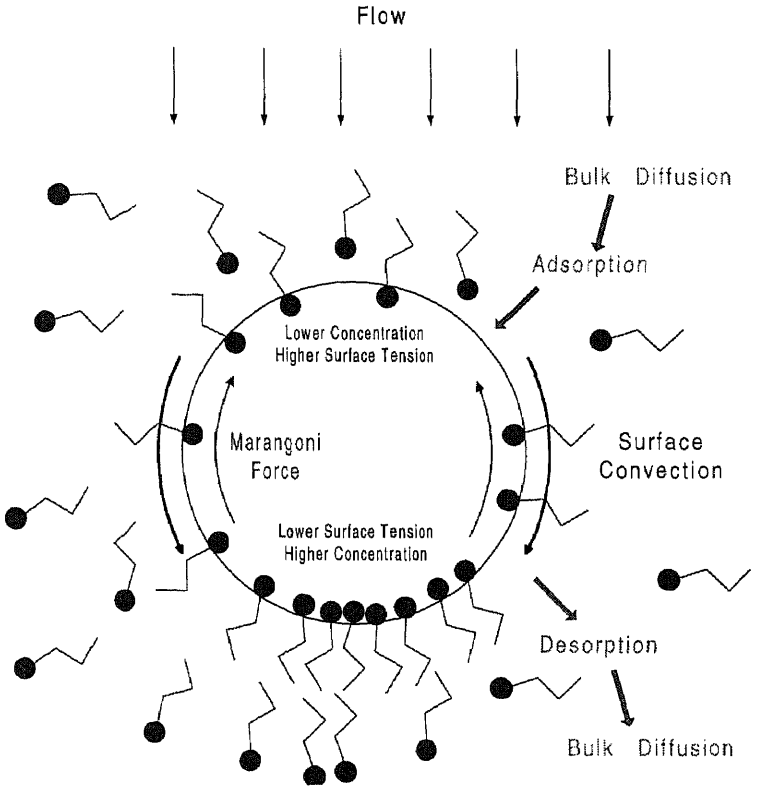

Figure 1.1 Retardation mechanism

In Chapter 2 we will derive the governing equations and thus set up the mathematical model for the cases of this study. Chapters 3 and 4 will focus on small Reynolds numbers with order one and higher Peclet numbers and the case of order one Reynolds numbers with order one and higher Peclet numbers, respectively. Our work on the asymptotic solution for high Peclet number will be described in Chapter 5.

1.1 Background

[Frumkin & Levich (1947)] first described the retardation mechanism on a particle moving in a surfactant solution. Here we describe this mechanism for the case in which surfactant is in the continuous phase only. As shown in Figure 1.1, when a particle moves in a fluid phase containing surfactants, surfactant adsorbs onto the surface of the particle at the leading edge, and is convected by the surface flow to the

particle's trailing end. Accumulation at the back end causes kinetic desorption into the bulk sublayer (fluid adjacent to the bubble surface), and the sublayer concentration increases above the value far from the interface. This difference gives rise to a diffusive flux away from the trailing end. Similarly at the front end kinetic adsorption occurs from the sublayer since the front surface is swept clean of surfactant. The sublayer concentration adjacent to the leading end of the particle decreases, creating a diffusive flux from the bulk to the front end. Eventually a steady state develops: In this state, the surface concentration at the back end has increased to the point where the desorption rate, proportional to the difference between the surface and sublayer concentration, balances the convective rate. In addition, the sublayer concentration increases sufficiently so that the diffusive flux away from the particle surface, proportional to the difference between the sublayer and far field concentration, balances the kinetic desorption. At the front end, the surface concentration becomes reduced enough so that kinetic adsorption balances convection, and the diffusion to the surface balances adsorption. Consequently, in this steady state the surface concentration is considerably higher at the rear than at the front of the particle. A gradient of surface concentration develops on the surface. Since surfactant reduces the surface tension, a surface tension gradient forms on the interface which opposes to the surface concentration gradient, implying that the surface tension at the back end is relatively lower than that at the front end. This interfacial tension gradient creates a surfactant Marangoni stress along the surface as the front end tugs the interface towards it. The direction of this surface stress is opposite to that of the surface flow, and thus the adsorption of surfactant onto the particle interface acts to reduce the surface flow, hence increases the drag on the particle and reduce the terminal velocity for rising

gas bubbles, for instance. Similar retardations are observed in thermocapillary flows also (see [Kim & Subramanian (1989b)] and [Nadim & Borhan (1989)]).

The retardation is much more significant for thermocapillary flows. In this case, the temperature at one side of the particle is relatively higher than the opposite side. Since the surface tension decreases as temperature increases, the side with the higher temperature has the lower surface tension, and vice versa. The low temperature region tugs the surface towards it, effectively developing a surface flow in the same direction and pulling the particle from the colder side to the warmer side. The magnitudes of this thermocapillary migration and the retardation caused by surfactant adsorption onto the particle surface are of the same order as they are both produced by a surface tension gradient, but in opposite directions. This makes the thermocapillary migration very sensitive to the presence of the surfactant as [Kim & Subramanian (1989a)], [Kim & Subramanian (1989b)] and [Nadim & Borhan (1989)] pointed out.

Using the Levich framework, several authors have studied, at steady state, the increase in drag for a particle moving at constant velocity due to the Marangoni forces created by the convective redistribution of surfactant along the surface. Roughly speaking they fall into two categories: when the convection of the surfactant along the surface is much greater than either the bulk diffusion or kinetic exchange, and, when they are of the same order.

When the surface Peclet number is large and the bulk concentration is small enough, the ratio of diffusion to convection is very small. This scenario belongs to the first category. In this case surfactant accumulates at the back end of the bubble and a stagnant cap develops there. This stagnant cap drastically increases the bubble drag, and increases it more as the cap angle gets larger.

Various theoretical studies of the dependence of the drag on the cap angle have been completed with the assumption that the Peclet number is infinite. [Savic (1953)] first observed the stagnant cap phenomenon. He also began its theoretical study, for the case of spherical drops (viscous and inertial forces are small compared to capillary forces) moving in creeping flow, with negligibly interior viscosity and bearing small stagnant cap, assuming that the surface pressure reaches its upper bound for a given surfactant. The problem is generally formulated in terms of an infinite set of algebraic equations for the coefficients of a series. Savic truncated this series after six terms. [Davis & Acrivos (1966)] improved his approximate numerical solution by retaining 150 terms for bubbles. [Harper (1973)] and [Harper (1982)] worked on small cap angles and carried out an asymptotic analysis. [Holbrook & Levan (1983a)], [Sadhal & Johnson (1983)] and [He, Maldarelli & Dagan (1991a)] worked on droplets. While these studies are for buoyancy driven motion, [Kim & Subramanian (1989b)] worked on thermocapillary driven motion of drops. The cap angle is obtained by computing the surfactant distribution in the cap region. [Griffith (1962)] first introduced the method, but the study was incomplete since he did not have the proper hydrodynamic solution. [Sadhal & Johnson (1983)] solved for the stream-function analytically for a given cap angle of arbitrary size—the solution is an infinite series involving the Gegenbauer polynomials whose coefficients are functions of the cap angle. They obtained the cap angle by using a linear relation between the surface tension gradient and surface concentration, and assuming that no diffusive boundary layer exists around the particle, i.e. the concentration in the liquid adjacent to the interface equals to the concentration at infinity. [He, Maldarelli & Dagan (1991a)] used a nonlinear relation, but they also ignore the existence of a boundary layer along the surface.

The question of how the concentration distribution of surfactant in the flow and on the surface affects the motion of the particle was not considered in these papers and still remains to be answered. In the case when the continuous phase inertia is not negligible (order one Reynolds number), [Bel Fdhila & Duineveld (1996)] (for a spherical bubble shape) and [McLaughlin (1997)] (for a deformed shape) computed the drag for buoyancy driven motion as a function of the cap angle, and the cap angle as a function of concentration for kinetic control. They demonstrated that at sufficiently large Reynolds number and cap angles, the immobility of the cap causes a recirculation at the back.

For thermocapillary driven motion, the effect of surfactant has only recently been studied by [Kim & Subramanian (1989a)], [Kim & Subramanian (1989b)] and [Nadim & Borhan (1989)]. They found the retardation on the thermocapillary driven is much greater than on the buoyancy driven motion. Since the magnitudes of Marangoni force and thermocapillary force are at the same order, Marangoni stress reduces the velocity to nearly zero.

Recent numerical results of [Cuenot, Magnaudet & Spennato (1997)] for the buoyancy driven motion of a spherical bubble at order one Reynolds number illustrate a cap by the collection of surfactant at the back end due to the high Peclet number and confirm the formation of a wake at order one Reynolds number as noted by [Bel Fdhila & Duineveld (1996)] and [McLaughlin (1997)].

In the second case when surfactant transport from the bulk to the surface matches the convective transport, if the kinetic rate is fast relative to convection, the surface and sublayer are in equilibrium. Bulk diffusion then governs the surfactant transport. All studies in this regime considered the case of a slightly soluble surfactant or a surfactant at low bulk concentration. Several studies examined

the case of large Peclet numbers, and used a boundary layer analysis to describe the diffusive flux. (c.f. [Deryagin, Dukhin & Lisichenko (1959)], [Saville (1973)], [Levich (1962)], [Harper (1974)] and [Harper (1982)] for negligible inertia and a spherical particle, and [Andrews, Fike & Wong (1988)] for a deformed particle at order one Reynolds number; all these studies are for buoyancy driven motion). The first studies in the direction of solving the convective diffusion directly were by [Levan & Newman (1976)] and [Holbrook & Levan (1983b)] for the case of buoyancy driven motion of a spherical particle in the absence of inertia. Levan demonstrated that the drag increases as the bulk concentration increases. This is because the surface concentration gradient increases as the bulk concentration increases at low concentration.

Most of the above studies for small bulk concentrations apply to the retarding effects due to the surfactant impurities unavoidably present in the bulk phase (see [Subramanian (1992)]), which is also the focus of many experimental studies. As noted above, the bubble velocity monotonically decreases as the bulk concentration increases. However, [Edge & Grant (1972)] and [Bel Fdhila & Duineveld (1996)] demonstrated the retardation by the intentional addition of surfactant with high Peclet number. They both found that there exists a critical concentration. The bubble velocity rapidly decreases to that of a solid sphere when the concentration is larger than the critical concentration. In addition the critical concentration increases as the bubble radius increases. [Barton & Subramanian (1989)] carried out similar experiments for the thermocapillary driven case.

1.2 Summary of Results

As described above, not much work has been done on the retarding effects of the surfactant for thermocapillary driven motion. In both buoyancy driven motion and thermocapillary driven motion, the general question of the effect of increasing bulk concentration remains open. The question of how to remobilize (remove the surfactant gradient on the surface) the particle has yet to be answered.

In this study we will show that the bubble surface can be remobilized by increasing the bulk concentration. In Chapter 3, we will show that the bubble surface can be remobilized by increasing the bulk concentration of surfactant at low Reynolds number. We illustrate numerically that, for a fixed Peclet number, a surface concentration gradient develops near the rear stagnation point at small bulk concentration, it spreads to the whole surface as the bulk concentration increases at the first, and then reduces to nearly zero as the bulk concentration gets large. This uniform distribution of surfactant on the bubble surface at large bulk concentration reduces the Marangoni force to nearly zero, hence decreases the drag and increases the velocity to the clean surface values. For any fixed bulk concentration, the bubble velocity decreases with increasing Peclet number. The larger the Peclet number is the larger the required bulk concentration needed to bring the velocity back to the clean surface value. Our numerical results in Chapter 4 show that, at order one Reynolds numbers, the remobilization still remains effective. We demonstrate that the drag monotonically decreases as a function of bulk concentration at order one and large concentration. Wakes form at higher Reynolds numbers as a rigid film develops near the rear stagnation point when the rate of convection on the surface is much larger than the rate of bulk diffusion, which cause a negative surface velocity in the stagnant cap region that drastically reduces the terminal

velocity. As we increase the bulk concentration for a fixed Peclet number, wakes become smaller, and disappear at large bulk concentration as the surfactant distribution on the bubble surface becomes more uniform. An asymptotical analysis for large Peclet numbers is presented in Chapter 5. The asymptotic structures are given along with the governing boundary layer equations. We found that in order to satisfy the zero net flux condition, the size of the clean part of the surface is very small. The boundary layer thickness along the stagnant cap region is found to be as the same for a solid sphere, and the boundary layer thickness along the clean part of the surface is found to be larger than that for a clean bubble sphere.

In industrial processes such as the environmental cleansing of poisonous gas, the purification of materials and the extraction of materials from mixtures, a remobilizing technique can be very useful. Other examples of potential applications include gap solidification, glass processing and composite preparation, etc. The technique can be especially valuable for material processing in microgravity environments. In such environments, because of the absence of buoyancy, other methods are necessary to induce the particles motion. Thermocapillary based driving forces are the most promising because of their high sensitivity to the interfacial and bulk surfactant concentration.

CHAPTER 2
DERIVATION OF EQUATIONS

We examine the motion of a spherical bubble rising steadily in an unbounded Newtonian fluid. The fluid contains surfactant, and it is assumed to be incompressible. We also assume the flow is axisymmetric and uniform at infinity, the concentration of surfactant far from the interface is uniform, the bubble remains spherical. The assumption of the bubble remaining spherical is reasonable if the inertial force is small compared to the surface tension, i.e. the Weber number ($\mathrm{We} = \frac{\rho U^2 a}{\gamma}$) and the capillary number ($\mathrm{Ca} = \frac{\mu U}{\gamma}$) are small.

2.1 Governing Equations

The mathematical model is based on a fixed coordinate system. The center of the bubble is taken to be the origin.

The governing equations for the fluid field are the incompressible Navier-Stokes equations

$$\rho \frac{D\tilde{\boldsymbol{u}}}{Dt} = -\nabla \tilde{P} + \mu \nabla^2 \tilde{\boldsymbol{u}}, \tag{2.1}$$

together with the equation of continuity

$$\nabla \cdot \tilde{\boldsymbol{u}} = 0, \tag{2.2}$$

where ρ is the density of the fluid and μ is the shear viscosity.

The governing equation for the surfactant transport in the bulk is the convection-diffusion equation

$$\frac{\partial \tilde{C}}{\partial t} + \nabla \cdot (\tilde{C}\tilde{\boldsymbol{u}}) = D\nabla^2 \tilde{C} \tag{2.3}$$

where $\tilde{C}$ is the surface-active surfactant concentration in the bulk and D is the diffusion coefficient of the continuous surfactant concentration..

Applying the continuity equation (2.2) to equations (2.1) and (2.3), the Navier-Stokes equations and the convection-diffusion equation become

$$\rho\left[\frac{\partial\tilde{\boldsymbol{u}}}{\partial t}+\tilde{\boldsymbol{u}}\cdot(\nabla\tilde{\boldsymbol{u}})\right]=-\nabla\tilde{p}+\mu\nabla^2\tilde{\boldsymbol{u}}, \tag{2.4}$$

$$\frac{\partial\tilde{C}}{\partial t}+\tilde{\boldsymbol{u}}\cdot\nabla\tilde{C}=D\nabla^2\tilde{C}. \tag{2.5}$$

By the nature of the problem, it is most convenient to express the equations in spherical coordinates (r,θ,ϕ), with $\theta=0$ representing the upstream direction. Since the flow is axisymmetric, the solution is independent of the azimuthal angle ϕ. The velocity in the azimuthal direction is zero and the only non-zero vorticity component is the azimuthal component, $\tilde{\omega}_\phi$, which is independent of ϕ. We examine the Navier-Stokes equations in terms of vorticity and stream-function. To do so, we write velocity in terms of stream-function $\tilde{\psi}$ as

$$\tilde{u}_r=-\frac{1}{\tilde{r}^2\sin\theta}\frac{\partial\tilde{\psi}}{\partial\theta}, \qquad \tilde{u}_\theta=\frac{1}{\tilde{r}\sin\theta}\frac{\partial\tilde{\psi}}{\partial\tilde{r}}, \tag{2.6}$$

in which case the continuity equation (2.2) is automatically satisfied.

Taking the curl of equation (2.4), and using the identity

$$\tilde{\boldsymbol{u}}\cdot\nabla\tilde{\boldsymbol{u}}=\frac{1}{2}\nabla|\tilde{\boldsymbol{u}}|^2+\tilde{\boldsymbol{\omega}}\times\tilde{\boldsymbol{u}}, \tag{2.7}$$

where $\tilde{\boldsymbol{\omega}}=\nabla\times\tilde{\boldsymbol{u}}$, the Navier-Stokes equations in vorticity form become

$$\frac{\partial\tilde{\boldsymbol{\omega}}}{\partial t}+\tilde{\boldsymbol{u}}\cdot(\nabla\tilde{\boldsymbol{\omega}})=\tilde{\boldsymbol{\omega}}\cdot(\nabla\tilde{\boldsymbol{u}})+\nu\nabla^2\tilde{\boldsymbol{\omega}}, \tag{2.8}$$

where $\nu = \mu/\rho$ is the kinematic viscosity.

Since the flow is axisymmetric, the solution is independent of the azimuthal angle ϕ, and the velocity component in that direction is zero. i.e. $\tilde{\boldsymbol{u}} = (\tilde{u}_r(\tilde{r},\theta), \tilde{u}_\theta(\tilde{r},\theta), 0)$. By the definition of vorticity, we have

$$\begin{aligned} \tilde{\boldsymbol{\omega}} &= \nabla \times \tilde{\boldsymbol{u}} \\ &= \left(0, 0, \frac{1}{\tilde{r}}\left[\frac{\partial(\tilde{r}\tilde{u}_\theta)}{\partial \tilde{r}} - \frac{\partial \tilde{u}_r}{\partial \theta}\right]\right). \end{aligned} \tag{2.9}$$

It follows that the vorticity has only one component in the azimuthal direction, $\tilde{\omega}_\phi$, which can be written in terms of the stream-function as

$$\begin{aligned} \tilde{\omega}_\phi &= \frac{1}{\tilde{r}}\left[\frac{\partial(\tilde{r}\tilde{u}_\theta)}{\partial \tilde{r}} - \frac{\partial \tilde{u}_r}{\partial \theta}\right] \\ &= \frac{1}{\tilde{r}}\tilde{E}^2\tilde{\psi}. \end{aligned} \tag{2.10}$$

The Navier-Stokes equations (2.8) in terms of vorticity and stream-function become, then,

$$\frac{\partial \tilde{\omega}_\phi}{\partial t} + \frac{\partial}{\partial \tilde{r}}(\tilde{r}\tilde{u}_r\tilde{\omega}_\phi) + \frac{\partial}{\partial \theta}(\tilde{u}_\theta\tilde{\omega}_\phi) = \nu\tilde{E}^2(\tilde{r}\tilde{\omega}_\phi \sin\theta), \tag{2.11}$$

where

$$\tilde{E}^2 = \frac{1}{\sin\theta}\frac{\partial^2}{\partial \tilde{r}^2} + \frac{1}{\tilde{r}^2}\frac{\partial}{\partial \theta}\left(\frac{1}{\sin\theta}\frac{\partial}{\partial \theta}\right). \tag{2.12}$$

2.2 Mixed Boundary Conditions

2.2.1 Hydrodynamics

The boundary conditions at the axes of symmetry are

$$\tilde{\psi} = 0 \qquad \text{at} \qquad \theta = 0, \pi, \tag{2.13}$$

$$\tilde{\omega}_\phi = 0 \qquad \text{at} \qquad \theta = 0, \pi. \tag{2.14}$$

The flow is uniform at infinity implying that the boundary conditions there are

$$\tilde{\psi} = \frac{1}{2} U \tilde{r}^2 \sin^2 \theta \qquad \text{as} \qquad \tilde{r} \to \infty, \tag{2.15}$$

$$\tilde{\omega}_\phi = 0 \qquad \text{as} \qquad \tilde{r} \to \infty, \tag{2.16}$$

where U is the uniform flow velocity far from the interface.

Since there is no deformation on the bubble surface, the normal velocity at the interface is zero. This leads to

$$\tilde{\psi} = 0 \qquad \text{at} \qquad \tilde{r} = a. \tag{2.17}$$

It follows that the first and second derivatives of stream-function with respect to θ are zero and so we have from equation (2.10)

$$\tilde{\omega}_\phi = \frac{1}{a \sin \theta} \frac{\partial^2 \tilde{\psi}}{\partial \tilde{r}^2} \qquad \text{at} \qquad \tilde{r} = a. \tag{2.18}$$

In the presence of surfactant, as explained in Chapter 1, the concentration, $\tilde{\Gamma}(\theta)$ say, varies from point to point on the surface of the bubble; i.e. $\tilde{\Gamma} = \tilde{\Gamma}(\theta)$. Since an increase in surfactant lowers the surface tension, the surface tension γ is a function of

surface concentration $\tilde{\Gamma}$ and it also varies along the surface. The relation between the surface tension and the surface concentration is expressed by the Langmuir equation (see [Levich (1962)])

$$\gamma = \gamma_c + RT\Gamma_\infty \ln(1 - \frac{\tilde{\Gamma}}{\Gamma_\infty}), \tag{2.19}$$

where γ_c is the surface tension on a clean bubble, Γ_∞ is the maximum packing density of surfactant, R is the gas constant and T is the temperature.

This surface tension gradient causes a Marangoni force on the bubble surface that must be compensated by a viscous tangential stress on the interface. This is expressed as (see [Leal (1992)])

$$\tilde{\tau}_{r\theta} = -\frac{1}{a}\frac{\partial \gamma}{\partial \theta} \qquad \text{at} \qquad \tilde{r} = a. \tag{2.20}$$

Differentiating equation (2.19) with respect to $\tilde{\Gamma}$, gives

$$\frac{\partial \gamma}{\partial \tilde{\Gamma}} = -\frac{RT\Gamma_\infty}{\Gamma_\infty - \tilde{\Gamma}}. \tag{2.21}$$

If we rewrite equation (2.20) as

$$\tilde{\tau}_{r\theta} = -\frac{1}{a}\frac{\partial \gamma}{\partial \tilde{\Gamma}}\frac{\partial \tilde{\Gamma}}{\partial \theta}, \tag{2.22}$$

and substitute equation (2.21) into equation (2.22), we obtain the shear stress in terms of the surface concentration as follows,

$$\tilde{\tau}_{r\theta} = \frac{1}{a}\frac{RT\Gamma_\infty}{\Gamma_\infty - \tilde{\Gamma}}\frac{\partial \tilde{\Gamma}}{\partial \theta}. \tag{2.23}$$

On the other hand, the shear stress on the surface in terms of the stream-function can be expressed as

$$\tilde{\tau}_{r\theta} = \frac{\mu}{a \sin\theta} \left(\frac{\partial^2 \tilde{\psi}}{\partial \tilde{r}^2} - \frac{2}{a} \frac{\partial \tilde{\psi}}{\partial \tilde{r}} \right). \tag{2.24}$$

From equations (2.23) and (2.24), we deduce the following form of the tangential stress balance,

$$\frac{\partial^2 \tilde{\psi}}{\partial \tilde{r}^2} = \frac{2}{a} \frac{\partial \tilde{\psi}}{\partial \tilde{r}} + \frac{\sin\theta}{\mu} \frac{RT\Gamma_\infty}{\Gamma_\infty - \tilde{\Gamma}} \frac{\partial \tilde{\Gamma}}{\partial \theta}. \tag{2.25}$$

Hence the balance of Marangoni force and shear stress on the surface, leads to a boundary condition for the vorticity, namely

$$\tilde{\omega}_\phi = \frac{2}{a^2 \sin\theta} \frac{\partial \tilde{\psi}}{\partial \tilde{r}} + \frac{1}{a\mu} \frac{RT\Gamma_\infty}{\Gamma_\infty - \tilde{\Gamma}} \frac{\partial \tilde{\Gamma}}{\partial \theta}. \tag{2.26}$$

In order to solve for the flow field, the surface surfactant concentration, $\tilde{\Gamma}(\theta)$, must be known. This couples the Navier-Stokes equations with the convection-diffusion equation, as explained next.

2.2.2 Surfactant Transport

The amount of material adsorbed per unit area satisfies a mass conservation law, which, in the case of a bubble, can be expressed as ([Levich (1962)])

$$j_n = \nabla_s \cdot (\tilde{\Gamma} \tilde{u}_\theta) - \nabla \cdot (D_s \nabla_s \tilde{\Gamma}) + \frac{\partial \tilde{\Gamma}}{\partial t}, \tag{2.27}$$

where $\tilde{\Gamma}\tilde{u}_\theta$ is the flux of adsorbed material transferred along the surface by the tangential velocity component of the flow, and $\nabla_s \cdot (\tilde{\Gamma}\tilde{u}_\theta)$ is the surface divergence

of that flux. The quantity j_n represents the flux of material removed into the bulk of the medium ($j_n < 0$) or conveyed ($j_n > 0$) to a unit area of the bubble from the solution; $(-D_s \nabla_s \tilde{\Gamma})$ expresses the diffusion flux of adsorbed material on the surface of the bubble. Here D_s designates the surface diffusion coefficient of the surface-active material. Thus, in the expression for the total flux of surface-active material, the right side expresses the full divergence of the diffusional and convective fluxes of material along the surface of the bubble. The left side gives the flux of material to or from the bulk of the solution. The magnitude of the latter is evidently a function of the velocity distribution near the surface of bubble, while the magnitude of convective flux along the surface of the bubble is determined by the velocity on the bubble surface.

The magnitude j_n of the flux of surface-active material from the surface of the bubble into the bulk of the liquid, is determined by the rate of adsorption-desorption or the rate of transfer of molecules of surface-active material from the bulk of the liquid to the surface of the bubble. If the rate of adsorption-desorption is small compared to the rate at which the material is transferred to the surface of the bubble, the rate j_n of surface-active molecules leaving (or arriving at) per unit area of surface per unit time is determined by the total number of desorbed (or adsorbed) molecules. If, on the other hand, the kinetics of adsorption and desorption are rapid compared to the rate of transfer of surface-active molecules from the bulk of the solution to the interface, the number of surface-active molecules leaving (or arriving at) per unit area of surface per unit time is equal to the diffusional flux to the bulk. Here we assume the later case (see [Levich (1962)]). i.e.

$$j_n = D \left. \frac{\partial \tilde{C}}{\partial \tilde{r}} \right|_{\tilde{r}=a} . \tag{2.28}$$

Therefore in the case of rapid kinetics, j_n in the surface concentration conservation equation (2.27) has the form of expression (2.28). If we assume the surface diffusion is negligible compared to the convection on the surface, the surfactant interfacial conservation without surface deformation is described by the equation

$$\frac{\partial \tilde{\Gamma}}{\partial t} + \frac{1}{a \sin\theta} \frac{\partial}{\partial \theta} \left(\tilde{u}_\theta \tilde{\Gamma} \sin\theta \right) = D \left. \frac{\partial \tilde{C}}{\partial \tilde{r}} \right|_{\tilde{r}=a} . \tag{2.29}$$

The over-all rate of the exchange of surface-active material is determined by its rate of transfer from the bulk of the medium to the surface of the bubble. i.e. by the rate of convective-diffusion. The kinetics of the adsorption-desorption process in this case, may be considered to be as rapid as desired, so that the concentration of the solution near the surface has a value $\tilde{C}(\tilde{r} = a)$ which is in equilibrium with $\tilde{\Gamma}$, but differs from the concentration $\tilde{C}$ in the bulk of the solution. The flux of surfactant reaching the interface obeys Langmuir's law ([Levich (1962)]; [Probstein (1994)])

$$D \frac{\partial \tilde{C}}{\partial \tilde{r}} = \beta [\tilde{C}(\Gamma_\infty - \tilde{\Gamma}) - k_a^{-1} \tilde{\Gamma}] \qquad \text{at} \qquad \tilde{r} = a \tag{2.30}$$

where β and k_a are the parameters of the adsorption and desorption rate of constants respectively. For fast kinetic exchange, $\beta \gg 1$. That is the kinetics of adsorption and desorption are rapid compared to diffusional flux to the bulk phase. This reduces the equation (2.30) to a equilibrium dependence of $\tilde{\Gamma}$ on the concentration near the surface,

$$\tilde{\Gamma} = \left. \frac{k_a \Gamma_\infty \tilde{C}}{1 + k_a \tilde{C}} \right|_{\tilde{r}=a} \tag{2.31}$$

The boundary conditions are, due to axisymmetry,

$$\frac{\partial \tilde{C}}{\partial \theta} = 0 \qquad at \qquad \theta = 0, \pi, \tag{2.32}$$

and the uniform concentration in the far field provides the boundary condition at infinity

$$\tilde{C} = C_\infty \qquad \text{as} \qquad \tilde{r} \to \infty. \tag{2.33}$$

2.3 Force on the Surface

2.3.1 Pressure on the Surface

The steady state Navier-Stokes equations for incompressible flow are

$$\rho \tilde{\boldsymbol{u}} \cdot (\nabla \tilde{\boldsymbol{u}}) = -\nabla \tilde{p} + \mu \nabla^2 \tilde{\boldsymbol{u}}. \tag{2.34}$$

For axisymmetric flow, the Navier-Stokes equation in the tangential direction (θ) takes the form

$$\rho \left(\tilde{\boldsymbol{u}} \cdot \nabla \tilde{u}_\theta + \frac{\tilde{u}_\theta \tilde{u}_r}{\tilde{r}} \right) = -\frac{1}{\tilde{r}} \frac{\partial \tilde{p}}{\partial \theta} + \mu \left(\nabla^2 \tilde{u}_\theta + \frac{2}{\tilde{r}^2} \frac{\partial \tilde{u}_r}{\partial \theta} - \frac{\tilde{u}_\theta}{\tilde{r}^2 \sin^2 \theta} \right). \tag{2.35}$$

Since the normal velocity on the surface is zero, the equation on the surface reduces to

$$\begin{aligned} \rho \tilde{u}_\theta \frac{\partial \tilde{u}_\theta}{\partial \theta} = & -\frac{\partial \tilde{p}}{\partial \theta} \\ & + \mu \left(a \frac{\partial^2 \tilde{u}_\theta}{\partial \tilde{r}^2} + 2 \frac{\partial \tilde{u}_\theta}{\partial \tilde{r}} + \frac{1}{a} \frac{\partial^2 \tilde{u}_\theta}{\partial \theta^2} + \frac{\cot \theta}{a} \frac{\partial \tilde{u}_\theta}{\partial \theta} + \frac{2}{a} \frac{\partial \tilde{u}_r}{\partial \theta} - \frac{\tilde{u}_\theta}{a \sin^2 \theta} \right). \end{aligned} \tag{2.36}$$

Also, from the continuity equation (2.2), we have

$$\frac{1}{\tilde{r}^2} \frac{\partial (\tilde{r}^2 \tilde{u}_r)}{\partial \tilde{r}} + \frac{1}{\tilde{r} \sin \theta} \frac{\partial (\tilde{u}_\theta \sin \theta)}{\partial \theta} = 0. \tag{2.37}$$

Differentiating equation (2.37) with respect to $\tilde{r}$ and evaluating on the surface yields

$$a\frac{\partial^2 \tilde{u}_r}{\partial \tilde{r}\partial\theta} + 2\frac{\partial \tilde{u}_r}{\partial\theta} + \frac{\partial^2 \tilde{u}_\theta}{\partial\theta^2} + \cot\theta\frac{\partial \tilde{u}_\theta}{\partial\theta} - \frac{\tilde{u}_\theta}{\sin^2\theta} = 0. \tag{2.38}$$

By combining equations (2.36) and (2.38), we find that the pressure gradient on the surface can be expressed as

$$\begin{aligned}\frac{\partial \tilde{p}}{\partial\theta} &= \mu\left(a\frac{\partial^2 \tilde{u}_\theta}{\partial \tilde{r}^2} + 2\frac{\partial \tilde{u}_\theta}{\partial \tilde{r}} - \frac{\partial^2 \tilde{u}_r}{\partial \tilde{r}\partial\theta}\right) - \rho\tilde{u}_\theta\frac{\partial \tilde{u}_\theta}{\partial\theta} \\ &= \mu\frac{\partial(\tilde{r}\omega)}{\partial \tilde{r}} - \tilde{u}_\theta\frac{\partial \tilde{u}_\theta}{\partial\theta}.\end{aligned} \tag{2.39}$$

2.3.2 Total Drag Acting on the Bubble

The resultant force, due to the stresses, exerted by the surrounding fluid on the bubble is

$$\boldsymbol{F} = \int \boldsymbol{\sigma}\cdot\boldsymbol{n}\, dS, \tag{2.40}$$

where $\boldsymbol{\sigma}$ is the stress tensor, which for an incompressible viscous fluid is given by

$$\boldsymbol{\sigma} = -p\boldsymbol{I} + 2\mu\boldsymbol{e}, \tag{2.41}$$

with $\boldsymbol{e} = \frac{1}{2}(\nabla\tilde{\boldsymbol{u}} + \nabla\tilde{\boldsymbol{u}}^T)$ being the rate of strain tensor.

The stress vector acting across an element of surface area whose outer normal is $\boldsymbol{n}$ is then of the form

$$\begin{aligned}\boldsymbol{\sigma}_n &= \boldsymbol{\sigma}\cdot\boldsymbol{n} \\ &= \boldsymbol{n}\left(-\tilde{p} + 2\mu\frac{\partial \tilde{u}_r}{\partial \tilde{r}}\right) + \boldsymbol{\theta}\mu\left[\tilde{r}\frac{\partial}{\partial \tilde{r}}\left(\frac{\tilde{u}_\theta}{\tilde{r}}\right) + \frac{1}{\tilde{r}}\frac{\partial \tilde{u}_r}{\partial\theta}\right].\end{aligned} \tag{2.42}$$

Owing to the symmetry of the flow, the cumulative effect of the stresses acting over the entire surface of the bubble give rise to only one significant dynamic parameter-a force acting parallel to the axis of revolution. Take the upstream direction to be the positive direction; then, the force exerted on the bubble is given by

$$\begin{aligned} F_z &= \int_0^\pi \left\{ \left(-\tilde{p} + 2\mu \frac{\partial \tilde{u}_r}{\partial \tilde{r}} \right) \cos\theta - \mu \left[\tilde{r} \frac{\partial}{\partial \tilde{r}} \left(\frac{\tilde{u}_\theta}{\tilde{r}} \right) + \frac{1}{\tilde{r}} \frac{\partial \tilde{u}_r}{\partial \theta} \right] \sin\theta \right\} \Bigg|_{\tilde{r}=a} \cdot 2\pi a^2 \sin\theta \, d\theta \\ &= 2\pi a^2 \int_0^\pi \left(\frac{\sin^2\theta}{2} \frac{\partial \tilde{p}}{\partial \theta} - \frac{\mu}{a} \frac{\partial^2 \tilde{\psi}}{\partial \tilde{r}^2} \sin\theta \right) \Bigg|_{\tilde{r}=a} d\theta \\ &= \pi a^2 \int_0^\pi \sin^2\theta \frac{\partial \tilde{p}}{\partial \theta} \, d\theta - 2\pi a\mu \int_0^\pi \frac{\partial^2 \tilde{\psi}}{\partial \tilde{r}^2} \sin\theta \, d\theta \\ &= \pi a^2 \int_0^\pi \sin^2\theta \frac{\partial \tilde{p}}{\partial \theta} \, d\theta - 2\pi a\mu \int_0^\pi \left(\frac{2}{a} \frac{\partial \tilde{\psi}}{\partial \tilde{r}} + \frac{\sin\theta}{\mu} \frac{RT\Gamma_\infty}{\Gamma_\infty - \tilde{\Gamma}} \frac{\partial \tilde{\Gamma}}{\partial \theta} \right) \sin\theta \, d\theta. \end{aligned} \tag{2.43}$$

2.4 Nondimensionalization

2.4.1 Governing Equations and Mixed Boundary Conditions

We make the equations dimensionless by nondimensionalizing using the following transformations:

$$r = \frac{\tilde{r}}{a}, \qquad \boldsymbol{u} = \frac{\tilde{\boldsymbol{u}}}{U}, \qquad \psi = \frac{\tilde{\psi}}{Ua^2}, \qquad \omega = \frac{\tilde{\omega}_\phi}{U/a}, \tag{2.44}$$

$$\Gamma = \frac{\tilde{\Gamma}}{\Gamma_\infty}, \qquad C = \frac{\tilde{C}}{C_\infty}. \tag{2.45}$$

Since we are interested in steady state solutions, the time scale does not play a significant role. We keep the time derivative term for numerical convenience.

The nondimensionalized governing equations become, then,

$$\frac{\partial \omega}{\partial t} + \frac{\partial}{\partial r}(r u_r \omega) + \frac{\partial}{\partial \theta}(u_\theta \omega) = \frac{1}{\mathrm{Re}} E^2 (r\omega \sin\theta) \qquad \text{by (2.11)}, \tag{2.46}$$

$$\omega = \frac{1}{r} E^2 \psi \qquad \text{by (2.10)}, \tag{2.47}$$

$$\frac{\partial C}{\partial t} + \boldsymbol{u} \cdot \nabla C = \frac{1}{\mathrm{Pe}} \nabla^2 C \qquad \text{by (2.5)}, \tag{2.48}$$

where

$$u_r = -\frac{1}{r^2 \sin\theta} \frac{\partial \psi}{\partial \theta}, \qquad u_\theta = \frac{1}{r \sin\theta} \frac{\partial \psi}{\partial r}, \tag{2.49}$$

$$E^2 = \frac{1}{\sin\theta} \frac{\partial^2}{\partial r^2} + \frac{1}{r^2} \frac{\partial}{\partial \theta} \left(\frac{1}{\sin\theta} \frac{\partial}{\partial \theta} \right), \tag{2.50}$$

from formula (2.6) and equation (2.12) respectively, $\mathrm{Re} = \dfrac{Ua}{\nu}$ is the Reynolds number, and $\mathrm{Pe} = \dfrac{Ua}{D}$ is the Peclet number.

The nondimensional boundary conditions for the hydrodynamics are

$$\psi = 0 \qquad at \qquad \theta = 0, \pi, \tag{2.51}$$

$$\psi = 0 \qquad at \qquad r = 1, \tag{2.52}$$

$$\psi = \frac{1}{2} r^2 \sin^2\theta \qquad as \qquad r \to \infty, \tag{2.53}$$

$$\omega = 0 \qquad at \qquad \theta = 0, \pi, \tag{2.54}$$

$$\omega = 0 \qquad as \qquad r \to \infty, \tag{2.55}$$

and

$$\omega = \frac{2}{\sin\theta} \frac{\partial \psi}{\partial r}\bigg|_{r=1} + \frac{\mathrm{Ma}}{1-\Gamma} \frac{\partial \Gamma}{\partial \theta}, \tag{2.56}$$

where $\mathrm{Ma} = \dfrac{RT\Gamma_\infty}{\mu U}$ is the Marangoni number, and Γ is the dimensionless surface concentration to be found from the concentration field.

The nondimensional boundary conditions for the surfactant transport equations are

$$\frac{\partial C}{\partial \theta} = 0 \qquad at \qquad \theta = 0, \pi, \tag{2.57}$$

$$C = 1 \qquad as \qquad r \to \infty, \tag{2.58}$$

and the equation of interfacial surfactant conservation becomes

$$\frac{\partial \Gamma}{\partial t} + \frac{1}{\sin\theta}\frac{\partial}{\partial \theta}(u_\theta \Gamma \sin\theta) = \left.\frac{\chi k}{\mathrm{Pe}}\frac{\partial C}{\partial r}\right|_{r=1}. \tag{2.59}$$

The equilibrium equation between the surface concentration Γ, and the sublayer surfactant concentration is, in dimensionless form,

$$\Gamma = \left.\frac{kC}{1+kC}\right|_{r=1}. \tag{2.60}$$

In equations (2.59) and (2.60) above the parameters appearing are given by, $\chi = \dfrac{a}{k_a \Gamma_\infty}$ and $k = k_a C_\infty$ which is a measure of the bulk concentration.

2.4.2 Drag on the Body

2.4.2.1 Creeping Flow

For small Reynolds number, we nondimensionalize pressure and drag using the following scales

$$p_1 = \frac{\tilde{p}}{\mu U/a}, \qquad C_{D1} = \frac{F_z}{\pi \mu U a}. \tag{2.61}$$

Then, the nondimensional pressure gradient on the surface given by equation (2.39), becomes

$$\frac{\partial p_1}{\partial \theta} = \frac{\partial (r\omega)}{\partial r}, \tag{2.62}$$

and consequently the dimensionless drag coefficient for small Reynolds number is given by

$$\begin{aligned} C_{D1} &= \int_0^{\pi} \sin^2\theta \frac{\partial p_1}{\partial \theta} d\theta - 2\int_0^{\pi} \frac{\partial^2 \psi}{\partial r^2} \sin\theta d\theta \\ &= \int_0^{\pi} \sin^2\theta \frac{\partial p_1}{\partial \theta} d\theta - 2\int_0^{\pi} \left(2\frac{\partial \psi}{\partial r} + \frac{\mathrm{Ma}\sin\theta}{1-\Gamma}\frac{\partial \Gamma}{\partial \theta} \right) \sin\theta d\theta. \end{aligned} \tag{2.63}$$

2.4.2.2 Order One Reynolds Numbers

For order one Reynolds numbers, we rescale pressure and drag as

$$p_2 = \frac{\tilde{p}}{\rho U^2}, \qquad C_{D2} = \frac{F_z}{\pi a^2 \rho U^2}. \tag{2.64}$$

Then, from equations (2.39) and (2.43), the dimensionless pressure gradient on the surface and the drag coefficient are

$$\frac{\partial p_2}{\partial \theta} = \frac{1}{\mathrm{Re}} \frac{\partial (r\omega)}{\partial r} - u_\theta \frac{\partial u_\theta}{\partial \theta}, \tag{2.65}$$

and

$$\begin{aligned} C_{D2} &= \int_0^{\pi} \sin^2\theta \frac{\partial p_2}{\partial \theta} d\theta - 2\int_0^{\pi} \frac{\partial^2 \psi}{\partial r^2} \sin\theta d\theta \\ &= \int_0^{\pi} \sin^2\theta \frac{\partial p_2}{\partial \theta} d\theta - 2\int_0^{\pi} \left(2\frac{\partial \psi}{\partial r} + \frac{\mathrm{Ma}\sin\theta}{1-\Gamma}\frac{\partial \Gamma}{\partial \theta} \right) \sin\theta d\theta, \end{aligned} \tag{2.66}$$

respectively.

CHAPTER 3

CONTROLLING BUBBLE VELOCITY IN SURFACTANT SOLUTION AT LOW REYNOLDS NUMBER

3.1 Introduction

When a bubble rises in the fluid containing surfactant, the surfactant is adsorbed onto the interface at the leading edge of the bubble, convects to the trailing edge by the surface flow and diffuses into the bulk along the surface. Accumulation of surfactant at the back end makes the surface concentration at the back end relatively higher than that at the front end. This surface concentration gradient creates a surface tension gradient on the bubble surface, since surfactant lower the surface tension. A Marangoni force which is in the opposite direction of the surface velocity is created as the surface has the higher surface tension (the front end) tugs the surface towards it. It reduces the surface velocity, hence increases the drag. When the rate of surface convection is large compared to the rate of bulk diffusion, a stagnant cap develops near the rear stagnation point, as shown in Figure 3.1. The mechanism of this retardation is presented in detail in Chapter 1.

Various studies have been concerned with the effects of surfactant on the motion of particles rising in surfactant solution. As we described on Chapter 1, most of the works were focused on trace amount of surfactant due to the material impurities, in which the drag monotonically increases as a function of bulk concentration. The retardation effects of intentional addition of surfactant are demonstrated experimentally by [Edge & Grant (1972)] on drops and [Bel Fdhila & Duineveld (1996)] on bubbles for buoyancy driven motion with high Peclet number. Edge & Grant observed that the motion of drops in contaminated water is indistinguishable from the motion of drops in pure water when the surfactant concentration is very small,

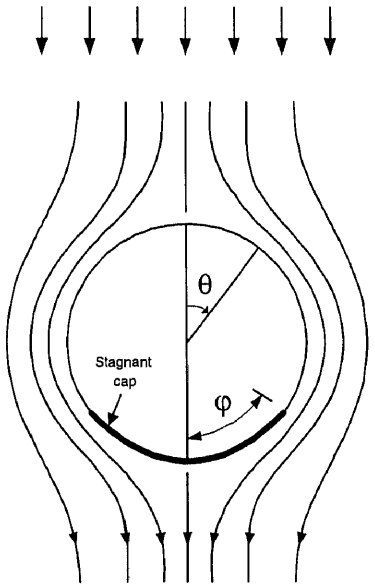

Figure 3.1 Flow around bubble, where φ is the cap angle

and the drag increases as the bulk concentration increases. Wakes form at high enough bulk concentration and are similar to the attached wakes behind solid spheres. Duineveld found that the bubble velocity decreases with increasing bulk concentration. For all bubble sizes there is a critical concentration, below which the velocity is almost equal to the clean surface value, and above which the velocity decreases rapidly to the solid sphere value. This critical concentration value increases as the bubble size increases. [Barton & Subramanian (1989)] carried out similar experiments for the thermocapillary driven case.

In this chapter, we demonstrate that the bubble interface can be remobilized by increasing the bulk concentration of surfactant. The surfactant concentration distribution on the surface for a fixed Peclet number and various bulk concentrations is given in Section 3.3.1. Numerical results show that the amount of surfactant adsorbed onto the surface increases as the bulk concentration increases. A surface concentration gradient develops near the rear stagnation point when the bulk concentration is very small. As the bulk concentration increases, the surface concentration gradient

spreads onto the whole interface at first, and disappears at large concentration. The removal of retardation of the surface velocity is shown in Section 3.3.2, where the surface velocities for a fixed Peclet number with different bulk concentrations are calculated. When the bulk concentration is very small, the surface velocity near the front is almost the same as the clean surface value, but it is much smaller than the clean surface value near the back end (corresponding to the surface concentration gradient there). As the bulk concentration increases, the surface velocity decreases at first, and then increases to the clean surface velocity as the surface concentration distribution becomes more uniform at large bulk concentration. In Section 3.3.3, we show that for a fixed Peclet number, the drag increases monotonically as a function of bulk concentration when the bulk concentration is small, and, after it reaches a maximum the drag decreases monotonically to the clean surface value. For fixed concentration, the drag increases with increasing Peclet number. For larger Peclet numbers, higher bulk concentration is required to reduce the drag to the clean surface value. Numerical results also show the development of a cap near the rear stagnation point when $\frac{k\chi}{\mathrm{Pe}} \ll 1$.

3.2 Mathematical Model and Numerical Algorithm

We examine the dynamics of a spherical, buoyancy driven gas bubble rising steadily in an infinite Newtonian fluid containing surfactant. The Reynolds number of the flow is small and we consider the case of bulk diffusion controlled surfactant transport with order one and large Peclet number. In addition, we assume that the fluid is incompressible, the flow is uniform at infinity, the surfactant concentration far from the bubble surface is uniform, and there is no interfacial deformation thus keeping the

bubble spherical (small Weber numbers). The mathematical model and the relevant boundary conditions were given in Chapter 2. Since the governing equations are nonlinear, and coupled by the nonlinear boundary conditions, it is unlikely that the full problem can be solved analytically. We will examine the problem in nondimensional form by addressing numerically equations (2.46)-(2.48) with the corresponding boundary conditions (2.51)-(2.60). Since the problem considered in this chapter is for small Reynolds number, the equation (2.46) is reduced to

$$\frac{\partial \omega}{\partial t} = E^2(r\omega \sin\theta).$$

The numerical method is described below.

The problem is to solve simultaneously the differential equations (2.46)-(2.48) subject to the boundary conditions (2.51)-(2.60). Since the equations are nonlinear and coupled by the nonlinear boundary conditions, an appropriate approach we found to be efficient and stable is to use a numerical method involving an iterative procedure. The iterative procedure can be outlined as follows:

1. Choose initial conditions for the fluid field and concentration fields (usually taken from a known analytical solution such as flow past a clean surface sphere).

2. Obtain an approximation to the stream-function subject to the boundary conditions (2.51)-(2.53). Use the relation (2.49) to find the radial and tangential velocities.

3. Substitute the tangential velocity found in (2) in equation (2.59), and solve for Γ using an explicit method.

4. Find the boundary condition on the surface for the vorticity by using the results found in (2) and (3) on equation (2.56), and get an approximation for the vorticity subject to boundary conditions (2.54)-(2.56).

5. Solve the convection-diffusion equation (2.48) subject to boundary conditions (2.57)-(2.60) using the results found in (2) and (3).

6. Check the convergence criteria. If the criteria is not satisfied, upgrade the initial conditions in (1) and repeat the steps (2)-(5).

3.2.1 A Finite Difference Method

A variety of finite-difference schemes exist which can be used to solve the coupled nonlinear system (2.46)-(2.48), and it is not possible to compare them exhaustively to ensure an optimal approach for each particular problem. The Alternating Directions Implicity (ADI) method is used for the pseudo-unsteady system. We make this choice because the ADI method are been widely used and tested in fluid dynamics problems (see [Peyret & Taylor (1983)]), it is easy to implement and has good stability properties. Generally, the method is unconditionally stable with second order accuracy.

To illustrate this method, it is best to combine equations (2.46)-(2.48) into the following general form:

$$\frac{\partial G}{\partial t} + q_1 L_1(G) + q_2 L_2(G) = f \tag{3.1}$$

where G stands for the vorticity ω, or the stream function ψ, or the concentration C, q_1 and q_2 are functions of vorticity ω, stream-function ψ and velocity $\boldsymbol{u}$, f is the

force term, and L_1 and L_2 are differential operators in the normal and transverse directions, respectively.

With the ADI scheme, each time step is divided into two equal parts. Applying the ADI scheme on equation (3.1) at each step provides the recursions

$$\frac{G^{n+\frac{1}{2}} - G^n}{\frac{\Delta t}{2}} + q_1^n \left[L_1(G)\right]^{n+\frac{1}{2}} + q_2^n \left[L_2(G)\right]^n = f^{n+\frac{1}{2}} \qquad \text{(Step I)} \quad (3.2)$$

$$\frac{G^{n+1} - G^{n+\frac{1}{2}}}{\frac{\Delta t}{2}} + q_1^{n+\frac{1}{2}} \left[L_1(G)\right]^{n+\frac{1}{2}} + q_2^{n+\frac{1}{2}} \left[L_2(G)\right]^{n+1} = f^{n+1} \qquad \text{(Step II)} \quad (3.3)$$

Applying the ADI scheme on equations (2.46), (2.47) and (2.48) yields three systems of equations at each step, which can be written in three tridiagonal matrix forms if we treat the boundary conditions (2.51)-(2.60) carefully.

3.2.2 Special Treatment for the Boundary Conditions

With the finite difference method, one has to limit the radial direction to some finite radius r_∞. Applying directly the boundary condition at infinity, (2.53), on $r = r_\infty$ would introduce an error, and the proper way to minimize this error is to obtain a correction term for the stream-function and use the corrected stream-function at infinity.

For axisymmetric creeping flow, the stream-function satisfies the differential equation (see [Happel & Brenner (1973)])

$$E^4 \psi = 0, \quad (3.4)$$

where E is given by equation (2.50) in Chapter 2. The general solution of equation (3.4) is

$$\psi = \sum_{n=0}^{\infty}(A_n r^{-n+3} + B_n r^{-n+1} + C_n r^{n+2} + D_n r^n)C_n^{-\frac{1}{2}}(\cos\theta), \tag{3.5}$$

where $C_n^{-\frac{1}{2}}(x)$ are Gegenbauer polynomials of degree $-\frac{1}{2}$. Applying the boundary conditions (2.51)-(2.53) to the above solution, one obtains

$$\psi = \frac{1}{2}(r^2 - r)\sin^2\theta + \sum_{n=2}^{\infty} B_n(r^{-n+1} - r^{-n+3})C_n^{-\frac{1}{2}}(\cos\theta), \tag{3.6}$$

where B_n are constants to be determined.

It follows from equation (2.63) that

$$\begin{aligned} C_{D1} &= \int_0^{\pi}\left(\sin^2\theta\frac{\partial p_1}{\partial\theta} - 2\sin\theta\frac{\partial^2\psi}{\partial r^2}\right)\Big|_{r=1} d\theta \\ &= -\int_0^{\pi}\left[3\sin^2\theta + 2\sum_{n=2}^{\infty}(3n-5)(n+1)B_n C_n^{-\frac{1}{2}}(\cos\theta)\right]\sin\theta d\theta \\ &= -4 - 4B_2, \end{aligned} \tag{3.7}$$

where we have used the relations

$$\int_0^{\pi} C_n^{-\frac{1}{2}}(\cos\theta)\sin\theta\, d\theta = \begin{cases} 2 & \text{if } n = 0, \\ \frac{2}{3} & \text{if } n = 2, \\ 0 & \text{otherwise.} \end{cases} \tag{3.8}$$

This implies

$$B_2 = -\frac{C_{D1}}{4} - 1,$$

and substituting this into equation (3.6), gives

$$\psi = \frac{1}{2}r^2\sin^2\theta + \frac{C_{D1}}{8}r\sin^2\theta + \cdots, \qquad \text{as} \quad r \to \infty, \tag{3.9}$$

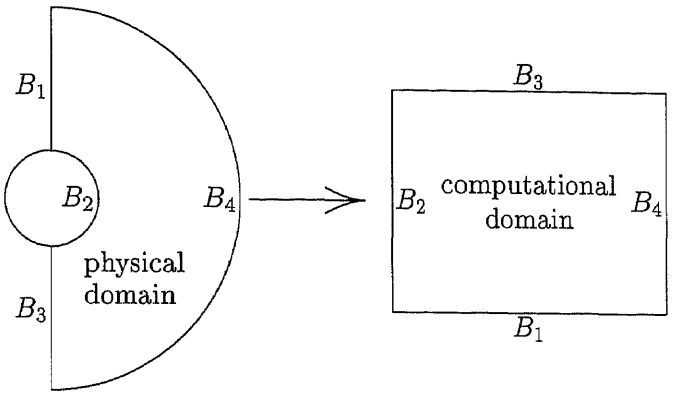

Figure 3.2 Domain transformation schematic.

for creeping flow, where C_{D1} is the total drag on the particle non-dimensionalized by $\pi\mu Ua$, with μ being the viscosity. We found that the drag on the particle is about 6% higher, if we apply the uniform stream condition directly at $r = r_\infty$, as opposed to using the correction term.

Since the solutions are axisymmetric, we will solve the problem on half of the domain. Discretizing the equations directly on the physical domain would give an expanding mesh as r increases. To avoid this problem we use the following transformation,

$$x = \frac{\ln r}{\ln r_\infty}, \qquad y = \frac{\theta}{\pi}, \tag{3.10}$$

which transforms the physical domain (r, θ) onto a unit square (x, y) as shown in Figure 3.2.

3.2.3 Accuracy - Code Validation

To check the code, we consider special cases for which analytical solutions exist. We found that there are two problems that can be solved analytically when there is no

flow—one takes the particle as an infinite sink ($C = 0$ on the surface), while the other is $k \ll 1$ (small bulk concentration). The solutions are (see Appendix A for more details)

$$C = 1 - \frac{1}{r} + \frac{1}{r}\,\mathrm{erf}\left(\frac{r-1}{2\sqrt{t\mathrm{Pe}}}\right)$$

for the former, and

$$C = 1 - \frac{1}{\pi r}\int_0^\infty \frac{\chi\sqrt{y}\cos[\sqrt{y}(r-1)] + (\chi - y)\sin[\sqrt{y}(r-1)]}{(\chi-y)^2 + \chi^2 y} e^{-yt\mathrm{Pe}}\,dy$$

for the latter.

We compared the numerical and analytical results for these two special cases and found the agreement between solutions to be excellent for large t.

As an additional accuracy test of the numerics, we developed an analytical solution for the drag C_{D1} for the full problem when $k \ll 1$ and $\mathrm{Pe} = O(k)$. We found that the drag C_{D1} is given by (see Appendix B for details)

$$C_{D1} = -4 - \frac{2Q\mathrm{Ma}}{3\chi}k^2 + \frac{4Q\mathrm{Ma}}{3\chi}k^3 + \cdots \quad ,$$

where $\mathrm{Pe} = Qk$, with Q being a constant. We found that the difference between the analytical and numerical solutions was less than 0.5%.

Finally, we also computed the nondimensional steady surfactant mass transfer, the Nusselt number which is defined as

$$\mathrm{Nu} = \int_0^\pi \left.\frac{\partial C}{\partial r}\right|_{r=1} \sin\theta\, d\theta, \tag{3.11}$$

for a spherical bubble rising in creeping flow as an infinite sink ($C_s = 0$) with order one Peclet numbers ($\mathrm{Pe} = 3, 10, 40, 70$), and found excellent agreement with Masliyah and Epstein's [Masliyah & Epstein (1971)] numerical data for the Nusselt number (their mean Nusselt number).

3.3 Results

The results were computed on a 50×50 grid. The radial distance is truncated at $r_\infty = 20$, and the time steps were about 2×10^{-2} for most calculations. However, for high surfactant concentration, since the diffusion is much faster than surfactant convection along the surface, equation (2.59) becomes stiff and the time step has to be reduced accordingly (see [Peyret & Taylor (1983)] for more details). The criterion of convergence for the results is $\text{Max}|\psi_{n+100} - \psi_n| < 10^{-6}$, with n being nth time step. We checked a few results on a 100×100 grid and found that the difference of the results between the two grids is less than 0.3%. A few results are calculated for $r_\infty = 30$ and $r_\infty = 40$, the difference on drags for different r_∞ (20, 30, 40) is less than 0.05%.

To illustrate remobilization, we consider results from a computation which varies the bulk concentration k and Peclet number Pe about a reference case having $\text{Ma} = 5$ and $\chi = 1$, with $\theta = 0$ being the leading edge and $\theta = \pi$ being the trailing edge. We will present plots of the drag, surface concentration distribution and surface velocity profile, as well as contours of bulk concentration to show that the bubble motion can be controlled by bulk concentration. All results shown below are in dimensionless form as outlined in Section 2.4.

3.3.1 Surface Concentration Distribution

Surfactant adsorbs onto the particle surface at the leading edge, is convected to the trailing edge by the surface flow, and then diffuses into the bulk as the particle migrates in the fluid. The adsorption of surfactant onto the liquid interface develops a gradient of surfactant on the surface. In Figure 3.3, we plot the surface concentration distribution as a function of θ for $\text{Pe} = 10$ and various bulk concentration

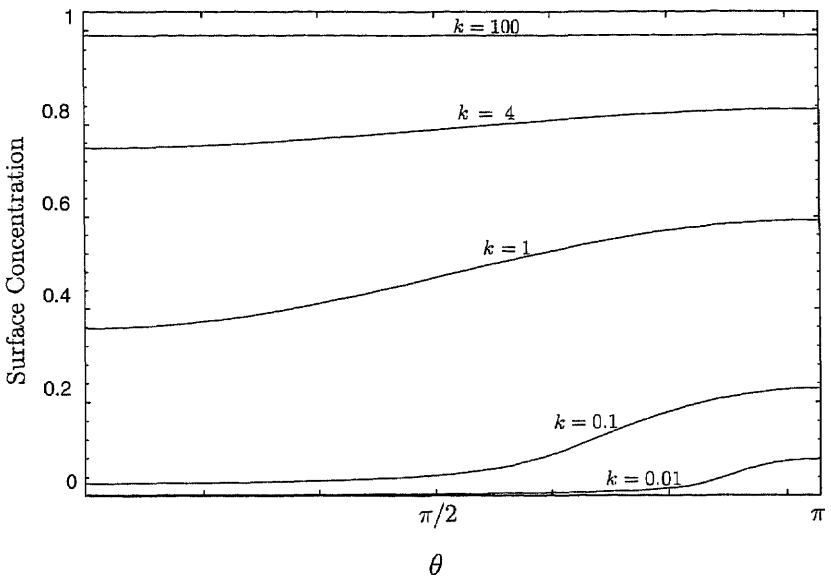

Figure 3.3 The surface concentration distribution, for Pe = 10, Ma = 5 and $\chi = 1$, and $k = k_a C_\infty$ is the measurement of bulk concentration.

values, k. The Figure shows that for any k (bulk concentration), the surface concentration at the trailing edge is higher than that at the leading edge. It is evident that, when the bulk concentration is very small ($k = 0.01$), not only is the amount of surfactant absorbed onto the surface very small, but also the surface concentration gradient is only in a very small region near the rear stagnation point. When the bulk concentration increases to about $k = 1$, the amount of surfactant absorbed onto the surface increases and a surface concentration gradient develops on the entire sphere. And as we increase the bulk concentration further to $k = 100$, the amount of surfactant adsorbed onto the surface is much larger, but more importantly, the distribution of surfactant on the surface is almost uniform (the bubble surface has been remobilized). This argument readily follows from the surface concentration conservation equation (2.59) and equation of equilibrium between the surface concentration and the sublayer (2.60). When k is small, the ratio $\frac{\chi k}{\mathrm{Pe}}$ is small, so the diffusional flux

to the bulk is small compared to the convection on the surface, which is clear from equation (2.59). Surfactant accumulate at the back end. On the other hand, from equation (2.60), the amount of surfactant adsorbed onto the surface is small when k is small. Hence a surface concentration gradient develops only in a small region at the back end. As k increases, although the ratio $\frac{\chi k}{\mathrm{Pe}}$ increases, the amount of surfactant adsorbed onto the surface increases and a surface concentration gradient develops on a larger region at the back end. As k increases further, the amount of surfactant adsorbed onto the surface is large. But the diffusional flux is large compared to the convection on the surface and surfactant does not accumulate at the back end. The surface concentration gradient disappears.

We now observe some implications of our numerical results for the existence of the stagnant cap at the rear stagnation point as first observed by [Savic (1953)]. For large Peclet numbers, when the ratio $\frac{k\chi}{\mathrm{Pe}}$ is small, the convection on the surface is much larger than the diffusion to the bulk, (this is clear from equation (2.59)), and surfactant accumulate at the back end to form a stagnant cap. This phenomenon is supported in the surface concentration distributions given above for $k = 0.01$; the front end is free of surfactant, while a sharp surface concentration gradient develops in a small region near the rear stagnation point. When $\mathrm{Pe} \gg 1$, the cap size increases as k increases, and eventually the cap covers the entire surface as [Edge & Grant (1972)], [Barton & Subramanian (1989)] and [Bel Fdhila & Duineveld (1996)] observed. Since the stagnant cap acts like a solid boundary, the flow may separate at the back end at order one Reynolds number. Flow separation and its effect on terminal velocities for different bulk concentrations and order one Reynolds numbers is considered in Chapter 4.

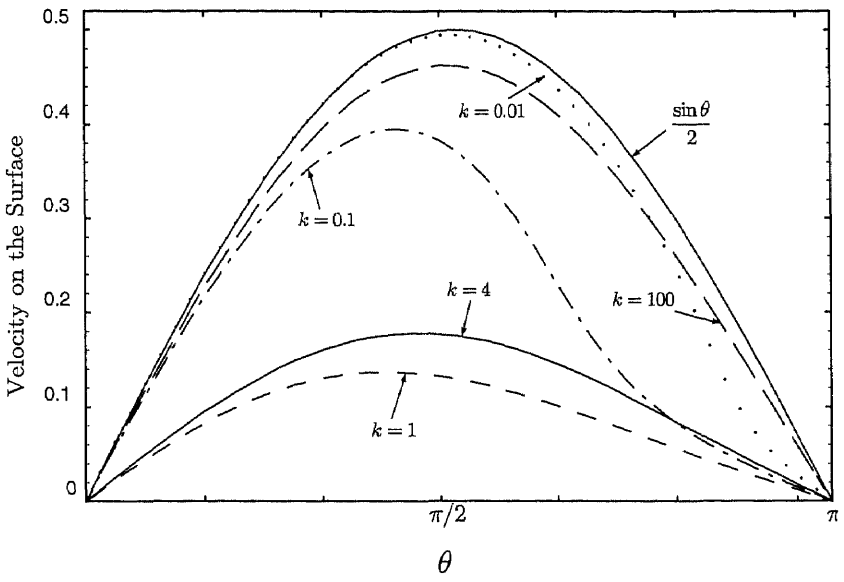

Figure 3.4 Surface velocity, for Pe = 10, Ma = 5 and $\chi = 1$, and $k = k_a C_\infty$ is the measurement of bulk concentration.

3.3.2 Surface Velocity

As a surface concentration gradient develops, a surface tension gradient is set up that creates a Marangoni force opposing the surface flow and hence reduces the surface velocity. But, as shown in Figure 3.3, the surface concentration becomes uniform as k increases for a fixed Peclet number. The increase of surface velocity as the bubble surface remobilizes is evident in Figure 3.4 which plots the surface velocity as a function of tangential angle θ and bulk concentration k with the same values of Marangoni number Ma, Peclet number pe and χ as in Figure 3.3. Note that for a clean interface, the surface velocity is equal to $\frac{\sin\theta}{2}$, so at any point on the surface the velocity cannot be larger than $\frac{\sin\theta}{2}$ for any k. That is exactly what is shown in Figure 3.4. When the bulk concentration is small, the surface velocity is the same as that for the clean surface near the leading edge ($\theta = 0$), but it is smaller near the rear stagnant point ($\theta = \pi$) which corresponds to the surface concentration gradient

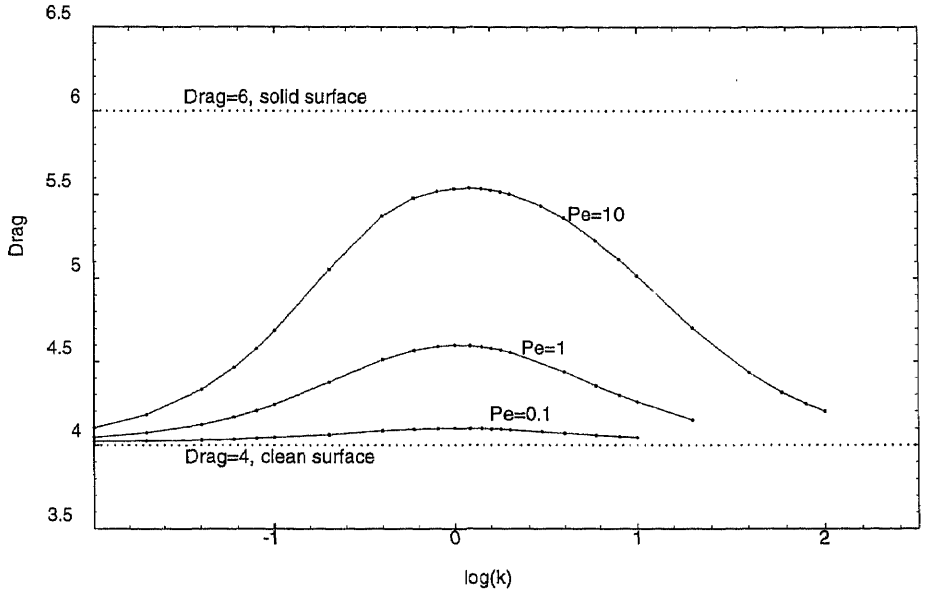

Figure 3.5 The effect of concentration on the drag, for Ma = 5 and $\chi = 1$, and $k = k_a C_\infty$ is the measurement of bulk concentration. The dots are the actual points calculated

in Figure 3.3. As k increases, the surface velocity decreases from the clean value $\frac{\sin\theta}{2}$ at first. This is the retardation, that as we noted in the Introduction, has been well documented in the literature. However as k increases further, the velocity increases and at $k = 100$ the velocity profile is very close to that for clean surfaces. This is because for $k = 100$, the surfactant diffusion at the back end is large compared to the surfactant convection along the surface, and the surface concentration gradient tends to zero. Hence, the surface tension gradient disappears, and the Marangoni force tends to zero. The bubble interface has been remobilized.

3.3.3 Total Drag on the Bubble

The effect of bulk concentration on the terminal velocity is examined in Figure 3.5 by inspecting the way in which the drag on the bubble is affected by the bulk surfactant concentration. The dots on the drag profile are the actual points calculated. Three

different Peclet numbers are used (Pe = 0.1, 1.0, and 10.0). We found that, for a fixed Peclet number, as we vary the bulk concentration k from 0.01 to 100, the drag increases monotonically as a function of concentration when the concentration is small (corresponding to the decrease in the interfacial mobility observed in Figure 3.3), but decreases to the clean surface case when the concentration gets large as the interface remobilizes. With concentration fixed, the drag increases as the Peclet number increases. The larger the Peclet number, the larger the concentration needed to bring the drag down to the clean surface case, as shown in Figure 3.5. Note that the drag always lies between the values $Drag = 4$ (drag for a clean bubble) and $Drag = 6$ (drag for a solid sphere).

3.3.4 Bulk Concentration Distribution

As the bulk surfactant concentration increases and the surface surfactant concentration becomes more uniform, the sublayer concentration (in equilibrium with the surface concentration) also becomes more uniform. In Figure 3.6, we give contours of bulk surfactant concentration for Pe = 10 with varying k. For $k = 0.1$, the concentration near the leading edge is much smaller than that near the trailing edge, and the sublayer concentration at the front end is almost uniform. As k increase to 1, although the difference in concentration near the back end and the front end is smaller than that for $k = 0.1$, the sublayer concentration varies along the whole surface. The tendency towards a more uniform concentration with increasing k is clearly evidenced. At $k = 100$, the concentration in the bulk approaches unity as the diffusion driving force disappears; the sublayer concentration also approaches one. It is clear that as the interface remobilizes and the bulk concentration becomes uniform.

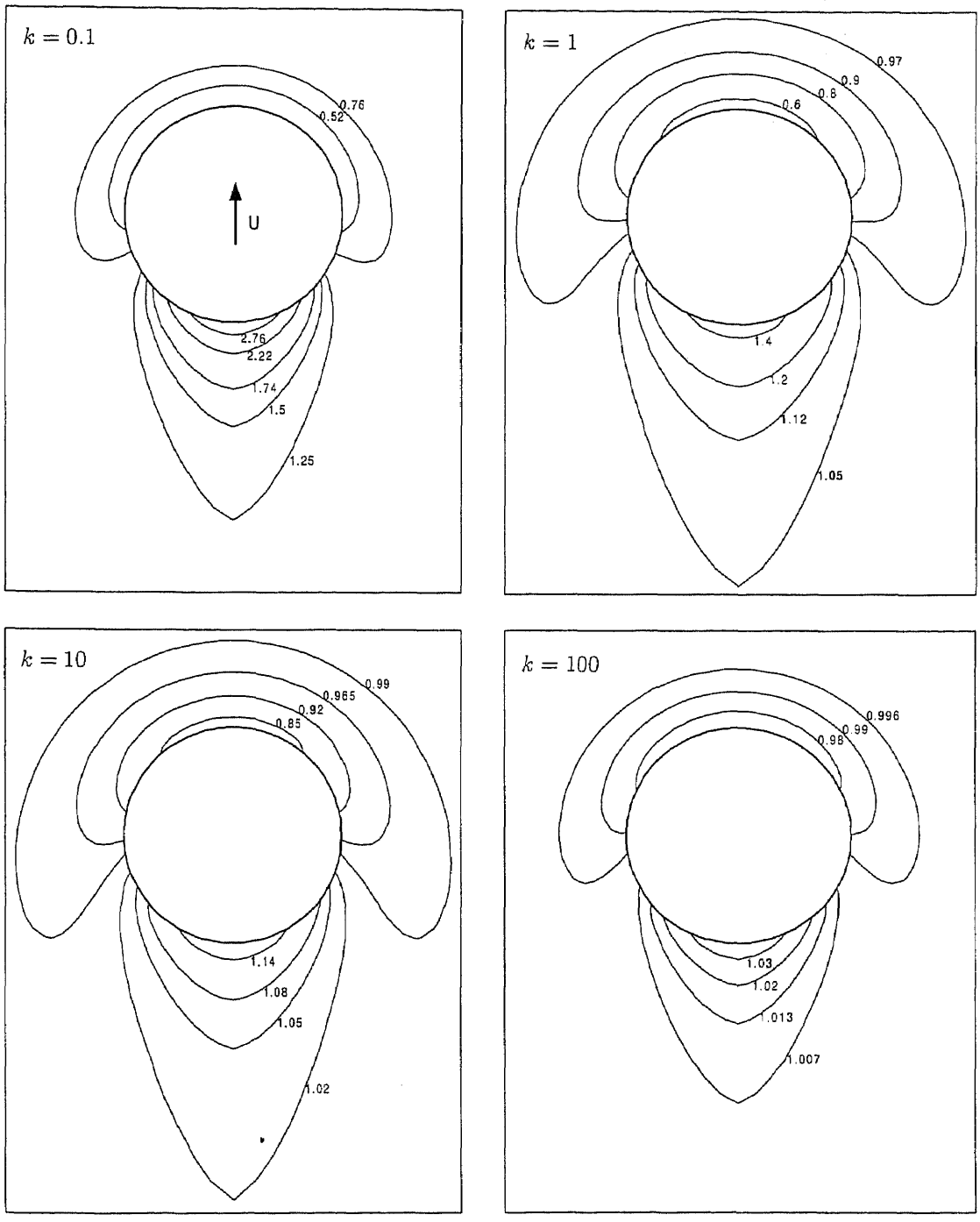

Figure 3.6 Contour of concentration for Pe = 10, Ma = 5 and $\chi = 1$. $k = k_a C_\infty$ is the measurement of bulk concentration and U is the terminal velocity

3.4 Conclusion and Discussion

In the previous section, we have given numerical solutions which show that the bubble interface can be remobilized by controlling the bulk concentration. The ratio of bulk diffusion to convection $\frac{k\chi}{\mathrm{Pe}}$ plays a very important role in this problem. For a fixed Peclet number, when the ratio $\frac{k\chi}{\mathrm{Pe}} \ll 1$, the total amount of surfactant adsorbed onto the surface is very small according to equation (2.60) since the bulk concentration k is small. Although a stagnant cap may develop near the rear stagnation point ($\theta = \pi$), the cap size should be very small. The Marangoni force is small and so is the retardation on the bubble motion. When $\frac{k\chi}{\mathrm{Pe}} = O(1)$, a surface concentration gradient develops on the entire surface, the Marangoni force reaches a maximum and the bubble terminal velocity reduces to a minimum. At $\frac{k\chi}{\mathrm{Pe}} \gg 1$, although the total amount of surfactant adsorbed onto the surface is large, the surface concentration becomes uniform (we say the bubble interface remobilizes). Since the diffusion to the bulk is much larger than the convection on the surface (as can be seen from equation (2.59)), surfactant will not accumulate at the back end as we showed in Figure 3.3. Hence the Marangoni force disappears and the bubble regains the velocity it would have with a clean surface. The larger the Peclet number is the larger the bulk concentration needed to remobilize the bubble interface as shown in Figure 3.5. For fixed bulk surfactant concentration, the drag increases as the Peclet number increases.

Thus, we have shown numerically, how to control the motion of a bubble rising in a fluid containing surfactant, for low Reynolds numbers and buoyancy driven motion. Similar results are expected for fluid-fluid particles, order one Reynolds numbers and thermocapillary migration. The case of order one Reynolds numbers is considered next.

CHAPTER 4

SURFACTANT EFFECTS ON BUBBLE MOTION AT ORDER ONE REYNOLDS NUMBERS

4.1 Introduction

A numerical study of the flow around a spherical bubble rising steadily in a surfactant solution at order one Reynolds numbers ($0.5 \sim 50$) with relatively large Peclet numbers (100, 200) is presented, where the Reynolds number and Peclet number are defined in Section 2.4 in Chapter 2. When a bubble rises through a fluid phase containing surfactant, the fluid motion near its surface can be slowed down or even stopped. At large Peclet number, surfactant accumulate near the back end of the bubble and make the surface there act like rigid boundary. Wakes can form at order one Reynolds number as shown schematically in Figure 4.1, which drastically decrease the surface velocity and hence increases the drag. The mechanism of this retardation is discussed in detail in Chapter 1.

Various studies have been carried out concerning the effect of surfactant on bubble motion. As we described in Section 1.1 of Chapter 1, most of the works are focused on trace amounts of surfactant (small concentration) or slightly soluble surfactant, and in addition, low Reynolds numbers. [Edge & Grant (1972)] and [Bel Fdhila & Duineveld (1996)] demonstrated experimentally the retardation by the intentional addition of surfactant for buoyancy driven motion at order one Reynolds numbers. Edge & Grant observed that the velocity of drops falling through contaminated water decreases with increasing bulk concentration. They found that wakes form at larger concentration, similar to the wakes behind solid spheres, the fluid inside the drops being stagnant. Duineveld examined the retardation effect on rising bubbles. He found that there exists a critical concentration

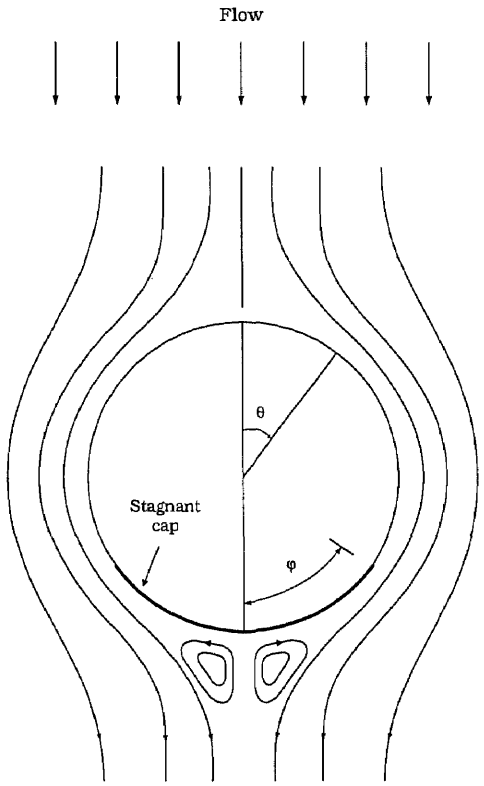

Figure 4.1 Flow around bubble at order one Reynolds number

above which the bubble velocity rapidly decreases to that of a solid sphere. It is also found that the critical concentration increases as the bubble radius increases. [Barton & Subramanian (1989)] carried out similar experiments for thermocapillary driven motion. [Bel Fdhila & Duineveld (1996)] have extended the approach of [Sadhal & Johnson (1983)] to finite Reynolds numbers by solving the Navier-Stokes equations numerically subject to the stagnant cap boundary condition described in Section 5.2 in the next chapter. Leppinen, Renksizbulut & Haywood (1996a,b) investigated the effect of an insoluble surfactant on the flow around and inside a deforming drop surrounded by air. For that purpose they couple the Navier-Stokes equations in both phases to the surface concentration balance, assuming a high surface diffusivity and a linear dependence of surface tension on surfactant concentration. When the droplet is maintained spherical, they find a weak overall

effect of the contamination on the drag because the tangential velocity at the droplet surface is small even in the absence of surfactant, owing to the low viscosity of the surrounding fluid. In contrast, when the droplet is allowed to deform, a significant increase of the amplitude of shape oscillations is observed when contamination is present. The work of [McLaughlin (1997)] considers the effect of an insoluble surfactant on the flow around a deforming bubble rising steadily in water at high Reynolds number. In that work the Navier-Stokes equation are solved around the bubble under the assumptions of the stagnant cap model. By successive adjustments of the cap angle the computations are able to reproduce properly the rise velocities measured by [Haberman & Morton (1954)] in tap water and by [Bel Fdhila & Duineveld (1996)] in a dilute solution of Triton-X100. The most recent study to date is by [Cuenot, Magnaudet & Spennato (1997)] of the buoyancy driven motion of a spherical bubble at order one Reynolds number. They solved the Navier-Stokes equations together with the convection-diffusion equation for nonlinear interfacial boundary conditions at large Peclet number ($\sim 10^5$) and small bulk concentration (large surface convection compared to the bulk diffusion). Their numerical results illustrate a cap at the back end, and confirm the formation of a wake at order one Reynolds numbers as noted by [Bel Fdhila & Duineveld (1996)] and [McLaughlin (1997)].

The aim of this chapter is to illustrate that the retardation of the bubble velocity can be reduced by using bulk concentration for order one Reynolds numbers. In Section 4.3 we present numerical results by plotting surface velocities, surface surfactant concentrations, drag and stream lines for different Peclet numbers (100, 200), and various Reynolds numbers and bulk concentration. The surface concentration distributions for fixed Peclet numbers and different values of bulk concen-

tration given in Section 4.3.1, illustrate that a stagnant cap develops near the rear stagnation point when the bulk concentration is very small, and the bubble surface remobilizes at large bulk concentration. The formation of wakes in the stagnant cap regime for order one Reynolds numbers is discussed in Section 4.3.3 where it is also show that wakes disappear as the bubble remobilizes. The larger the Peclet number is, the larger the concentration needed to remove the wake. Surface velocity profiles show that the surface velocity becomes negative at the stagnant cap region when there are wakes behind the bubble. The velocity increases with increasing bulk concentration for larger concentration, and the drag decreases with increasing bulk concentration.

4.2 Mathematical Model and Algorithm

Consider a spherical, buoyancy driven gas bubble rising steadily in an infinite Newtonian fluid containing surface active surfactant, at order one Reynolds numbers with bulk diffusion controlled surfactant transport characterized by order one or large Peclet number. We assume that the fluid is incompressible, the flow is uniform at infinity, the surfactant concentration far from the bubble surface is uniform, and there is no interfacial deformation thus keeping the bubble spherical. The mathematical model and the relevant boundary conditions were given in Chapter 2. We examine the problem in nondimensional form by addressing numerically equations (2.46)-(2.48) with the corresponding boundary conditions (2.51)-(2.60). The numerical method and algorithm are described in Section 3.2.

The results were computed on a 50×50 grid and the radial distance is truncated at $r_\infty = 20$. The time steps were about 2×10^{-2} for most calculations. However, for high surfactant concentration, since the diffusion is much faster than surfactant

convection along the surface, equation (2.59) becomes stiff and the time step has to be reduced accordingly (see [Peyret & Taylor (1983)] for more details). The criteria of convergence for the results is $\text{Max}|\psi_{n+100} - \psi_n| < 10^{-6}$, with n being nth time step.

The corrected boundary condition (3.9) is no longer valid for order one Reynolds numbers. The boundary condition (2.53) is applied directly on $r = r_\infty$. We calculated a few results for $r_\infty = 30$ with $\text{Re} = 50$. Compare the drag coefficient C_{D2} (nondimensionalized by $\pi a^2 \rho U^2$) to the value for $r_\infty = 20$, we found the drag coefficient is 1.5% higher. We also checked a few results on a 100×100 grid and found that the difference of the results between the two grids is less than 2%.

4.3 Numerical Results

To illustrate remobilization, we consider results from a computation which varies the concentration k and Reynolds number Re about a reference case having $\text{Ma} = 5$, $\chi = 1$ and $\text{Pe} = 100, 200$, with $\theta = 0$ being the leading edge and $\theta = \pi$ being the trailing edge. We will present plots of the drag, surface concentration distribution and surface velocity, as well as steam lines to show that the bubble motion can be controlled by bulk concentration. All results shown below are in dimensionless form as outlined in Section 2.4.

4.3.1 Surface Concentration Distributions

Surfactant adsorbs onto the particle surface at the leading edge, is convected to the trailing edge by the surface flow, and then diffuses into the bulk as the particle migrates in the fluid. The adsorption of surfactant onto the liquid interface develops a gradient of surfactant on the surface. In Figure 4.2, we plot the surface concentration

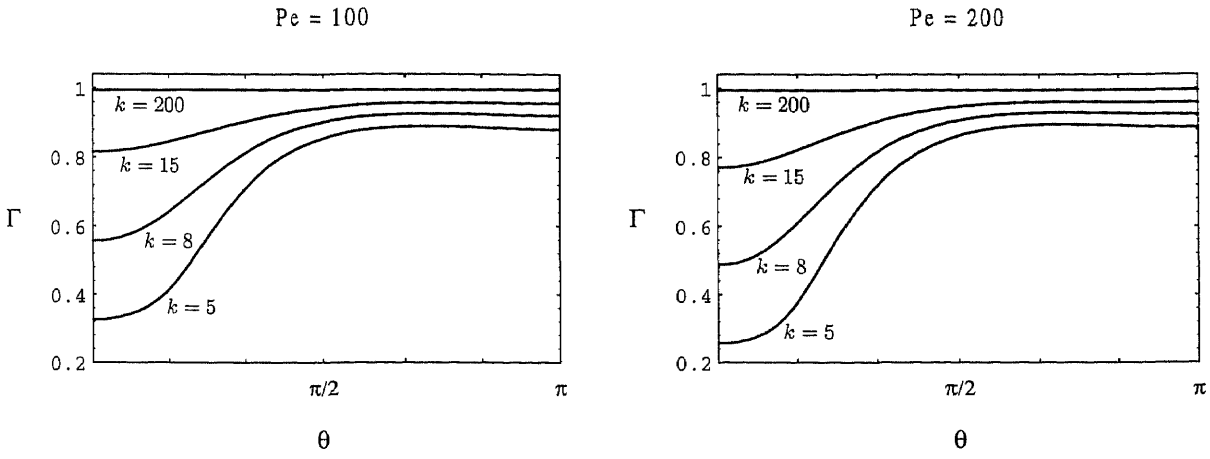

Figure 4.2 The surface concentration distribution, for Re = 50, Ma = 5 and $\chi = 1$, and $k = k_a C_\infty$ is the measurement of bulk concentration.

distribution as a function of θ at various bulk concentration values, k, with Re = 50 and different Peclet numbers, Pe = 100 and Pe = 200. The Figure shows that for any k (bulk concentration), the surface concentration at the trailing edge is higher than that at the leading edge. It is evident that, when the bulk concentration is small ($k = 5$), the surface concentration near the front stagnation point is small and the surfactant distribution is almost uniform in that region, a sharp surface concentration gradient develops in the region near the rear stagnation point and the surface concentration is high in that region. This is the so called stagnant cap regime owing to the fact that the surface convection is much larger than the bulk diffusion when the ratio $\frac{\chi k}{\mathrm{Pe}}$ is small (this is easily seen from equation (2.59)). Surfactant adsorb onto the surface at the front, and are quickly swept to the back by strong surface convection. Since the surface concentration is always in equilibrium with the sublayer concentration, which is expressed in equation (2.60), small bulk diffusion (compared to surface convection) means slow surfactant desorption at the back end. Surfactant accumulate at the back end, and this makes the interface act like rigid boundary there. As k increases, the amount of surfactant adsorbed

onto the surface increases, which follows from the equilibrium relation (2.60). But the surface concentration gradient decreases as k increases. When we increase k to 200, the surface concentration gradient almost disappears (the bubble surface has been remobilized). This is because the ratio $\frac{\chi k}{\mathrm{Pe}}$ increases as k increases, hence the diffusion at the back end balances the surface convection at large k. Comparing the surface concentration distributions for $\mathrm{Pe} = 100$ and $\mathrm{Pe} = 200$, one observes that the larger the Peclet number, the larger the bulk concentration needed to remobilize the interface. Another interesting feature to notice, is the slight decrease in value of the surface concentration near the rear stagnation point, which is caused by a negative surface velocity at the back end as discussed in detail in next Section.

4.3.2 Surface Velocity Distributions

Since surfactant lower the surface tension, a surface concentration gradient causes a surface tension gradient that in turn creates a Marangoni force opposing the surface flow and hence reducing the surface velocity. This retardation is evidenced in Figure 4.3. In figure(A) and figure(B), we plot the surface velocity, v_s, as a function of θ, for the same value of Reynolds number Re, Marangoni number Ma and χ as shown in Figure 4.2, and various bulk concentration values k, for different Peclet numbers ($\mathrm{Pe} = 100, 200$). In both graphs, there are negative velocities when the bulk concentration k is small, which are shown in figure(C) and figure(D), the magnifications near the rear stagnation point of figure(A) and figure(B) respectively. This is because when $\frac{\chi k}{\mathrm{Pe}} \ll 1$, a stagnant cap develops near the rear stagnation point that makes the interface at the back end act like rigid boundary. Reverse flow occurs at order one Reynolds number, which causes a negative velocity near the surface in the vicinity of the stagnant cap region. This negative velocity pushes surfactant on

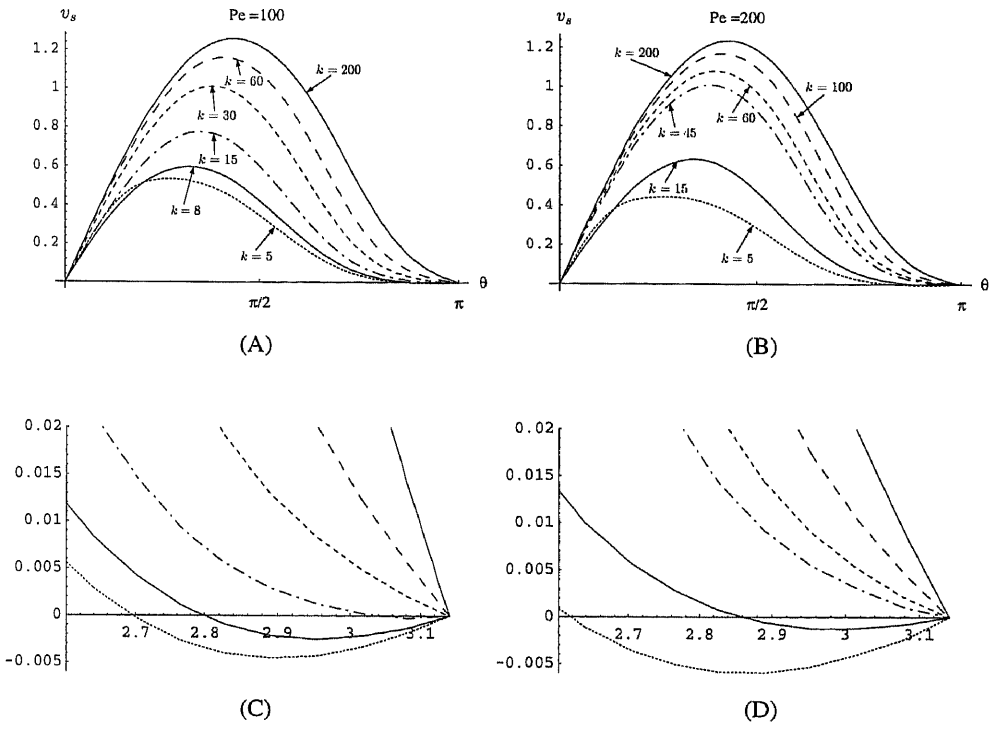

Figure 4.3 Surface velocity, for Re = 50, Ma = 5 and $\chi = 1$, and $k = k_a C_\infty$ is the measurement of bulk concentration.

the surface away from the back stagnation point and so causes a negative velocity on the surface near the back end. This negative velocity also causes a decrease in surface concentration near the rear stagnation point as we observed in Figure 4.2. It is evident from Figure 4.3, that as k increases the velocity increases for a fixed Peclet number, and the velocity profile becomes more symmetric about $\theta = \frac{\pi}{2}$, corresponding to the remobilization in Figure 4.2. Note that, when k increases from the value $k = 5$, the surface velocity near the front stagnation point decreases at the first. The reason is that in the stagnant cap regime, surfactant convect to the back end after adsorbing onto the surface at the front end and very little material is left at the front making the surface concentration gradient there small. As k increases, a larger surface concentration gradient develops near the front end at first as the ratio $\frac{\chi k}{\mathrm{Pe}}$ becomes larger (but not large enough for remobilization).

4.3.3 The Flow Field in the Bulk

When the rate of surface convection is much larger compared to the bulk diffusion ($\frac{\chi k}{\mathrm{Pe}} \ll 1$), surfactant accumulate near the back and the interface there becomes immobile. Wakes form at order one Reynolds numbers ($\mathrm{Re} = Ua/\nu$) as shown in Figure 4.4. The Figure shows the flow around the bubble by plotting the stream lines at steady state for different Reynolds numbers, with Peclet number $\mathrm{Pe} = 100$, $k = 5$ ($k = k_a C_\infty$ is a measure of bulk concentration), Marangoni number $\mathrm{Ma} = 5$ and $\chi = 1$. Wakes first form between Reynolds numbers $\mathrm{Re} = 15$ and $\mathrm{Re} = 20$, which is larger than the value for a solid sphere ($\mathrm{Re} \sim 12.5$), and as expected the recirculation zone expands as the Reynolds number increases. In Figures 4.5 and 4.6, we plot the stream lines around the bubble for Reynolds number $\mathrm{Re} = 50$, Marangoni number $\mathrm{Ma} = 5$ and $\chi = 1$, and Peclet numbers $\mathrm{Pe} = 100$ and 200 respectively. It is evident

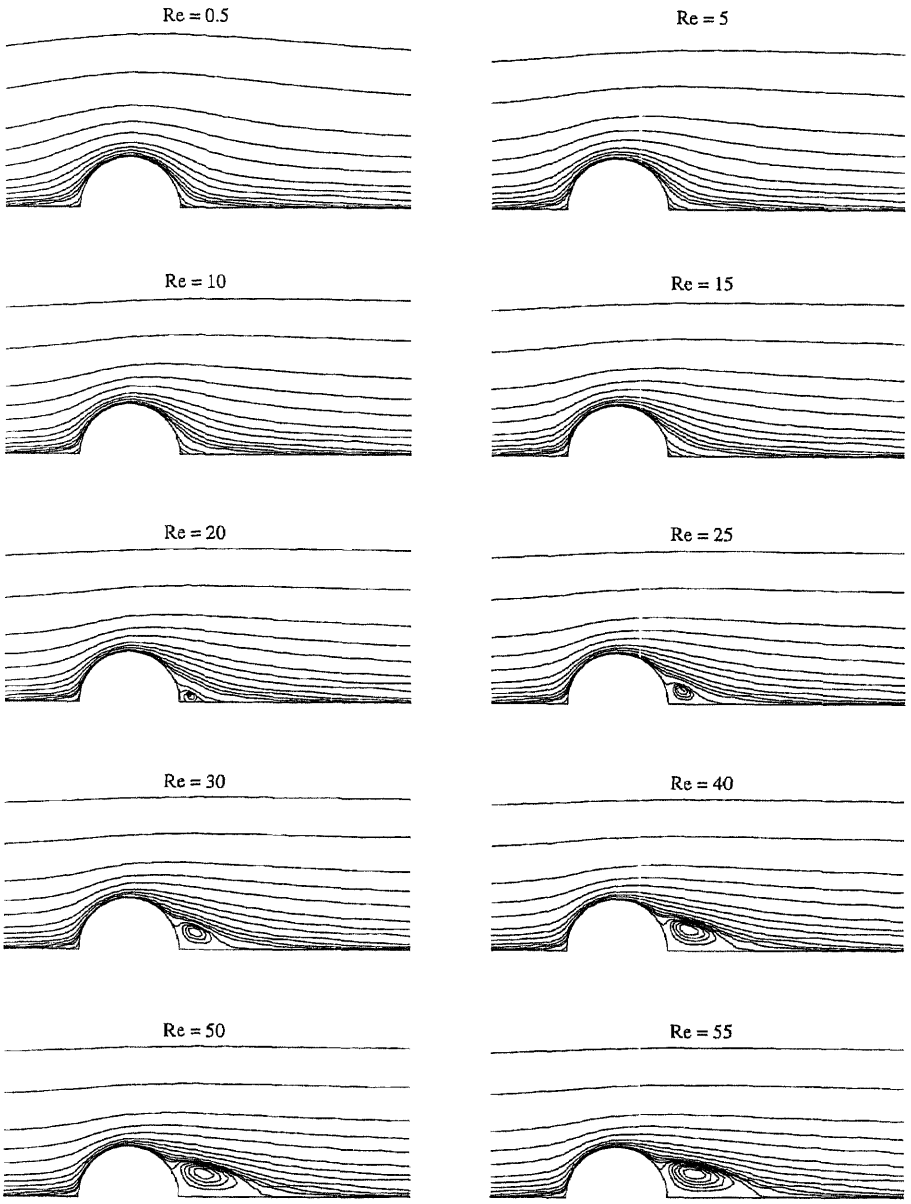

Figure 4.4 Flow around the bubble for Pe = 100, Ma = 5, $\chi = 1$ and $k = 5$.

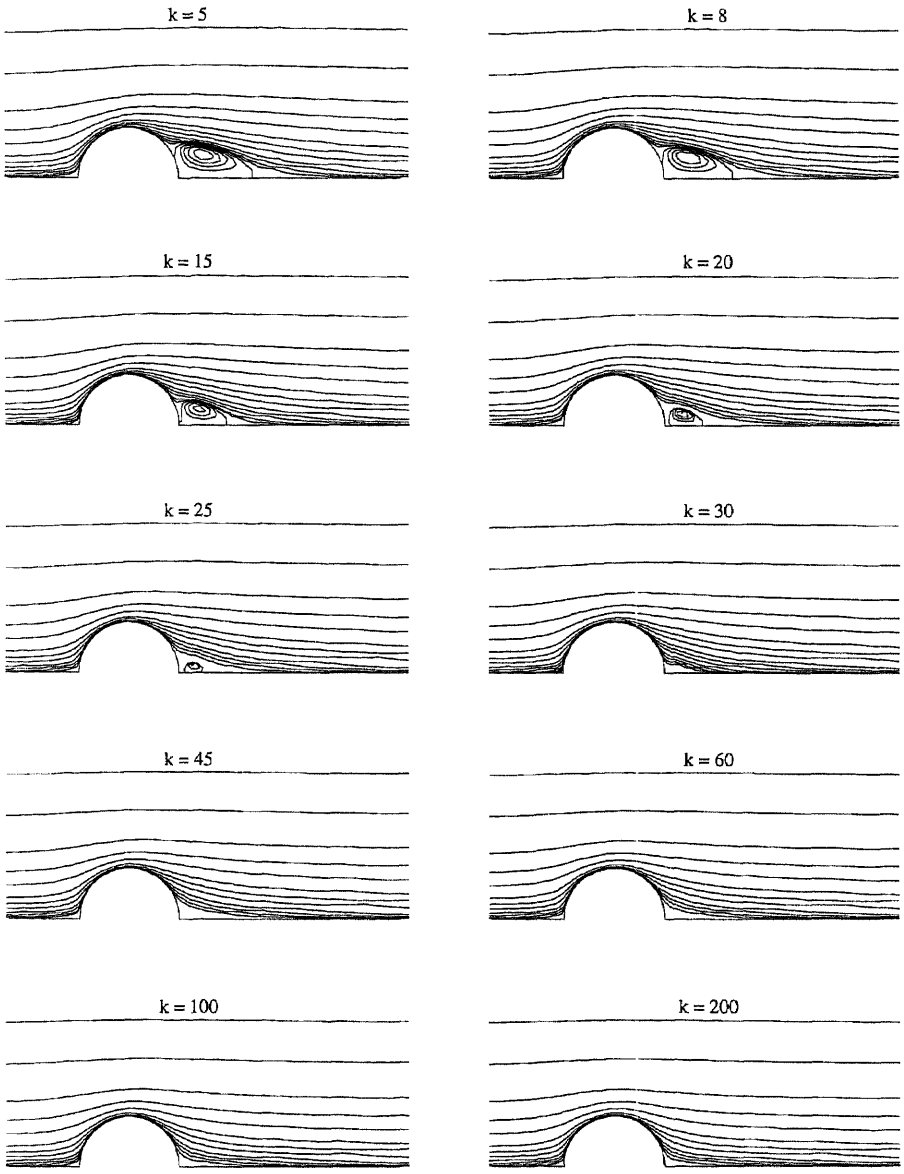

Figure 4.5 Flow around the bubble for Pe = 100, Ma = 5, $\chi = 1$ and Re = 50.

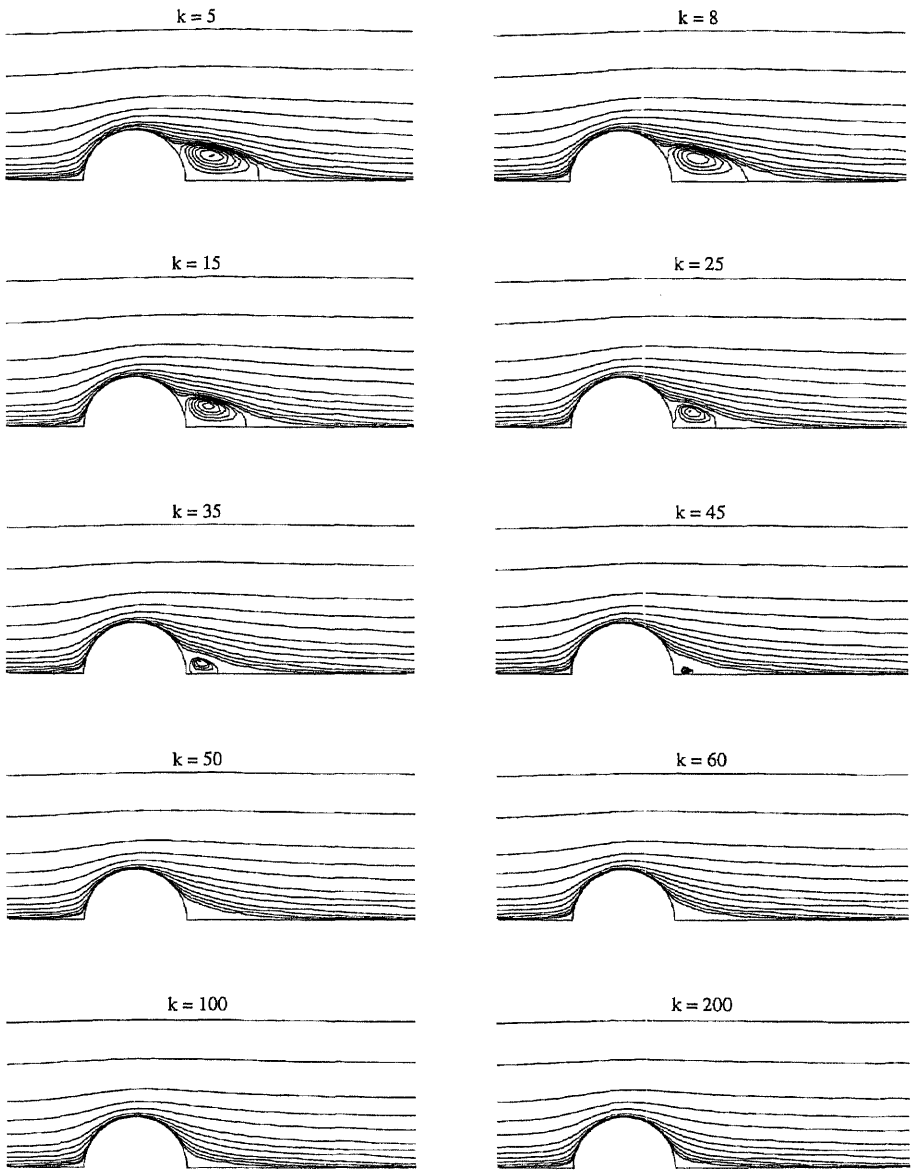

Figure 4.6 Flow around the bubble for Pe = 200, Ma = 5, $\chi = 1$ and Re = 50.

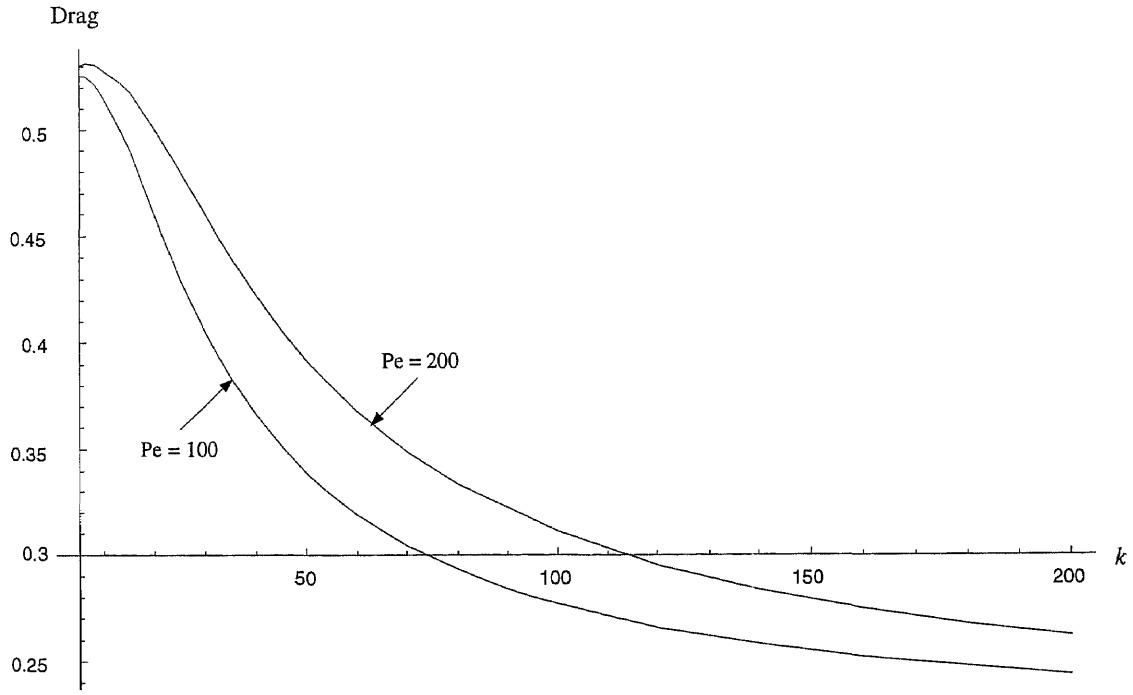

Figure 4.7 The effect of concentration on the drag, for Re = 50, Ma = 5 and $\chi = 1$, and $k = k_a C_\infty$ is the measurement of bulk concentration.

that for a fixed Reynolds number, the recirculating eddies shrink as k increases and disappear altogether at large k. In addition the stream lines become more symmetric about $\theta = \frac{\pi}{2}$ as the surface remobolizes. For the same value of k, the wake is bigger for Pe = 200 than that corresponding to Pe = 100. Wakes disappear between the values of $k = 25$ and 30 for Pe = 100, and between $k = 45$ and 50 for Pe = 200. These results confirm that higher bulk surfactant concentrations are required to remobilize the bubble surface for larger Peclet number.

4.3.4 Total Drag on the Bubble

The effect of bulk concentration k on drag is examined in Figure 4.7. Here we plot the drag coefficient C_{D2} (nondimensionalized by $\pi a^2 \rho U^2$) as a function of bulk concentration (k ranges from 5 to 200), for two different Peclet numbers (Pe =

100, and 200), with Reynolds number Re = 50, Marangoni number Ma = 5 and $\chi = 1$. We found that, for a fixed Peclet number, the drag decreases as the bulk concentration k increases corresponding to the increase of the interfacial mobility observed in Figure 4.2. Since the smallest bulk concentration k we examined in this chapter is 5, the drag is not seen to increase monotonically at first as observed for the zero Reynolds number case in Chapter 3; the monotonic increase takes place as bulk concentrations increase from small values. With the concentration fixed, however, the drag increases as the Peclet number increases in agreement with our low Reynolds number results.

4.4 Conclusion and Discussion

The numerical results we presented in the previous section show that control of bubble migration velocity by using surfactant concentration, is still effective for order one Reynolds numbers. As in the low Reynolds number case, the ratio of bulk diffusion to convection $\frac{\chi k}{\mathrm{Pe}}$ plays a very important role for order one Reynolds numbers. For any order one Peclet number, when the ratio $\frac{\chi k}{\mathrm{Pe}} \ll 1$, surfactant collect near the rear stagnation point ($\theta = \pi$) making the interface there immobile and allowing wakes to form at order one Reynolds numbers. The reverse flow near the surface pushes surfactant away from the rear stagnation point towards front stagnation point, and causes a negative surface velocity near the back end which drastically reduces the migration velocity. As k increases, although the amount of surfactant adsorbed onto the surface increases, the surface concentration gradient decreases since the ratio $\frac{\chi k}{\mathrm{Pe}}$ increases. In turn wakes disappear as the interface near the rear stagnation point becomes more mobile. At $\frac{\chi k}{\mathrm{Pe}} \gg 1$, although the total amount of surfactant adsorbed onto the surface is large, the surface concen-

tration becomes uniform (we say the bubble interface remobilizes) as shown in Figure 4.2. Hence the Marangoni force disappears and the bubble velocity increases with increasing bulk concentration. The larger the Peclet number is the larger the bulk concentration needed to remobilize the bubble interface as shown in Figure 4.7. For fixed bulk surfactant concentration, the drag increases as the Peclet number increases.

We have shown numerically, how to control the motion of a bubble rising in a fluid containing surfactant, for order one Reynolds numbers and buoyancy driven motion. Similar results are expected for fluid-fluid particles and thermocapillary migration.

CHAPTER 5

DIFFUSIVE BOUNDARY LAYER ANALYSIS (Pe $\gg$ 1)

5.1 Introduction

When Pe $\gg$ 1, diffusion into the bulk is very weak and consequently surfactant which adsorbs onto the surface at the leading edge is swept quickly to the rear where it builds up and makes the surface immobile, it acts like a solid. This implies that part of the bubble acts like a liquid surface and part like a solid. [Savic (1953)] was the first to observe this phenomenon. It has since been confirmed experimentally by many researchers: see [Huang & Kintner (1969)], [Griffith (1962)], [Bel Fdhila & Duineveld (1996)], and [McLaughlin (1997)]. Savic also began a theoretical study for the case of spherical drops moving in creeping flow, with negligible interior viscosity and small caps. His numerical results were improved by [Davis & Acrivos (1966)]. By requiring the net flux of surfactant to the surface to be zero at steady state, [Harper (1973)] obtained an asymptotic solution for small cap angles. [Holbrook & Levan (1983a)] assumed a uniformly retarded velocity and obtained an asymptotic solution while [Sadhal & Johnson (1983)] solved the velocity field analytically in terms of an infinite series of Gegenbauer polynomials with constant coefficients as a function of a given cap angle of arbitrary size. The mass transfer rates on the surface and cap were obtained by assuming a linear relation between surface tension variation and surface concentration (this assumption is valid for very low surfactant concentration), resulting in underpredictions. [He, Dagan & Maldarelli (1991b)] obtained a more realistic value for the cap angle by connecting the surface tension variation and surface concentration with a nonlinear equation. However, the convection-diffusion equation

was not solved and the cap angle was connected to the bulk concentration by assuming that no diffusive boundary layer exists around the bubble, i.e. the bulk concentration adjacent to the surface equals the concentration at infinity. [Cuenot, Magnaudet & Spennato (1997)] solved the bulk concentration numerically for a spherical bubble at order one Reynolds number with large surface and bulk Peclet number ($\sim 10^5$) and low bulk concentration. Their numerical results illustrate a cap at the back end, and confirm the formation of a wake at order one Reynolds number as noted by [Edge & Grant (1972)] and [McLaughlin (1997)].

In this chapter, we consider a spherical bubble rising steadily in creeping flow for strong convective surfactant transport (Pe $\gg$ 1). A boundary layer analysis for the bulk concentration is presented. As we described in Chapter 1, a boundary layer develops along the bubble surface when Pe $\gg$ 1. The boundary layer thickness for a solid sphere is of $O(\mathrm{Pe}^{-\frac{1}{3}})$, and for a clean gas bubble is of $O(\mathrm{Pe}^{-\frac{1}{2}})$ (see [Leal (1992)]). In the stagnant cap regime, part of the bubble surface is covered with surfactant and acts as rigid boundary, while the other part is free of surfactant and is completely mobile. When the Peclet number is asymptotically large, a boundary layer develops along the bubble surface, but with different thickness along the stagnation cap region and along the clean part surface as shown in Figure 5.1. The governing equations and the stagnant cap boundary conditions are given in Section 5.2. The leading order solution for the velocity field is given in Section 5.3. In Section 5.4.2.1 we derive the leading order boundary layer equation valid in the stagnant cap region, and show that the boundary layer thickness is of $\mathrm{O}(\mathrm{Pe}^{-\frac{1}{3}})$, which is the same as for a solid sphere. In Section 5.4.2.2 we derive the leading order boundary layer equation along the clean part of the surface, and show that the boundary layer thickness is of $\mathrm{O}(\mathrm{Pe}^{-\frac{7}{15}})$, which is larger than that for a clean

surface bubble. The size of the clean part surface is found to be of $O(Pe^{-\frac{1}{15}})$. A boundary layer analysis is given in Section 5.4.3.

5.2 Stagnant Cap Model

We examine the problem in dimensionless form with the scaling groups given in Section 2.4 in Chapter 2. For simplicity, we write $\epsilon = \dfrac{1}{Pe}$ through this chapter. The stream-function for axisymmetric creeping flow satisfies the partial differential equation

$$E^4\psi = 0, \tag{5.1}$$

and the steady state convection-diffusion equation is given by

$$\boldsymbol{u} \cdot \nabla C = \epsilon \nabla^2 C, \tag{5.2}$$

subject to the boundary conditions (2.51) - (2.60), where E is given by equation (2.50) in Section 2.4 and $\epsilon \ll 1$.

When $Pe \gg 1$, the boundary condition (2.59) reduces to, at the leading order,

$$\frac{\partial}{\partial \theta}(u_\theta \Gamma \sin\theta) = 0. \tag{5.3}$$

Integrating the above equation gives (see [Sadhal & Johnson (1983)] for more detail)

$$u_\theta \Gamma = 0. \tag{5.4}$$

This implies that to leading order the interface at the stagnant cap acts as solid surface and the interface elsewhere on the bubble is clean of surfactant. i.e.

$$\Gamma = 0 \qquad 0 < \theta < \pi - \varphi, \tag{5.5}$$

$$u_\theta = 0 \qquad \pi - \varphi < \theta < \pi. \tag{5.6}$$

The relation (2.23) between shear stress and Marangoni force on the surface in dimensionless form is given by

$$\tau_{r\theta} = \frac{\mathrm{Ma}}{1-\Gamma}\frac{\partial \Gamma}{\partial \theta}, \tag{5.7}$$

where $\tau_{r\theta}$ is nondimensionalized by $\frac{\mu U}{a}$. It follows, by substitution of equation (5.5) into equation (5.7), that the interface on the clean part of the bubble surface is stress free. This together with the zero tangential velocity condition on the stagnant cap leads to the mixed boundary conditions for the stream-function on the surface

$$\left.\frac{\partial^2 \psi}{\partial r^2} - 2\frac{\partial \psi}{\partial r}\right|_{r=1} = 0, \qquad 0 < \theta < \pi - \varphi. \tag{5.8}$$

$$\left.\frac{\partial \psi}{\partial r}\right|_{r=1} = 0, \qquad \pi - \varphi < \theta < \pi. \tag{5.9}$$

Note that the cap angle φ is unknown and must be determined as part of the solution.

5.3 Fluid Field

We assume an asymptotic expansion for the stream function ψ in the form

$$\psi = \psi_0 + \sum_{n=1}^{\infty} F_n(\epsilon)\psi_n, \tag{5.10}$$

where $F_{n+1}(\epsilon) \ll F_n(\epsilon)$ for all n. Then the first order stream function obeys the partial differential equation (5.1), and satisfies the boundary conditions (2.51)-(2.53), (5.8) and (5.9). As we showed in Section 3.2.2 in Chapter 3, a general solution which satisfies the boundary conditions (2.51)-(2.53) is of the form

$$\psi_0 = \frac{1}{2}(r^2 - r)\sin^2\theta + \sum_{n=2}^{\infty} B_n(r^{-n+1} - r^{-n+3})C_n^{-\frac{1}{2}}(\cos\theta), \tag{5.11}$$

where $C_n^{-\frac{1}{2}}(x)$ are the Gegenbauer polynomials of degree $-\frac{1}{2}$.

Applying the boundary conditions (5.8) and (5.9) to the solution (5.11), we have the following dual series equations (there arise due to the mixed boundary conditions),

$$\begin{cases} \sum_{n=2}^{\infty}(2n-1)B_n C_n^{-\frac{1}{2}}(\cos\theta) = 0 & 0 < \theta < \pi - \varphi, \\ \sum_{n=2}^{\infty} B_n C_n^{-\frac{1}{2}}(\cos\theta) = \frac{1}{4}\sin^2\theta & \pi - \varphi < \theta < \pi. \end{cases} \tag{5.12}$$

Using the properties of $C_n^{-\frac{1}{2}}$ we express above dual series in terms of P_n^{-1} as follows,

$$\begin{cases} \sum_{n=0}^{\infty}(2n+3)B_{n+2}P_{n+1}^{-1}(\cos\theta) = 0 & 0 < \theta < \pi - \varphi, \\ \sum_{n=0}^{\infty} B_{n+2}P_{n+1}^{-1}(\cos\theta) = -\frac{1}{4}\sin\theta, & \pi - \varphi < \theta < \pi \end{cases} \tag{5.13}$$

where $P_n^{-1}(x)$ are the Associated Legendre polynomials with order -1 and their relation to the Gegenbauer polynomials $C_n^{-\frac{1}{2}}(x)$ is given in equation (C.11) in Appendix C.

[Sadhal & Johnson (1983)] solved the dual series by using the method introduced by [Collins (1961)], by expressing the velocities in terms of infinite series of Gegenbauer polynomials with constant coefficients as a function of given cap angle. The convection-diffusion equation was not solved and the cap angle was connected to the bulk concentration by assuming that no diffusive boundary layer exists around the bubble. Here, we will solve the convection-diffusion equation by carrying out a proper boundary layer analysis. To do so, we need to find both the velocity and the shear stress in closed form on the whole surface.

5.3.1 Shear Stress on the Surface

To find the shear stress on the surface, we define

$$h(\theta) = \sum_{n=0}^{\infty}(2n+3)B_{n+2}P_{n+1}^{-1}(\cos\theta) \qquad \pi - \varphi < \theta < \pi. \tag{5.14}$$

This is the value of the first series in (5.13) extended to the whole surface. Then,

$$\sum_{n=0}^{\infty}(2n+3)B_{n+2}P_{n+1}^{-1}(\cos\theta) = \begin{cases} 0 & 0 < \theta < \pi - \varphi, \\ h(\theta) & \pi - \varphi < \theta < \pi. \end{cases} \tag{5.15}$$

Applying the relation C.15 and the orthogonal property C.19 to equation (5.15), it follows that

$$B_{n+2} = -\frac{1}{2}\int_{\pi-\varphi}^{\pi} h(\zeta)P_{n+1}^{1}(\cos\zeta)\sin\zeta\, d\zeta, \tag{5.16}$$

where $P_n^1(x)$ are the associated Legendre polynomials with order 1. Substituting this expression into the second part of dual series equations (5.13), we have

$$\sum_{n=0}^{\infty}\left[P_{n+1}^{-1}(\cos\theta)\int_{\pi-\varphi}^{\pi} h(\zeta)P_{n+1}^{1}(\cos\zeta)\sin\zeta\, d\zeta\right] = \frac{1}{2}\sin\theta \quad (\pi - \varphi < \theta < \pi).$$

If we now interchange the order of summation and integration of the above equation we obtain

$$\int_{\pi-\varphi}^{\pi} h(\zeta)S(\theta,\zeta)\sin\zeta\, d\zeta = \frac{1}{2}\sin\theta \qquad (\pi - \varphi < \theta < \pi), \tag{5.17}$$

where

$$S(\theta,\zeta) = \sum_{n=0}^{\infty} P_{n+1}^{-1}(\cos\theta)P_{n+1}^{1}(\cos\theta). \tag{5.18}$$

To sum $S(\theta,\zeta)$ we use the following theorem for Legendre polynomials:

$$\begin{aligned} P_l(\cos w) &= P_l(\cos\theta)P_l(\cos\zeta) \\ &\quad + 2\sum_{m=1}^{l}(-1)^m\cos(mz)P_l^{-m}(\cos\theta)P_l^m(\cos\zeta), \quad l=1,2,3,\ldots \quad , \end{aligned} \tag{5.19}$$

where

$$\cos w = \cos\theta\cos\zeta + \sin\theta\sin\zeta\cos z.$$

First, multiply both sides of the equation (5.19) by $\cos z$, and integrate from 0 to 2π with respect to z to obtain

$$P_{n+1}^{-1}(\cos\theta)P_{n+1}^{1}(\cos\theta) = -\frac{1}{2\pi}\int_0^{2\pi} P_{n+1}(\cos w)\cos z\,dz. \tag{5.20}$$

Thus we can write

$$\begin{aligned} S(\theta,\zeta) &= -\frac{1}{2\pi}\sum_{n=0}^{\infty}\int_0^{2\pi} P_{n+1}(\cos w)\cos z\,dz \\ &= -\frac{1}{2\pi}\sum_{n=0}^{\infty}\int_0^{2\pi} P_n(\cos w)\cos z\,dz, \end{aligned} \tag{5.21}$$

since

$$\int_0^{2\pi} P_0(\cos w)\cos z\,dz = 0.$$

On interchanging the order of summation and integration in equation (5.21), and by noting that

$$\sum_{n=0}^{\infty} P_n(x) = \frac{1}{\sqrt{2-2x}},$$

we obtain

$$S(\theta,\zeta) = -\frac{1}{2\pi}\int_0^{2\pi} \frac{\cos z\, dz}{\sqrt{2-2\cos w}}$$
$$= -\frac{1}{2\pi}\int_0^{2\pi} \frac{\cos z\, dz}{\sqrt{s_1^2+s_2^2-2s_1s_2\cos z}},$$

where

$$s_1 = 2\sin\frac{\theta}{2}\cos\frac{\zeta}{2}, \qquad s_2 = 2\sin\frac{\zeta}{2}\cos\frac{\theta}{2},$$

and both s_1 and s_2 are positive for all θ and ζ, since $0 < \theta, \zeta < \pi$. Using a lemma of [Copson (8)], it follows that

$$S(\theta,\zeta) = -\frac{2}{\pi s_1 s_2}\int_0^{\min(s_1,s_2)} \frac{s^2\, ds}{\sqrt{(s_1^2-s^2)(s_2^2-s^2)}}. \tag{5.22}$$

Since $s_1 < s_2$ when $\theta < \zeta$, and $s_1 > s_2$ when $\theta > \zeta$, we split the integral in equation (5.17) at $\zeta = \theta$ and then substitute the summation (5.22) into the integrals, it follows that

$$\int_{\pi-\varphi}^{\theta} h(\zeta)\int_0^{s_2} \frac{s^2\, ds}{\sqrt{(s_1^2-s^2)(s_2^2-s^2)}}\, d\zeta + \int_{\theta}^{\pi} h(\zeta)\int_0^{s_1} \frac{s^2\, ds}{\sqrt{(s_1^2-s^2)(s_2^2-s^2)}}\, d\zeta \tag{5.23}$$
$$= -\frac{\pi}{4}\sin^2\theta \qquad (\pi-\varphi < \theta < \pi).$$

We next make the change of variable

$$s = 2\sin\frac{\theta}{2}\sin\frac{\zeta}{2}\cot\frac{u}{2} \qquad (\pi-\varphi < \theta < \pi),$$

it follows, then, from equation (5.23)

$$\int_{\pi-\varphi}^{\theta} h(\zeta)\int_{\theta}^{\pi} \frac{\sin^2\frac{\zeta}{2}\cot^2\frac{u}{2}\, du}{\sqrt{(\cos\zeta-\cos u)(\cos\theta-\cos u)}}\, d\zeta$$
$$+ \int_{\theta}^{\pi} h(\zeta)\int_{\zeta}^{\pi} \frac{\sin^2\frac{\zeta}{2}\cot^2\frac{u}{2}\, du}{\sqrt{(\cos\zeta-\cos u)(\cos\theta-\cos u)}}\, d\zeta$$
$$= -\frac{\pi}{2}\cos^2\frac{\theta}{2} \qquad (\pi-\varphi < \theta < \pi).$$

By inverting the order of integrations in above equation, we obtain

$$\int_\theta^\pi \cot^2\frac{u}{2}\,du \int_{\pi-\varphi}^{\theta} \frac{h(\zeta)\sin^2\frac{\zeta}{2}\,d\zeta}{\sqrt{(\cos\zeta-\cos u)(\cos\theta-\cos u)}} + \int_\theta^\pi \cot^2\frac{u}{2}\,du \int_\theta^u \frac{h(\zeta)\sin^2\frac{\zeta}{2}\,d\zeta}{\sqrt{(\cos\zeta-\cos u)(\cos\theta-\cos u)}} = -\frac{\pi}{2}\cos^2\frac{\theta}{2} \qquad (\pi-\varphi<\theta<\pi).$$

It follows that

$$\int_\theta^\pi \frac{\cot^2\frac{u}{2}\,du}{\sqrt{\cos\theta-\cos u}} \int_{\pi-\varphi}^{u} \frac{h(\zeta)\sin^2\frac{\zeta}{2}\,d\zeta}{\sqrt{\cos\zeta-\cos u}} = -\frac{\pi}{2}\cos^2\frac{\theta}{2}.$$

Let

$$H(u) = \int_{\pi-\varphi}^{u} \frac{h(\zeta)\sin^2\frac{\zeta}{2}}{\sqrt{\cos\zeta-\cos u}}\,d\zeta. \tag{5.24}$$

Then

$$\int_\theta^\pi \frac{H(u)\cot^2\frac{u}{2}}{\sqrt{\cos\theta-\cos u}}\,du = -\frac{\pi}{2}\cos^2\frac{\theta}{2} \qquad (\pi-\varphi<\theta<\pi). \tag{5.25}$$

To find $H(u)$, we multiply both sides of equation (5.25) by $\dfrac{\sin\theta}{\sqrt{\cos v-\cos\theta}}$ and integrate both sides of the equation from v to π with respect to θ, then

$$\int_v^\pi \frac{\sin\theta\,d\theta}{\sqrt{\cos v-\cos\theta}} \int_\theta^\pi \frac{H(u)\cot^2\frac{u}{2}\,du}{\sqrt{\cos\theta-\cos u}} = -\frac{\pi}{2}\int_v^\pi \frac{\sin\theta\cos^2\frac{\theta}{2}}{\sqrt{\cos v-\cos\theta}}\,d\theta. \tag{5.26}$$

Invert the order of integrations in equation (5.26), we have

$$\int_v^\pi H(u)\cot^2\frac{u}{2}\,du \int_v^u \frac{\sin\theta\,d\theta}{\sqrt{(\cos\theta-\cos u)(\cos v-\cos\theta)}} = -\frac{\pi}{2}\int_v^\pi \frac{\sin\theta\cos^2\frac{\theta}{2}}{\sqrt{\cos v-\cos\theta}}\,d\theta. \tag{5.27}$$

Applying the integral formula (C.20) directly on the second integral on the left hand side of equation (5.27) gives the value π. The integral on the right hand side of equation (5.27) can be evaluated using integration by parts, which is given as (see equation (C.1) in Appendix C for more details)

$$\int_v^\pi \frac{\sin\theta \cos^2\frac{\theta}{2}}{\sqrt{\cos v - \cos\theta}}\, d\theta = \frac{2}{3}(1+\cos v)^{\frac{3}{2}}.$$

It follows, then,

$$\int_v^\pi H(u)\cot^2\frac{u}{2}\, du = -\frac{1}{3}(1+\cos v)^{\frac{3}{2}}. \tag{5.28}$$

Differentiating equation (5.28) with respect to v gives,

$$H(v) = -\frac{1}{2}(1+\cos v)^{\frac{1}{2}}\sin v \tan^2\frac{v}{2}. \tag{5.29}$$

Substituting (5.29) into equation (5.24), we have

$$\int_{\pi-\varphi}^u \frac{h(\zeta)\sin^2\frac{\zeta}{2}}{\sqrt{\cos\zeta - \cos u}}\, d\zeta = -\frac{1}{2}(1+\cos v)^{\frac{1}{2}}\sin u \tan^2\frac{u}{2}. \tag{5.30}$$

To find $h(\zeta)$, we multiply both sides of equation (5.30) by $\dfrac{\sin u}{\sqrt{\cos u - \cos v}}$ and then integrate with respect to u from $\pi-\varphi$ to v. It follows that,

$$\begin{aligned}\int_{\pi-\varphi}^v \frac{\sin u\, du}{\sqrt{\cos u - \cos v}} \int_{\pi-\varphi}^u \frac{h(\zeta)\sin^2\frac{\zeta}{2}}{\sqrt{\cos\zeta - \cos u}}\, d\zeta \\ = -\frac{1}{2}\int_{\pi-\varphi}^v \frac{\sin^2 u \tan^2\frac{u}{2}\sqrt{1+\cos u}}{\sqrt{\cos u - \cos v}}\, du.\end{aligned} \tag{5.31}$$

Interchange the order of integrations on the left side of equation (5.31), we have

$$\begin{aligned}\int_{\pi-\varphi}^{v} h(\zeta)\sin^2\frac{\zeta}{2}\,d\zeta \int_{\zeta}^{v} \frac{\sin u\,du}{\sqrt{(\cos u-\cos v)(\cos\zeta-\cos u)}} \\ = -\sqrt{2}\int_{\pi-\varphi}^{v} \frac{\sin^3\frac{u}{2}\sin u}{\sqrt{\cos u-\cos v}}\,du.\end{aligned} \tag{5.32}$$

The second integral on the left hand side of equation (5.32) equals to π, which can be evaluated by directly applying the integral formula (C.1) in Appendix C. The integral on the right hand side of the equation is not obvious, but integrable. With a little effort, we found (see equation (C.2) in Appendix C for more details)

$$\begin{aligned}\int_{\pi-\varphi}^{v} \frac{\sin^3\frac{u}{2}\sin u}{\sqrt{\cos u-\cos v}}\,du = \frac{3}{2\sqrt{2}}\sin^4\frac{v}{2}\sin^{-1}\sqrt{\frac{\cos(\pi-\varphi)-\cos v}{1-\cos v}} \\ +\frac{1}{8}\cos\frac{\varphi}{2}(5+2\cos\varphi-3\cos v)\sqrt{\cos(\pi-\varphi)-\cos v}.\end{aligned} \tag{5.33}$$

Substituting this into equation (5.32) and differentiating with respect to v, we obtain,

$$\begin{aligned}h(v)\sin^2\frac{v}{2} = -\frac{\sin v}{\pi}\left\{\frac{3}{2}\left[\sin^2\frac{v}{2}\sin^{-1}\sqrt{\frac{\cos(\pi-\varphi)-\cos v}{1-\cos v}}+\frac{\sqrt{2}\cos\frac{\varphi}{2}\sin^2\frac{v}{2}}{4\sqrt{\cos(\pi-\varphi)-\cos v}}\right]\right. \\ \left.+\frac{\sqrt{2}\cos\frac{\varphi}{2}}{8}\left[3\sqrt{\cos(\pi-\varphi)-\cos v}+\frac{(5+2\cos\varphi-3\cos v)}{2\sqrt{\cos(\pi-\varphi)-\cos v}}\right]\right\}.\end{aligned}$$

i.e.

$$\begin{aligned}h(\theta) = -\frac{\sqrt{2}}{\pi}\left(\frac{3\sin\theta}{2\sqrt{2}}\sin^{-1}\sqrt{\frac{\cos(\pi-\varphi)-\cos\theta}{1-\cos\theta}}\right. \\ \left.+\frac{\cos\frac{\varphi}{2}\sin\theta}{\sqrt{\cos(\pi-\varphi)-\cos\theta}}+\frac{\cos\frac{\varphi}{2}}{2}\cot\frac{\theta}{2}\sqrt{\cos(\pi-\varphi)-\cos\theta}\right) \\ (\pi-\varphi<\theta<\pi).\end{aligned} \tag{5.34}$$

With $h(\theta)$ known, the velocity field can be found as shown next.

5.3.2 Velocity Field

We use $h(\theta)$ to find a closed form expression for the velocity on the clean part of the interface. We assume

$$g(\theta) = \sum_{n=0}^{\infty} B_{n+2} P_{n+1}^{-1}(\cos\theta) \qquad (0 < \theta < \pi - \varphi). \tag{5.35}$$

Then

$$\sum_{n=0}^{\infty} B_{n+2} P_{n+1}^{-1}(\cos\theta) = \begin{cases} g(\theta) & 0 < \theta < \pi - \varphi, \\ -\frac{\sin\theta}{4} & \pi - \varphi < \theta < \pi. \end{cases} \tag{5.36}$$

Substituting equation (5.16) into the equation (5.35) and interchanging the order of the summation and integration, we have,

$$\begin{aligned} g(\theta) &= -\frac{1}{2} \sum_{n=0}^{\infty} \int_{\pi-\varphi}^{\pi} h(\zeta) P_{n+1}^{1}(\cos\zeta) P_{n+1}^{-1}(\cos\theta) \sin\zeta \, d\zeta \\ &= -\frac{1}{2} \int_{\pi-\varphi}^{\pi} h(\zeta) \sin\zeta \sum_{n=0}^{\infty} P_{n+1}^{1}(\cos\zeta) P_{n+1}^{-1}(\cos\theta) \, d\zeta \\ &= -\frac{1}{2} \int_{\pi-\varphi}^{\pi} h(\zeta) S(\theta,\zeta) \sin\zeta \, d\zeta \qquad (0 < \theta < \pi - \varphi), \end{aligned} \tag{5.37}$$

where $S(\theta,\zeta)$ and $h(\zeta)$ are given in equation (5.22) and equation (5.34) respectively.

We now make the change of variable

$$s = 2\cos\frac{\theta}{2}\cos\frac{\zeta}{2}\tan\frac{u}{2} \qquad (0 < \theta < \pi - \varphi),$$

and note that $s_2 > s_1$ for all θ and ζ, since $0 < \theta < \pi - \varphi$ and $\pi - \varphi < \zeta < \pi$. Then,

$$\begin{aligned} S(\theta,\zeta) &= -\frac{2}{\pi s_1 s_2} \int_0^{s_1} \frac{s^2 \, ds}{\sqrt{(s_1^2 - s^2)(s_2^2 - s^2)}} \\ &= -\frac{2}{\pi \sin\theta \sin\zeta} \int_0^{\theta} \frac{2\cos^2\frac{\theta}{2}\cos^2\frac{\zeta}{2}\tan^2\frac{u}{2}}{\sqrt{(\cos u - \cos\theta)(\cos u - \cos\zeta)}} \, du \\ &= -\frac{2\cot\frac{\theta}{2}\cos^2\frac{\zeta}{2}}{\pi \sin\zeta} \int_0^{\theta} \frac{\tan^2\frac{u}{2} \, du}{\sqrt{(\cos u - \cos\theta)(\cos u - \cos\zeta)}}. \end{aligned}$$

Substituting this into equation (5.37) and inverting the order of integrations, we have,

$$\begin{aligned} g(\theta) &= \frac{\cot\frac{\theta}{2}}{\pi}\int_0^{\theta}\frac{\tan^2\frac{u}{2}}{\sqrt{\cos u-\cos\theta}}\int_{\pi-\varphi}^{\pi}\frac{h(\zeta)\cos^2\frac{\zeta}{2}\,d\zeta}{\sqrt{\cos u-\cos\zeta}}\,du \\ &= \frac{\cot\frac{\theta}{2}}{\pi}\int_0^{\theta}\frac{G(u)\tan^2\frac{u}{2}}{\sqrt{\cos u-\cos\theta}}\,du \qquad (0<\theta<\pi-\varphi), \end{aligned} \tag{5.38}$$

where

$$G(u) = \int_{\pi-\varphi}^{\pi}\frac{h(\zeta)\cos^2\frac{\zeta}{2}}{\sqrt{\cos u-\cos\zeta}}\,d\zeta. \tag{5.39}$$

Substitution equation (5.34) into equation (5.39), gives (see Appendix C for details),

$$\begin{aligned} G(u) &= -\frac{\sqrt{2}}{\pi}\int_{\pi-\varphi}^{\pi}\frac{\cos^2\frac{\zeta}{2}}{\sqrt{\cos u-\cos\zeta}}\left[\frac{3\sin\zeta}{2\sqrt{2}}\sin^{-1}\sqrt{\frac{\cos(\pi-\varphi)-\cos\zeta}{1-\cos\zeta}}\right. \\ &\quad \left.+\frac{\cos\frac{\varphi}{2}\sin\zeta}{\sqrt{\cos(\pi-\varphi)-\cos\zeta}}+\frac{1}{2}\cos\frac{\varphi}{2}\cot\frac{\zeta}{2}\sqrt{\cos(\pi-\varphi)-\cos\zeta}\right]d\zeta \\ &= -\frac{\sqrt{2}}{\pi}\left(\varphi\cos^3\frac{u}{2}-\frac{\sin\varphi}{2}\cos\frac{u}{2}+\frac{\sin^2 u-\cos u-\cos\varphi}{4\sin\frac{u}{2}}\ln\left|\frac{\cos\frac{u-\varphi}{2}}{\cos\frac{u+\varphi}{2}}\right|\right). \end{aligned} \tag{5.40}$$

The function $g(\theta)$ is obtained by combining equations (5.40) and (5.38) to give (see Appendix C for details),

$$\begin{aligned} g(\theta) &= -\frac{\sqrt{2}}{\pi^2}\cot\frac{\theta}{2}\int_0^{\theta}\left(\varphi\cos^3\frac{u}{2}-\frac{\sin\varphi}{2}\cos\frac{u}{2}\right. \\ &\quad \left.+\frac{\sin^2 u-\cos u-\cos\varphi}{4\sin\frac{u}{2}}\ln\left|\frac{\cos\frac{u-\varphi}{2}}{\cos\frac{u+\varphi}{2}}\right|\right)\frac{\tan^2\frac{u}{2}}{\sqrt{\cos u-\cos\theta}}\,du \\ &= -\frac{\varphi}{4\pi}\sin\theta+\frac{\sqrt{2}}{2\pi}\sin\frac{\varphi}{2}\tan\frac{\theta}{2}\sqrt{\cos\varphi+\cos\theta} \\ &\quad -\frac{\sin\theta}{4\pi^2}\int_0^{\theta}\ln\left|\frac{\cos\frac{u-\varphi}{2}}{\cos\frac{u+\varphi}{2}}\right|\frac{\sin u\,du}{\sqrt{(1+\cos u)(\cos u-\cos\theta)}} \\ &\qquad\qquad (0<\theta<\pi-\varphi). \end{aligned} \tag{5.41}$$

5.4 Surfactant Transport

The limit $\epsilon \to 0$ poses a singular perturbation problem as can be seen from equation (5.2). In the main part of the flow field a solution can be found which needs to be matched onto boundary layer solutions in the vicinity of the bubble surface. These two solutions in their respective regions are considered next.

5.4.1 Leading Order Outer Solution

In the limit $\epsilon \to 0$, equation (5.2) becomes

$$\boldsymbol{u} \cdot \nabla C = 0. \tag{5.42}$$

That is, the directional derivative of C in the direction of $\boldsymbol{u}$ vanishes. i.e.

$$\frac{DC}{D\boldsymbol{u}} = 0.$$

It follows, from the definition of the stream-function, that the bulk surfactant concentration C is constant along stream lines. Since the concentration far from interface is equal to one. This leads to the solution

$$C = 1, \tag{5.43}$$

everywhere in the fluid domain. This solution satisfies the boundary condition at infinity (2.58), but it does not satisfy the boundary conditions on the surface (2.60), (5.5) and (5.7).

The problem arises from neglecting the diffusion term on the right hand side of equation (5.2) everywhere. When $\epsilon \to 0$, the problem becomes singular. Diffusion is

negligible compared to convection away from the bubble surface, but is not negligible near the interface as a boundary layer develops there. In fact, the solution (5.43) is the first order outer solution of the problem. To find the inner solution, we need to introduce appropriately stretched boundary layer variables on perform a local analysis there.

5.4.2 Rescaling and Boundary Layer Equations

5.4.2.1 Stagnant Cap Region ($\pi - \varphi < \theta < \pi$)

We rescale the length in the inner region as

$$\eta_1 = \frac{r-1}{\delta_1}, \tag{5.44}$$

where $\delta_1 \ll 1$ depends on ϵ and is to be found from orders-of-magnitude (or balance of terms) arguments.

From equation (5.11), we have, the exact leading order velocities,

$$\begin{aligned} u_r &= (\frac{1}{r} - 1)\cos\theta + \sum_{n=2}^{\infty} B_n(r^{-n+1} - r^{-n-1})P_{n-1}(\cos\theta), \\ u_\theta &= (1 - \frac{1}{2r})\sin\theta \\ &\quad + \frac{1}{\sin\theta}\sum_{n=2}^{\infty} B_n[(n-3)r^{-n+1} - (n-1)r^{-n-1}]C_n^{-\frac{1}{2}}(\cos\theta). \end{aligned} \tag{5.45}$$

We now substitute $r = 1 + \delta_1\eta_1$ into equations (5.45), and linearize the velocities for small δ_1. Note that

$$\frac{1}{(1+\delta_1\eta_1)^l} = 1 - l\delta_1\eta_1 + \frac{l(l+1)}{2}\delta_1^2\eta_1^2 - \frac{l(l+1)(l+2)}{3!}\delta_1^3\eta_1^3 + \ldots$$

Then

$$\begin{aligned} u_r &\sim (-\delta_1\eta_1 + \delta_1^2\eta_1^2)\cos\theta \\ &\quad + \sum_{n=2}^{\infty} B_n[2\delta_1\eta_1 - (2n+1)\delta_1^2\eta_1^2]P_{n-1}(\cos\theta) + O(\delta_1^3), \\ \frac{u_\theta}{r} &\sim \frac{\sin\theta}{2} \\ &\quad + \frac{1}{\sin\theta}\sum_{n=2}^{\infty} B_n[-2 + 2(2n-1)\delta_1\eta_1]C_n^{-\frac{1}{2}}(\cos\theta) + O(\delta_1^2). \end{aligned} \tag{5.46}$$

To evaluate the infinite sums in equations (5.46), we use the results in Section 5.3, where we obtained that,

$$\sum_{n=0}^{\infty} B_{n+2}P_{n+1}^{-1}(\cos\theta) = -\frac{1}{4}\sin\theta \qquad (\pi - \varphi < \theta < \pi), \tag{5.47}$$

$$\sum_{n=0}^{\infty}(2n+3)B_{n+2}P_{n+1}^{-1}(\cos\theta) = h(\theta) \quad (\pi - \varphi < \theta < \pi), \tag{5.48}$$

which is equivalent to writing

$$\sum_{n=2}^{\infty} B_n C_n^{-\frac{1}{2}}(\cos\theta) = \frac{1}{4}\sin^2\theta \qquad (\pi - \varphi < \theta < \pi), \tag{5.49}$$

$$\sum_{n=2}^{\infty}(2n-1)B_n C_n^{-\frac{1}{2}}(\cos\theta) = -\sin\theta h(\theta) \quad (\pi - \varphi < \theta < \pi). \tag{5.50}$$

Differentiating both sides of the above equations, we have,

$$\sum_{n=2}^{\infty} B_n P_{n-1}(\cos\theta) = \frac{1}{2}\cos\theta \qquad (\pi - \varphi < \theta < \pi), \tag{5.51}$$

$$\sum_{n=2}^{\infty}(2n-1)B_n P_{n-1}(\cos\theta) = -\cot\theta h(\theta) - h'(\theta) \qquad (\pi - \varphi < \theta < \pi). \tag{5.52}$$

Applying these results to equations (5.46), we obtain,

$$u_r \sim \delta_1^2\eta_1^2[\cot\theta h(\theta) + h'(\theta)] + O(\delta_1^3) \qquad (\pi - \varphi < \theta < \pi), \tag{5.53}$$

$$\frac{u_\theta}{r} \sim -2\delta_1\eta_1 h(\theta) + O(\delta_1^2) \qquad (\pi - \varphi < \theta < \pi). \tag{5.54}$$

We now propose an asymptotic expansion for the concentration field in the inner region of the stagnant cap region, of the form

$$C(\eta_1,\theta) = C_1(\eta_1,\theta) + \sum_{n=1}^{\infty} G_n(\epsilon) C_1^{(n)}(\eta_1,\theta). \tag{5.55}$$

Substituting equations (5.53), (5.54) and (5.55) into equation (5.2), yields,

$$\delta_1\eta_1[\cot\theta h(\theta) + h'(\theta)]\frac{\partial C_1}{\partial \eta_1} - 2\delta_1\eta_1 h(\theta)\frac{\partial C_1}{\partial \theta} + O(\delta_1^2) \sim \frac{\epsilon}{\delta_1^2}\frac{\partial^2 C_1}{\partial \eta_1^2} + O(\delta_1^2)$$
$$(\varphi - \pi < \theta < \pi).$$

It follows, by a balance of terms that,

$$\delta_1 \sim \frac{\epsilon}{\delta_1^2},$$

i.e. the boundary layer thickness on the stagnant cap region is

$$\delta_1 = \epsilon^{\frac{1}{3}} \qquad (\varphi - \pi < \theta < \pi). \tag{5.56}$$

This scaling is expected since it is that of the boundary layer on a solid sphere (see [Leal (1992)]). The boundary layer equation is

$$-\frac{\partial^2 C_1}{\partial \eta_1^2} + \eta_1^2[\cot\theta h(\theta) + h'(\theta)]\frac{\partial C_1}{\partial \eta_1} = 2\eta_1 h(\theta)\frac{\partial C_1}{\partial \theta} \quad (\pi - \varphi < \theta < \pi). \tag{5.57}$$

5.4.2.2 Clean Surface Region $(0 < \theta < \pi - \varphi)$

We begin our analysis by assuming that the angle $\pi - \varphi$ (the size of the clean part of the interface) is of order one. This implies that $\frac{\partial}{\partial\theta} \sim 1$ in the boundary layer and, as we show later, it leads to physically inconsistent solutions. This analysis is useful in deriving the correct asymptotic boundary layer structures. From Section 5.3, we have,

$$\sum_{n=0}^{\infty} B_{n+2} P_{n+1}^{-1}(\cos\theta) = g(\theta) \qquad (0 < \theta < \pi - \varphi), \tag{5.58}$$

$$\sum_{n=0}^{\infty} (2n+3) B_{n+2} P_{n+1}^{-1}(\cos\theta) = 0 \qquad (0 < \theta < \pi - \varphi), \tag{5.59}$$

which are equivalent to

$$\sum_{n=2}^{\infty} B_n C_n^{-\frac{1}{2}}(\cos\theta) = -\sin\theta g(\theta) \qquad (0 < \theta < \pi - \varphi), \tag{5.60}$$

$$\sum_{n=2}^{\infty} (2n-1) B_n C_n^{-\frac{1}{2}}(\cos\theta) = 0 \qquad (0 < \theta < \pi - \varphi). \tag{5.61}$$

Differentiating both sides of the above equations, we have

$$\sum_{n=2}^{\infty} B_n P_{n-1}(\cos\theta) = -\cot\theta g(\theta) - g'(\theta) \qquad (0 < \theta < \pi - \varphi), \tag{5.62}$$

$$\sum_{n=2}^{\infty} (2n-1) B_n P_{n-1}(\cos\theta) = 0 \qquad (0 < \theta < \pi - \varphi). \tag{5.63}$$

We introduce a boundary layer thickness $\delta_2(\epsilon)$, and rescale the radial coordinate near the surface as

$$\eta_2 = \frac{r-1}{\delta_2}. \tag{5.64}$$

The concentration concentration is also expanded as

$$C(\eta_2,\theta) = C_2(\eta_2,\theta) + \sum_{n=1}^{\infty} H(\epsilon) C_2^{(n)}(\eta_2,\theta). \tag{5.65}$$

Substituting $r = 1 + \delta_2\eta_2$ into equation (5.45), expanding for small δ_2, and using the summations (5.60) - (5.63), we have, for the leading order velocities,

$$u_r \sim -\eta_2\delta_2[\cos\theta - 2(\cot\theta g(\theta) + g'(\theta))] + O(\delta_2^2) \qquad (0 < \theta < \pi - \varphi), \tag{5.66}$$

$$\frac{u_\theta}{r} \sim 2g(\theta) + \frac{\sin\theta}{2} + O(\delta_2) \qquad (0 < \theta < \pi - \varphi). \tag{5.67}$$

Substitution of equations (5.65) - (5.67) into equation (5.2), yields,

$$-\eta_2[\cos\theta + 2\cot\theta g(\theta) + 2g'(\theta)]\frac{\partial C_2}{\partial \eta_2} + \left(2g(\theta) + \frac{\sin\theta}{2}\right)\frac{\partial C_2}{\partial\theta} \sim \frac{\epsilon}{\delta_2^2}\frac{\partial^2 C_2}{\partial \eta_2^2}. \tag{5.68}$$

Balancing the diffusion with convection gives

$$\delta_2 = \epsilon^{\frac{1}{2}},$$

which is the expected result for a clean surface (c.f. [Leal (1992)]). We indicate, next that this structure is physically inconsistent. This is done by consideration of the mass flux onto and off the interface. Using the boundary layer scalings just found, the mass flux onto the clean part of the surface is

$$\int_0^{\pi-\varphi} \left.\frac{\partial C}{\partial r}\right|_{r=1} \sin\theta\, d\theta = \frac{1}{\delta_2}\int_0^{\pi-\varphi} \left.\frac{\partial C_2}{\partial \eta_2}\right|_{\eta_2=0} \sin\theta\, d\theta \sim O(\epsilon^{-\frac{1}{2}}). \tag{5.69}$$

On the other hand, on the rigid part of the surface, $r = 1 + \epsilon^{\frac{1}{3}}\eta_1$, so the mass flux off this part of the surface is

$$\int_{\pi-\varphi}^{\pi} \left.\frac{\partial C}{\partial r}\right|_{r=1} \sin\theta\, d\theta = \frac{1}{\delta_1}\int_{\pi-\varphi}^{\pi} \left.\frac{\partial C_1}{\partial \eta_1}\right|_{\eta_1=0} \sin\theta\, d\theta \sim O(\epsilon^{-\frac{1}{3}}). \tag{5.70}$$

It is obvious that the order of the mass flux onto the clean part of the surface is asymptotically larger than that off the rigid part, and hence the mass flux off the surface cannot balance the mass flux onto the surface as $\epsilon \to 0$. This contradicts the fact that the total net diffusion flux to the surface vanishes at steady state. The problem lies in the assumption we made that the tangential angle both in stagnant cap region and clean part are of order one. In fact, when $\epsilon \to 0$ (Pe $\to \infty$), surfactant acts as if it is insoluble once it adsorbs onto the surface. As a result, surfactant almost covers the entire surface (as [Bel Fdhila & Duineveld (1996)] observed) at steady state. In what follows we provide the consistent asymptotic scalings in the limit $\epsilon \to 0$.

To get an appropriate boundary layer thickness along the clean part of the surface, we assume

$$\pi - \varphi = \lambda(\epsilon)\varphi_0, \tag{5.71}$$

with $\lambda(epsilon) \ll 1$ to be found and $\varphi_0 = O(1)$ being a constant that needs to be determined by matching the boundary layer solution along the clean part with the solution along the stagnant cap.

We next rescale the variable θ as

$$\xi = \frac{\theta}{\lambda(\epsilon)}, \tag{5.72}$$

which implies that

$$\frac{\partial C_2}{\partial \theta} = \frac{1}{\lambda}\frac{\partial C_2}{\partial \xi}. \tag{5.73}$$

The velocity field near the clean part of the surface now depends on both δ_2 and $\lambda(epsilon)$. To find the boundary layer thickness there, we need to expand the function $g(\theta)$ and its derivative $g'(\theta)$, in asymptotic series.

We substitute $\theta = \lambda\xi$ and $\varphi = \pi - \lambda\varphi_0$ into equation (5.41), and change to the variable $u = \lambda v$ in the integral of that equation. Then,

$$\begin{aligned}
g(\lambda\xi) &= -\frac{\varphi}{4\pi}\sin(\lambda\xi) + \frac{\sqrt{2}}{2\pi}\sin\frac{\varphi}{2}\tan\frac{\lambda\xi}{2}\sqrt{\cos\varphi + \cos(\lambda\xi)} \\
&\quad - \frac{\sin(\lambda\xi)}{4\pi^2}\int_0^{\xi} \ln\left|\frac{\sin\frac{(v+\varphi_0)\lambda}{2}}{\sin\frac{(v-\varphi_0)\lambda}{2}}\right| \frac{\lambda\sin(\lambda v)\,dv}{\sqrt{[1+\cos(\lambda v)][\cos(\lambda v)-\cos(\lambda\xi)]}} \\
&= -\frac{(\pi-\varphi_0\lambda)}{4\pi}\sin(\lambda\xi) + \frac{\sqrt{2}}{2\pi}\cos\frac{\lambda\varphi_0}{2}\tan\frac{\lambda\xi}{2}\sqrt{\cos(\lambda\xi)-\cos(\lambda\varphi_0)} \\
&\quad - \frac{\lambda^2\xi}{4\pi^2}\int_0^{\xi}\ln\left|\frac{v+\varphi_0}{v-\varphi_0}\right|\frac{v\,dv}{\sqrt{\xi^2-v^2}} \\
&\sim -\frac{(\pi-\varphi_0\lambda)}{4\pi}\lambda\xi + \frac{\sqrt{2}}{2\pi}\frac{\lambda\xi}{2}\frac{\lambda}{\sqrt{2}}\sqrt{\varphi_0^2-\xi^2} \\
&\quad + \frac{\lambda^2\xi}{4\pi^2}\left(\sqrt{\xi^2-v^2}\ln\left|\frac{v+\varphi_0}{v-\varphi_0}\right|\Bigg|_0^{\xi} - 2\varphi_0\int_0^{\xi}\frac{\sqrt{\xi^2-v^2}}{\varphi_0^2-v^2}\,dv\right) + O(\lambda^3) \\
&\sim -\frac{\xi\lambda}{4} + \frac{\varphi_0\xi\lambda^2}{4\pi} + \frac{\xi\lambda^2}{4\pi}\sqrt{\varphi_0^2-\xi^2} - \frac{\xi\varphi_0\lambda^2}{2\pi^2}\int_0^{\xi}\frac{\sqrt{\xi^2-v^2}}{\varphi_0^2-v^2}\,dv + O(\lambda^3) \\
&\sim -\frac{\xi\lambda}{4} + \frac{\varphi_0\xi\lambda^2}{4\pi} + \frac{\xi\lambda^2}{4\pi}\sqrt{\varphi_0^2-\xi^2} - \frac{\xi\lambda^2}{4\pi}\left(\varphi_0 - \sqrt{\varphi_0^2-\xi^2}\right) + O(\lambda^3) \\
&\sim -\frac{\xi}{4}\lambda + \frac{\xi\lambda^2}{2\pi}\sqrt{\varphi_0^2-\xi^2} + O(\lambda^3) \qquad (0<\xi<\varphi_0),
\end{aligned} \tag{5.74}$$

and

$$g'(\lambda\xi) \sim -\frac{1}{4} + \frac{1}{2\pi}\frac{\varphi_0^2-2\xi^2}{\sqrt{\varphi_0^2-\xi^2}}\lambda + O(\lambda^2) \qquad (0<\xi<\varphi_0). \tag{5.75}$$

Substitute $\theta = \lambda\xi$ into equations (5.66) and (5.67), expand the velocities for small λ and use the results (5.74) and (5.75), to obtain,

$$u_r \sim -\frac{\lambda\delta_2\eta_2}{\pi}\frac{2\varphi_0^2-3\xi^2}{\sqrt{\varphi_0^2-\xi^2}} + O(\delta_2^2\lambda) \qquad (0<\xi<\varphi_0), \tag{5.76}$$

$$\frac{u_\theta}{r} \sim \frac{\lambda^2\xi}{\pi}\sqrt{\varphi_0^2-\xi^2} + O(\delta_2\lambda^2) \qquad (0<\xi<\varphi_0). \tag{5.77}$$

Substitution of these along with equations (5.72) and (5.73) into the convection diffusion equation (5.2), yields

$$\boldsymbol{u}\cdot\nabla C_2 \sim \lambda\left(-\frac{\eta_2}{\pi}\frac{2\varphi_0^2-3\xi^2}{\sqrt{\varphi_0^2-\xi^2}}\frac{\partial C_2}{\partial \eta_2}+\frac{\xi}{\pi}\sqrt{\varphi_0^2-\xi^2}\frac{\partial C_2}{\partial \xi}\right)+O(\lambda^2,\lambda\delta_2) \qquad (0<\xi<\varphi_0), \tag{5.78}$$

and

$$\epsilon\nabla^2 C_2 \sim \frac{\epsilon}{\delta_2^2}\frac{\partial^2 C_2}{\partial \eta_2^2}+\frac{\epsilon}{\lambda^2}\left(\frac{1}{\xi}\frac{\partial C_2}{\partial \xi}+\frac{\partial^2 C_2}{\partial \xi^2}\right)+O(\frac{\epsilon}{\delta_2},\frac{\delta_2\epsilon}{\lambda^2},\frac{\epsilon}{\lambda}) \qquad (0<\xi<\varphi_0). \tag{5.79}$$

In the boundary layer region, we have to keep both the diffusion term and the convection term of equation (5.2). This means,

$$\lambda=\frac{\epsilon}{\delta_2^2}, \tag{5.80}$$

or

$$\lambda=\frac{\epsilon}{\lambda^2}. \tag{5.81}$$

At steady state, the total net flux to surface is zero, that is

$$\int_0^{\pi-\varphi}\frac{\partial C_2}{\partial r}\sin\theta\,d\theta=\int_{\pi-\varphi}^{\pi}\frac{\partial C_1}{\partial r}\sin\theta\,d\theta. \tag{5.82}$$

i.e.

$$\frac{\lambda^2}{\delta_2}\int_0^{\varphi_0}\frac{\partial C_2}{\partial \eta_2}\xi\,d\xi=\epsilon^{-\frac{1}{3}}\int_{\pi-\varphi}^{\pi}\frac{\partial C_1}{\partial \eta_1}\sin\theta\,d\theta.$$

It follows that,

$$\frac{\lambda^2}{\delta_2} = \epsilon^{-\frac{1}{3}} \qquad \text{as} \qquad \epsilon \to 0. \tag{5.83}$$

If we combine equation (5.83) with equation (5.81), then $\lambda = \epsilon^{\frac{1}{3}}$ and $\delta_2 = \epsilon$ which makes the diffusion term we keep (the second term in the right hand sides of equation (5.79)) to be much smaller than the term we throw away (the first term in the right hand sides of equation (5.79) as $\epsilon \to 0$. Obviously, balance of convection with the second term of equation (5.79) is not a right choice. The only possible correct answer is balancing the convection with the diffusion in radial direction. This could have been anticipated since we need the radial dependence in order to apply boundary conditions at $\eta_2 = 0, \infty$.

Combining equation (5.83) with equation (5.80), we obtain,

$$\delta_2 = \epsilon^{\frac{7}{15}}, \qquad \lambda = \epsilon^{\frac{1}{15}} \qquad (0 < \xi < \varphi_0). \tag{5.84}$$

That is the boundary layer thickness along the clean part of the surface is of $O(\epsilon^{\frac{7}{15}})$ and the size of the clean part surface is of $O(\epsilon^{\frac{1}{15}})$.

The boundary layer equation along the clean part of the surface is

$$-\frac{\eta_2(2\varphi_0^2 - 3\xi^2)}{\pi\sqrt{\varphi_0^2 - \xi^2}}\frac{\partial C_2}{\partial \eta_2} + \frac{\xi}{\pi}\sqrt{\varphi_0^2 - \xi^2}\frac{\partial C_2}{\partial \xi} = \frac{\partial^2 C_2}{\partial \eta_2^2} \qquad (0 < \xi < \varphi_0). \tag{5.85}$$

5.4.3 Boundary Layer Analysis

In the previous section, we found that a boundary layer develops along the bubble interface when $\epsilon \ll 1$ (Pe $\gg 1$), with thicknesses $\delta_1 = \epsilon^{\frac{1}{3}}$ in the stagnant cap region

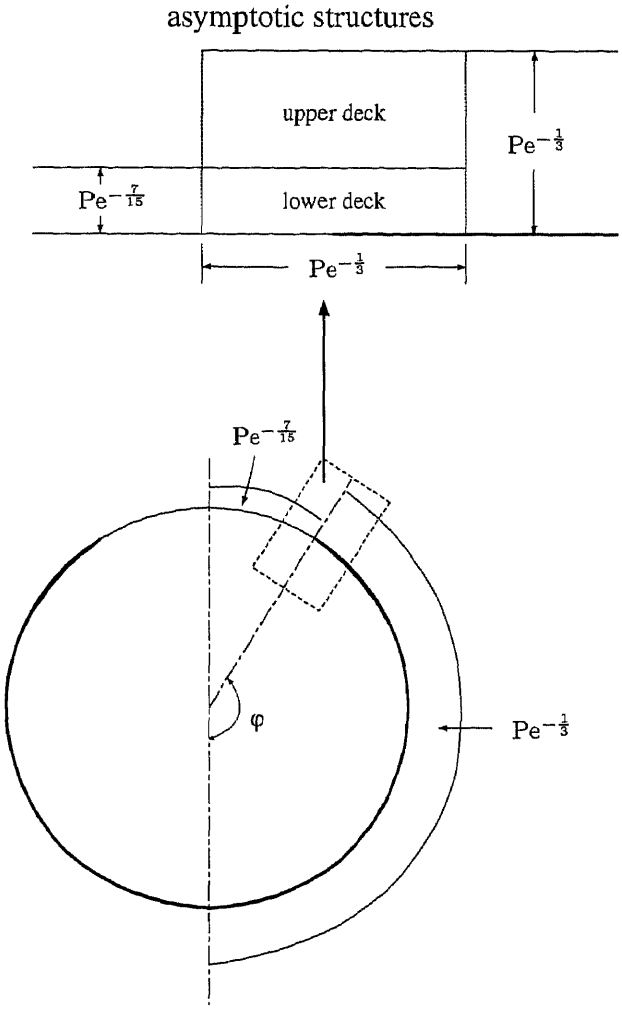

Figure 5.1 Boundary layer structure, where φ is the cap angle

and $\delta_2 = \epsilon^{\frac{7}{15}}$ in the clean surface region as illustrated in Figure 5.1. The size of the clean part of the surface is of $O(\epsilon^{\frac{1}{15}})$. That is the stagnant cap almost covers the entire bubble surface as $\epsilon \to 0$ (Pe $\to \infty$).

To find the leading order solution for the concentration field, we need to solve the boundary layer equations (5.57) and (5.85) subject to appropriate boundary conditions. The stagnant cap boundary conditions on the bubble surface hold for the equations. However, the boundary condition at infinity cannot be applied directly since the boundary layer solutions are only valid in the inner region near the surface. But the matching condition with the leading order outer solution (5.43) implies that

$$C_1 = 1 \qquad \text{as} \qquad \eta_1 \to \infty, \tag{5.86}$$

$$C_2 = 1 \qquad \text{as} \qquad \eta_2 \to \infty. \tag{5.87}$$

It follows that the boundary layer problems are:

1. In stagnant cap region $(\pi - \varphi < \theta < \pi)$

$$-\frac{\partial^2 C_1}{\partial \eta_1^2} + \eta_1^2[\cot\theta h(\theta) + h'(\theta)]\frac{\partial C_1}{\partial \eta_1} = 2\eta_1 h(\theta)\frac{\partial C_1}{\partial \theta}, \tag{5.88}$$

$$C_1 = \frac{\Gamma}{k(1-\Gamma)} \qquad \text{at} \qquad \eta_1 = 0, \tag{5.89}$$

$$\frac{\partial C_1}{\partial \theta} = 0 \qquad \text{at} \qquad \theta = \pi, \tag{5.90}$$

$$C_1 = 1 \qquad \text{as} \qquad \eta_1 \to \infty, \tag{5.91}$$

where $h(\theta)$ is given in equation (5.34), and $\Gamma(\theta)$ is obtained by solving differential equation (5.7) subject to the boundary condition $\Gamma(\pi - \varphi) = 0$, which is given by

$$\Gamma(\theta) = 1 - e^{f(\theta)}, \tag{5.92}$$

with

$$f(\theta) = \frac{1}{\pi \mathrm{Ma}} \left[(3\cos\theta - 1 + 2\cos\varphi) \sin^{-1} \sqrt{\frac{\cos(\pi-\varphi) - \cos\theta}{1-\cos\theta}} - 3\sqrt{2}\cos\frac{\varphi}{2}\sqrt{\cos(\pi-\varphi) - \cos\theta} \right]. \tag{5.93}$$

2. In clean surface region $(0 < \xi < \varphi_0)$

$$-\frac{\eta_2(2\varphi_0^2 - 3\xi^2)}{\pi\sqrt{\varphi_0^2 - \xi^2}} \frac{\partial C_2}{\partial \eta_2} + \frac{\xi}{\pi}\sqrt{\varphi_0^2 - \xi^2}\frac{\partial C_2}{\partial \xi} = \frac{\partial^2 C_2}{\partial \eta_2^2}, \tag{5.94}$$

$$C_2 = 0 \qquad \text{at} \qquad \eta_2 = 0, \tag{5.95}$$

$$\frac{\partial C_2}{\partial \eta_2} = 0 \qquad \text{at} \qquad \xi = 0, \tag{5.96}$$

$$C_2 = 1 \qquad \text{as} \qquad \eta_2 \to \infty. \tag{5.97}$$

At $\theta = \pi - \varphi$, both boundary layer equations (5.88) and (5.94) become singular. A double deck may need to be solved in a small region around $\theta = \pi - \varphi$, as is illustrated in Figure 5.1. Equation (5.94) is solved numerically by marching forward in ξ starting from an initial condition at $\xi = 0$. The solution is shown in Figure 5.2, where the horizontal axis represents the dimensionless concentration, the vertical axis represents $\eta' = \sqrt{\frac{\varphi_0}{\pi}}\eta_2$ and $\xi' = \frac{\xi}{\varphi_0}$. Note that there is a singularity in the solution as $\xi' \to 1$. Using the above rescalings, the equation can be written as

$$-\frac{\eta'(2 - 3\xi'^2)}{\sqrt{1-\xi'^2}} \frac{\partial C_2}{\partial \eta'} + \xi'\sqrt{1-\xi'^2}\frac{\partial C_2}{\partial \xi'} = \frac{\partial^2 C_2}{\partial \eta'^2}.$$

5.5 Conclusions

Once the solutions for boundary layer equations (5.88) and (5.94) are found, the solution for the bulk concentration C can be determined by matching the solutions

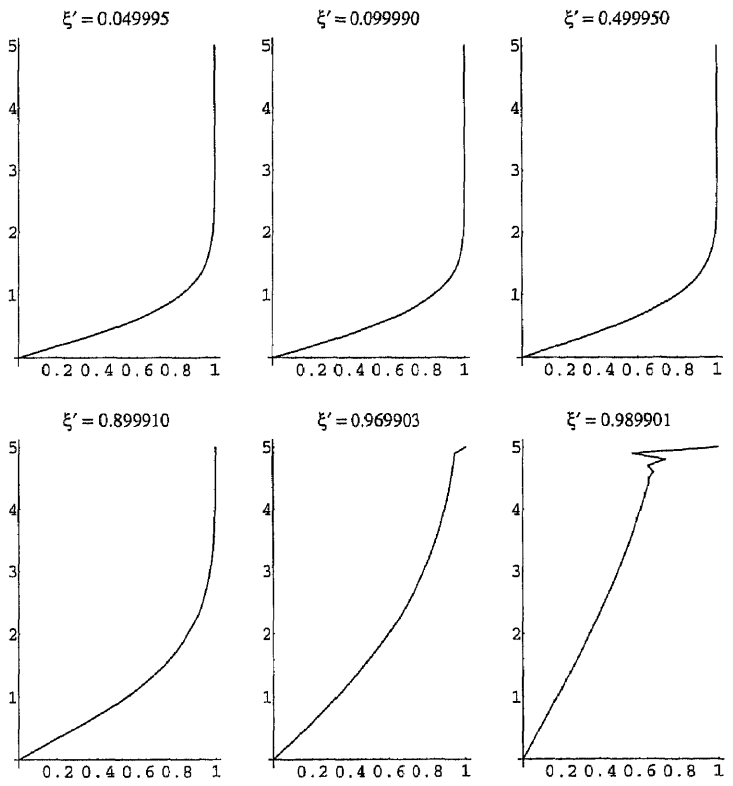

Figure 5.2 Boundary layer solution in clean surface region

near the singular point $\theta = \pi - \varphi$. The mass balance relation (5.82) can then be used to obtain the constant φ_0. Subsequently, with φ_0 known, we will be able to calculate the correction term to the drag. To find the drag, we first calculate the coefficient B_2 using the expression 5.16 and then substitute it into the relation 3.7. By using $\pi - \varphi = \epsilon^{\frac{1}{15}}\varphi_0$ and expanding the result for small ϵ, we have the following expression of drag:

$$Drag = -6 + \epsilon^{\frac{1}{3}}\frac{\varphi_0^5}{5\pi} + \cdots \quad ,$$

This expression of the drag is of ultimate use and can be used to check experiments.

APPENDIX A

ANALYTICAL SOLUTION FOR SMALL BULK CONCENTRATION AND PECLET NUMBER

The objective of this Appendix is the asymptotic evaluation of the drag C_{D1} experienced by the bubble in the limit of small bulk concentration k and small Peclet number of $O(k)$. It turns out that the $O(k)$ correction is zero and the asymptotic development is taken to $O(k^3)$ in order to provide an accurate enough result to compare with the simulations.

A.1 Hydrodynamics and Surfactant Transport

The exact system to be solved is

$$\begin{cases} E^4\psi = 0, & \\ \psi = 0 & \text{at} \quad r = 1, \quad \theta = 0, \pi, \\ \psi = \frac{1}{2} r^2 \sin^2\theta & \text{as} \quad r \to \infty, \\ \psi_{rr} - 2\psi_r|_{r=1} = \frac{\mathrm{Ma}}{1-\Gamma}\frac{\partial \Gamma}{\partial \theta}\sin\theta, & \end{cases} \tag{A.1}$$

for the hydrodynamics and

$$\begin{cases} \boldsymbol{u}\cdot\nabla C = \frac{1}{\mathrm{Pe}}\nabla^2 C, & \\ \Gamma = \frac{kC}{1+kC}, & \text{at} \quad r = 1 \\ C = 1, & \text{as} \quad r \to \infty, \\ \frac{1}{\sin\theta}\frac{\partial}{\partial\theta}(\sin\theta u_\theta \Gamma) = \frac{\chi k}{\mathrm{Pe}}\frac{\partial C}{\partial r}\Big|_{r=1}. & \end{cases} \tag{A.2}$$

for the convection-diffusion equation governing the concentration distribution in the bulk. It can be seen from equation (A.2) that in the limit $k \ll 1$ (here we also take $\mathrm{Pe} = Qk$ with Q a constant) the hydrodynamics decouples from the concentration dynamics. In addition, at higher order this remains the case and forced versions of equation (A.2) need to be addressed.

Formally, then, we expand dependent variables in powers of k,

$$\psi = \psi_0 + k\psi_1 + k^2\psi_2 + k^3\psi_3 + \cdots, \tag{A.3}$$

$$\Gamma = \Gamma_0 + k\Gamma_1 + k^2\Gamma_2 + k^3\Gamma_3 + \cdots, \tag{A.4}$$

$$C = C_0 + kC_1 + k^2C_2 + k^3C_3 + \cdots, \tag{A.5}$$

$$\boldsymbol{u} = \boldsymbol{u}_0 + k\boldsymbol{u}_1 + k^2\boldsymbol{u}_2 + k^3\boldsymbol{u}_3 + \cdots, \tag{A.6}$$

and substitute into (A.1) and (A.2), to obtain a sequence of problems at successive orders.

A.1.1 Leading Order Solution

The leading order problem is

$$\begin{cases} E^4\psi_0 = 0, & \\ \psi_0 = 0 & \text{at} \quad r = 1, \quad \theta = 0, \pi, \\ \psi_0 = \frac{1}{2}r^2\sin\theta & \text{as} \quad r \to \infty, \\ \frac{\partial^2\psi_0}{\partial r^2} - \frac{\partial\psi_0}{\partial r}\Big|_{r=1} = \frac{\mathrm{Ma}\sin\theta}{1-\Gamma_0}\frac{\partial\Gamma_0}{\partial\theta}. & \end{cases} \tag{A.7}$$

and

$$\begin{cases} \nabla^2 C_0 = 0, & \\ \Gamma_0 = 0, & \\ C_0 = 1, & \text{as} \quad r \to \infty, \\ \frac{1}{\sin\theta}\frac{\partial}{\partial\theta}(\sin\theta u_{0\theta}\Gamma_0) = \frac{\chi}{Q}\frac{\partial C_0}{\partial r}\Big|_{r=1}. & \end{cases} \tag{A.8}$$

From (A.8) we have $\Gamma_0 = 0$, and the boundary conditions for (A.7) and (A.8) become, respectively,

$$\frac{\partial^2\psi_0}{\partial r^2} - \frac{\partial\psi_0}{\partial r}\Big|_{r=1} = 0, \qquad \frac{\partial C_0}{\partial r}\Big|_{r=1} = 0.$$

The hydrodynamics decouples leading to the well-known Hadamard-Rybczynski solution

$$\psi_0 = \frac{1}{2}(r^2 - r)\sin^2\theta. \tag{A.9}$$

The general solution of (A.8) is

$$C_0 = \sum_{n=0}^{\infty} a_n r^{-n} P_n(\cos\theta),$$

and application of the boundary condition at infinity gives $a_0 = 1$, while the boundary condition at the bubble surface implies $a_i = 0$ for $i = 1, 2, \cdots$. Thus, the leading order solution for the concentration is

$$C_0 = 1. \tag{A.10}$$

A.1.2 Second Order Solution

At the next order, $O(k)$, the problem is

$$\begin{cases} E^4\psi_1 = 0, & \\ \psi_1 = 0 & \text{at} \quad r = 1, \quad \theta = 0, \pi, \\ \frac{\psi_1}{r^2} = 0 & \text{as} \quad r \to \infty, \\ \frac{\partial^2\psi_1}{\partial r^2} - \frac{\partial\psi_1}{\partial r}\Big|_{r=1} = \mathrm{Ma}\sin\theta\frac{\partial\Gamma_1}{\partial\theta}, & \end{cases} \tag{A.11}$$

and

$$\begin{cases} \nabla^2 C_1 = 0, & \\ \Gamma_1 = 1, & \\ C_1 = 0 & \text{as} \quad r \to \infty, \\ \frac{1}{\sin\theta}\frac{\partial}{\partial\theta}(\sin\theta u_{0\theta}\Gamma_1) = \frac{\chi}{Q}\frac{\partial C_1}{\partial r}\Big|_{r=1}, & \end{cases} \tag{A.12}$$

where

$$u_{0\theta}|_{r=1} = \frac{1}{\sin\theta}\frac{\partial\psi_0}{\partial r} = \frac{\sin\theta}{2},$$

follows from the leading order solutions. Since $\Gamma_1 = 1$ the boundary conditions involving Γ_1 in (A.11) and (A.12) become

$$\frac{\partial^2\psi}{\partial r^2} - 2\frac{\partial\psi}{\partial r}\bigg|_{r=1} = 0, \tag{A.13}$$

$$\frac{\partial C_1}{\partial r}\bigg|_{r=1} = \frac{Q}{\chi}\cos\theta. \tag{A.14}$$

Thus, the solution for (A.11) is

$$\psi_1 = 0, \tag{A.15}$$

and the general solution for (A.12) is of the form

$$C_1 = \sum_{n=0}^{\infty} b_n r^{-(n+1)} P_n(\cos\theta). \tag{A.16}$$

Applying boundary condition (A.14) on equation (A.16) implies

$$b_1 = -\frac{Q}{2\chi}, \qquad b_n = 0 \qquad \text{for} \qquad n \neq 1.$$

It follows, then, that the solution for (A.12) is

$$C_1 = -\frac{Q}{2\chi}\frac{\cos\theta}{r^2}. \tag{A.17}$$

A.1.3 Third Order Solution

At $O(k^2)$ the problem is

$$\begin{cases} E^4\psi_2 = 0, & \\ \psi_2 = 0 & \text{at} \quad r=1, \quad \theta = 0, \pi, \\ \frac{\psi_2}{r^2} = 0 & \text{as} \quad r \to \infty, \\ \frac{\partial^2\psi_2}{\partial r^2} - 2\frac{\partial\psi_2}{\partial r}\Big|_{r=1} = \mathrm{Ma}\sin\theta\frac{\partial\Gamma_2}{\partial\theta}, & \end{cases} \tag{A.18}$$

and for the concentration

$$\begin{cases} \nabla^2 C_2 = Q\left(u_{0r}\frac{\partial C_1}{\partial r} + \frac{u_{0\theta}}{r}\frac{\partial C_1}{\partial\theta}\right) & \\ C_2 = 0 & \text{as} \quad r \to \infty, \\ \Gamma_2 = C_{1s} - \Gamma_1 C_{0s}, & \\ \frac{1}{\sin\theta}\frac{\partial}{\partial\theta}(\sin\theta u_{0\theta}\Gamma_2) = \frac{\chi}{Q}\frac{\partial C_2}{\partial r}\Big|_{r=1}. & \end{cases} \tag{A.19}$$

As we showed in Section 3.2.2 in Chapter 3, the general solution for ψ_2 that satisfies the first two boundary conditions of (A.18) is

$$\psi_2 = \sum_{n=2}^{\infty} A_n(r^{-n+1} - r^{-n+3})C_n^{-\frac{1}{2}}(\cos\theta), \tag{A.20}$$

where $C_n^{-\frac{1}{2}}(x)$ are the Gegenbauer polynomials of order $-\frac{1}{2}$. Using this solution along with the known expression for Γ_2 (see (A.19) and (A.17)) provides the following equation connecting the unknown constants A_n,

$$\frac{Q\mathrm{Ma}}{2\chi}\sin^2\theta = 2\sum_{n=2}^{\infty}(2n-1)A_n C_n^{-\frac{1}{2}}(\cos\theta),$$

from which it follows (using the properties of the Gegenbauer polynomials) that

$$A_2 = \frac{Q\mathrm{Ma}}{6\chi}, \qquad A_n = 0 \qquad \text{otherwise.}$$

Hence,

$$\psi_2 = \frac{Q\mathrm{Ma}}{12\chi}\left(\frac{1}{r} - r\right)\sin^2\theta. \tag{A.21}$$

Next, with ψ_0 and C_1 known, the concentration C_2 in (A.19) satisfies

$$\nabla^2 C_2 = \frac{Q^2}{\chi}\left[\cos^2\theta\left(\frac{1}{r^4} - \frac{1}{r^3}\right) + \sin^2\theta\left(\frac{1}{2r^3} - \frac{1}{3r^4}\right)\right] \tag{A.22}$$

Seeking a solution of the form

$$C_2(r,\theta) = \sum_{n=0}^{\infty} f_n(r) P_n(\cos\theta), \tag{A.23}$$

we find that the unknown functions $f_n(r)$ satisfy

$$\frac{1}{r^2}\frac{d}{dr}(r^2 f_0') = \frac{Q^2}{6\chi r^4}, \tag{A.24}$$

$$\frac{1}{r^2}\frac{d}{dr}(r^2 f_2') - \frac{6}{r^2} f_2 = \frac{Q^2}{6\chi}\left(\frac{5}{r^4} - \frac{6}{r^3}\right), \tag{A.25}$$

$$\frac{1}{r^2}\frac{d}{dr}(r^2 f_n') - \frac{n(n+1)}{r^2} f_n = 0 \qquad \text{for} \qquad n \neq 0, 2. \tag{A.26}$$

The general solutions are,

$$f_0 = \frac{Q}{12\chi r^2} - \frac{d_0}{r} + b_0, \tag{A.27}$$

$$f_2 = \frac{Q^2}{6\chi}\left(\frac{1}{r} - \frac{5}{4r^2}\right) + \frac{d_2}{r^3} + b_2 r^2, \tag{A.28}$$

$$f_n = b_n r^n + d_n r^{-(n+1)} \qquad \text{for} \qquad n \neq 0, 2, \tag{A.29}$$

and since $C_2 \to 0$ as $r \to \infty$, we require $b_n = 0$ for all n. Hence the general solution for C_2 assumes the form

$$C_2 = \sum_{n=0}^{\infty} d_n r^{-(n+1)} P_n(\cos\theta) + \frac{Q^2}{12\chi r^2} + \frac{Q^2}{6\chi}\left(\frac{1}{r} - \frac{5}{4r^2}\right) P_2(\cos\theta), \tag{A.30}$$

and the constants d_n can be found by substitution into the surfactant concentration boundary condition in equation (A.19). The result is

$$d_0 = -\frac{Q^2}{6\chi}, \qquad d_1 = \frac{Q}{2\chi}, \tag{A.31}$$

$$d_2 = \frac{Q^2}{12\chi}\left(1+\frac{2}{\chi}\right), \qquad d_n = 0 \quad \text{for} \quad n \geq 3. \tag{A.32}$$

This together with (A.30) determines C_2, which is given by

$$C_2(r,\theta) = \frac{Q}{2\chi}\frac{P_1(\cos\theta)}{r^2} + \frac{Q^2}{6\chi}\left(\frac{2+\chi}{2\chi}\frac{1}{r^3} - \frac{3}{4r^2}\right)P_2(\cos\theta). \tag{A.33}$$

A.1.4 Fourth Order Solution

Finally we consider the $O(k^3)$ problems

$$\begin{cases} E^4\psi_3 = 0, \\ \psi_3 = 0 \qquad \text{at} \qquad r = 1, \quad \theta = 0, \pi, \\ \frac{\psi_3}{r^2} = 0 \qquad \text{as} \qquad r \to \infty, \\ \frac{\partial^2\psi_3}{\partial r^2} - 2\frac{\partial\psi_3}{\partial r}\Big|_{r=1} = \mathrm{Ma}\sin\theta\frac{\partial\Gamma_3}{\partial\theta} + \Gamma_1\left(\frac{\partial^2\psi_2}{\partial r^2} - 2\frac{\partial\psi_2}{\partial r}\right), \end{cases} \tag{A.34}$$

and

$$\begin{cases} \nabla^2 C_3 = Q\left(u_{0r}\frac{\partial C_2}{\partial r} + \frac{u_{0\theta}}{r}\frac{\partial C_2}{\partial\theta}\right) \\ C_3 = 0 \qquad\qquad \text{as} \qquad r \to \infty, \\ \Gamma_3 = C_{2s} - \Gamma_1 C_{1s} - C_{0s}\Gamma_2, \\ \frac{1}{\sin\theta}\frac{\partial}{\partial\theta}[\sin\theta(u_{0\theta}\Gamma_3 + u_{2\theta}\Gamma_1)] = \frac{\chi}{Q}\frac{\partial C_3}{\partial r}\Big|_{r=1}. \end{cases} \tag{A.35}$$

The solution for ψ_3 has the same form as that for ψ_2. Writing

$$\psi_3 = \sum_{n=2}^{\infty} B_n(r^{-n+1} - r^{-n+3})C_n^{-\frac{1}{2}}(\cos\theta),$$

the coefficients B_n are determined by substitution into the last boundary condition of (A.34) and use of the solutions already found for Γ_1, Γ_2, C_1 and C_2 (note that these determine Γ_3 which enters into the boundary conditions). The solution, then, is found to be

$$\begin{aligned}\psi_3(r,\theta) = &-\frac{Q\mathrm{Ma}}{3\chi}\left(\frac{1}{r}-r\right)C_2^{-\frac{1}{2}}(\cos\theta)\\ &-\frac{Q^2\mathrm{Ma}}{40\chi}\left(1+\frac{4}{\chi}\right)\left(\frac{1}{r^2}-1\right)C_3^{-\frac{1}{2}}(\cos\theta).\end{aligned} \tag{A.36}$$

Our interest is in computing the drag up to and including $O(k^3)$, so the solution for C_3 is not required.

A.2 Asymptotic Expression for the Drag

Letting the drag on the bubble be C_{D1}, the limit considered here implies the expansion

$$C_{D1} = D_0 + kD_1 + k^2D_2 + k^3D_3 + \cdots \quad . \tag{A.37}$$

The total drag on the bubble is found by integration of the forces acting on the interface and since the flow is axisymmetric, the drag is the magnitude of the total force acting along the axis of symmetry and opposing the motion. The drag is (see Section 2.4.2.1) (in what follows p_1 is the dimensionless pressure at the bubble surface)

$$\begin{aligned}C_{D1} &= \int_0^\pi \left(\sin^2\theta\frac{\partial p_1}{\partial\theta} - 2\sin\theta\frac{\partial^2\psi}{\partial r^2}\right)d\theta\\ &= \int_0^\pi \left(\sin\theta\frac{\partial^3\psi}{\partial r^3} - 6\sin\theta\frac{\partial\psi}{\partial r} - 2\mathrm{Ma}\frac{\sin^2\theta}{1-\Gamma}\frac{\partial\Gamma}{\partial\theta}\right)d\theta.\end{aligned}$$

Substituting equation (A.37) into above equation and using the solutions ψ_0, ψ_1, ψ_2, ψ_3, Γ_2 and Γ_3 given above determines the coefficients in the expansion (A.37) for the drag to be

$$
\begin{aligned}
D_0 &= \int_0^\pi \left(\frac{\partial^2 \psi_0}{\partial r^3} - 6\frac{\partial \psi_0}{\partial \theta} \right) \sin\theta \, d\theta = -4, \\
D_1 &= \int_0^\pi \left(\frac{\partial^2 \psi_1}{\partial r^3} - 6\frac{\partial \psi_1}{\partial \theta} \right) \sin\theta \, d\theta = 0, \\
D_2 &= \int_0^\pi \left(\frac{\partial^2 \psi_2}{\partial r^3} - 6\frac{\partial \psi_2}{\partial \theta} - 2\mathrm{Ma}\sin\theta \frac{\partial \Gamma_2}{\partial \theta} \right) \sin\theta \, d\theta \\
&= -\frac{Q\mathrm{Ma}}{2\chi} \int_0^\pi \sin^3\theta \, d\theta = -\frac{2Q\mathrm{Ma}}{3\chi}, \\
D_3 &= \int_0^\pi \left[\frac{\partial^2 \psi_3}{\partial r^3} - 6\frac{\partial \psi_3}{\partial \theta} - 2\mathrm{Ma}\sin\theta \left(\frac{\partial \Gamma_2}{\partial \theta} + \frac{\partial \Gamma_3}{\partial \theta} \right) \right] \sin\theta \, d\theta \\
&= \frac{2Q\mathrm{Ma}}{\chi} \int_{-1}^1 C_2^{-\frac{1}{2}}(z) \, dz + \frac{4Q^2\mathrm{Ma}}{5\chi} \left(1 + \frac{4}{\chi} \right) \int_{-1}^1 C_3^{-\frac{1}{2}}(z) \, dz \\
&= \frac{4Q\mathrm{Ma}}{3\chi}.
\end{aligned}
$$

The relation (3.8) in Chapter 3 has been used here. The asymptotic result for the drag C_{D1} follows, then,

$$
C_{D1} = -4 - \frac{2Q\mathrm{Ma}}{3\chi} k^2 + \frac{4Q\mathrm{Ma}}{3\chi} k^3 + \cdots \quad . \tag{A.38}
$$

APPENDIX B

ANALYTICAL SOLUTIONS WITHOUT FLOW

Two time dependent analytic solutions are provided for checking the accuracy of our numerical results. The problem is reduced to simple cases where it can be solved analytically, by assuming that there is no flow around the bubble. The solutions are obtained using Laplace transforms.

When there is no flow ($\boldsymbol{u} = \mathbf{0}$), the convection-diffusion equation (2.48) and equation (2.59) become

$$\frac{\partial C}{\partial t} = \frac{1}{\mathrm{Pe}} \nabla^2 C, \tag{B.1}$$

$$\frac{\partial \Gamma}{\partial t} = \frac{\chi_0}{\mathrm{Pe}} \left. \frac{\partial C}{\partial r} \right|_{r=1}, \tag{B.2}$$

where $\chi_0 = \chi k$.

Without loss of generality we rescale time as $t = \tau \mathrm{Pe}$ to obtain

$$\frac{\partial C}{\partial \tau} = \nabla^2 C, \tag{B.3}$$

$$\frac{\partial \Gamma}{\partial \tau} = \chi_0 \left. \frac{\partial C}{\partial r} \right|_{r=1}. \tag{B.4}$$

The problem can be solved analytically, if the bulk concentration is very small ($k \ll 1$) or the bubble is taken as an infinite sink ($C = 0$ on the surface).

B.1 Small Bulk Concentration

When $k \ll 1$, a linear relation between surface concentration Γ and sublayer concentration $C(r = 1)$ may be assumed, i.e. the boundary condition (2.60) can be written as

$$\Gamma = kC \qquad \text{at} \qquad r = 1.$$

Without loss of generality, we assume initially

$$C = 1, \qquad \Gamma = 0.$$

The initial boundary value problem reduces to

$$\begin{cases} \dfrac{\partial C}{\partial \tau} = \nabla^2 C & & \\ \dfrac{\partial \Gamma}{\partial \tau} = \chi_0 \left.\dfrac{\partial C}{\partial r}\right|_{r=1} & & \\ \Gamma = kC & \text{at} & r = 1 \\ \Gamma = 0 & \text{at} & \tau = 0 \\ C = 1 & \text{as} & r \to \infty \\ C = 1 & \text{at} & \tau = 0 \end{cases} \tag{B.5}$$

Since there is no flow around the bubble, the solution only depends on the radial distance r. The boundary condition at infinity suggests a solution of the form

$$C = 1 + \frac{\Phi(r, \tau)}{r}. \tag{B.6}$$

Substitution of equation (B.6) into system (B.5), gives

$$\frac{\partial \Phi}{\partial \tau} = \frac{\partial^2 \Phi}{\partial r^2}, \tag{B.7}$$

subject to the boundary conditions

$$|\Phi| < \infty \qquad \text{as} \qquad r \to \infty, \tag{B.8}$$

$$\Gamma = k(1 + \Phi) \qquad \text{at} \qquad r = 1, \tag{B.9}$$

$$\frac{\partial \Gamma}{\partial \tau} = \chi_0(\Phi_r - \Phi) \qquad \text{at} \qquad r = 1, \tag{B.10}$$

and the initial conditions

$$\Phi = 0, \qquad \Gamma = 0. \tag{B.11}$$

If we take the Laplace transform in time of the differential equation (B.7), we obtain

$$\frac{\partial^2 \hat{\Phi}}{\partial r^2} - s\hat{\Phi} = 0,$$

where $\hat{\Phi}$ is the Laplace transform of Φ defined as

$$\hat{\Phi} = \mathcal{L}[\Phi] = \int_0^\infty \Phi e^{-s\tau} d\tau. \tag{B.12}$$

The general solution for $\hat{\Phi}$ is

$$\hat{\Phi} = A(s)e^{-\sqrt{s}r}. \tag{B.13}$$

Here we choose the real part of $\sqrt{s}$ to be positive to give a bounded solution. Taking the Laplace transform of both sides of equations (B.9) and (B.10), and using the relation (B.13), we have,

$$s\hat{\Gamma} = -A\chi_0(\sqrt{s}+1)e^{-\sqrt{s}}, \tag{B.14}$$

$$\hat{\Gamma} = k(\frac{1}{s} + Ae^{-\sqrt{s}}), \tag{B.15}$$

where $\hat{\Gamma} = \mathcal{L}[\Gamma]$. It follows that

$$A = -\frac{ke^{\sqrt{s}}}{ks + \chi_0(\sqrt{s}+1)}. \tag{B.16}$$

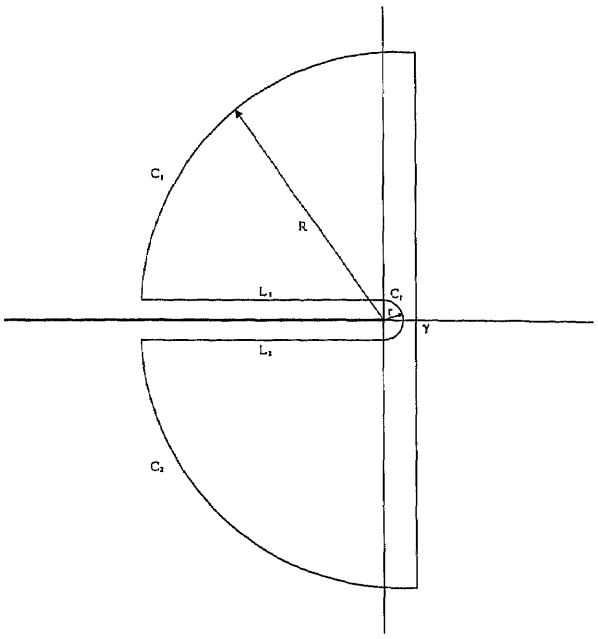

Figure B.1 Contour for integral of Eq. (B.18)

Substituting equation (B.16) into equation (B.13), gives

$$\hat{\Phi}(r,s) = -\frac{ke^{-\sqrt{s}(r-1)}}{ks + \chi_0(\sqrt{s}+1)}. \tag{B.17}$$

Now we use the contour L which is shown in Figure B.1 to find the inverse Laplace transform of $\hat{\Phi}$. Since $Re(\sqrt{s}) > 0$, the function $\hat{\Phi}$ has no singularity in the region that is bounded by the curve L, hence

$$\int_L \hat{\Phi} e^{s\tau} ds = 0. \tag{B.18}$$

This leads to

$$\begin{aligned} \Phi &= \frac{1}{2\pi i}\int_{\gamma-i\infty}^{\gamma+i\infty} \hat{\Phi} e^{s\tau} ds \\ &= -\frac{1}{2\pi i}\left(\int_{L_1} \hat{\Phi} e^{s\tau} ds + \int_{L_2} \hat{\Phi} e^{s\tau} ds + \int_{C_1+C_2} \hat{\Phi} e^{s\tau} ds + \int_{C_r} \hat{\Phi} e^{s\tau} ds\right). \end{aligned} \tag{B.19}$$

The last two terms of the above expression vanish as $R \to \infty$ and $r \to 0$. Hence

$$\begin{aligned}
\Phi &= -\frac{1}{2\pi i}\left(\int_{L_1} \hat{\Phi} e^{s\tau} ds + \int_{L_2} \hat{\Phi} e^{s\tau} ds\right) \\
&= \frac{1}{2\pi i}\left(\int_{L_1} \frac{k e^{-\sqrt{s}(r-1)}}{ks + \chi_0(\sqrt{s}+1)} e^{s\tau} ds + \int_{L_2} \frac{k e^{-\sqrt{s}(r-1)}}{ks + \chi_0(\sqrt{s}+1)} e^{s\tau} ds\right) \\
&= \frac{1}{2\pi i}\left(\int_{\infty}^{0} \frac{-k e^{-i\sqrt{y}(r-1)} e^{-y\tau}}{-ky + \chi_0(i\sqrt{y}+1)} dy + \int_{0}^{\infty} \frac{-k e^{i\sqrt{y}(r-1)} e^{-y\tau}}{-ky + \chi_0(-i\sqrt{y}+1)} dy\right) \\
&= \frac{k}{2\pi i}\int_0^{\infty} \left(\frac{e^{-i\sqrt{y}(r-1)}}{(\chi_0 - ky) + i\chi_0\sqrt{y}} - \frac{e^{i\sqrt{y}(r-1)}}{(\chi_0 - ky) - i\chi_0\sqrt{y}}\right) e^{-y\tau} dy \\
&= -\frac{k}{\pi}\int_0^{\infty} \frac{\chi_0\sqrt{y}\cos(\sqrt{y}(r-1)) + (\chi_0 - ky)\sin(\sqrt{y}(r-1))}{(\chi_0 - ky)^2 + \chi_0^2 y} e^{-y\tau} dy \\
&= -\frac{1}{\pi}\int_0^{\infty} \frac{\chi\sqrt{y}\cos(\sqrt{y}(r-1)) + (\chi - y)\sin(\sqrt{y}(r-1))}{(\chi - y)^2 + \chi^2 y} e^{-y\tau} dy
\end{aligned} \tag{B.20}$$

The solutions for system (B.5) follow by substitution of (B.20) into equations (B.6) and (B.9), and are

$$\begin{aligned}
C &= 1 - \frac{1}{\pi r}\int_0^{\infty} \frac{\chi\sqrt{y}\cos(\sqrt{y}(r-1)) + (\chi - y)\sin(\sqrt{y}(r-1))}{(\chi - y)^2 + \chi^2 y} e^{-y\tau} dy, \\
\Gamma &= k - \frac{k}{\pi}\int_0^{\infty} \frac{\chi\sqrt{y} e^{-y\tau}}{(\chi - y)^2 + \chi^2 y} dy.
\end{aligned} \tag{B.21}$$

These integrals are calculated numerically in carrying out code validation.

B.2 Infinite Sink

For the particle as an infinite sink, the initial boundary value problem becomes

$$\begin{cases}
\dfrac{\partial C}{\partial \tau} = \nabla^2 C, & & \\
C = 0 & \text{at} & r = 1, \\
C = 1 & \text{as} & r \to \infty, \\
C = 1 & \text{at} & \tau = 0.
\end{cases} \tag{B.22}$$

We seek the solution in the same form as in equation (B.6). Let

$$C = 1 + \frac{\Psi(r,\tau)}{r}. \tag{B.23}$$

Substitute this into system (B.22) to get

$$\frac{\partial \Psi}{\partial \tau} = \frac{\partial^2 \Psi}{\partial r^2}, \tag{B.24}$$

with

$$|\Psi| < \infty, \qquad \Psi|_{r=1} = -1, \qquad \Psi|_{\tau=0} = 0. \tag{B.25}$$

Taking Laplace transforms as discussed in the previous Section, the solution for the Laplace transform of Ψ is

$$\hat{\Psi} = B(s)e^{-\sqrt{s}r}. \tag{B.26}$$

Applying boundary conditions (B.25) on equation (B.26) gives,

$$B = -\frac{e^{\sqrt{s}}}{s}.$$

It follows, then, from equation (B.26), that

$$\hat{\Psi}(r,s) = -\frac{1}{s}e^{-\sqrt{s}(r-1)}. \tag{B.27}$$

To find the solution for Ψ, we first find the solution for Ψ_r. To do so, we differentiate the equation (B.27) with respect to r to obtain

$$\frac{\partial \hat{\Psi}}{\partial r} = \frac{1}{\sqrt{s}}e^{-\sqrt{s}(r-1)}. \tag{B.28}$$

It follows readily by inversion of (B.28), that

$$\frac{\partial \Psi}{\partial r} = \frac{1}{\sqrt{\pi \tau}} e^{-\frac{(r-1)^2}{4\tau}}. \tag{B.29}$$

Integrating equation (B.29) with respect to r, and using the boundary conditions (B.25), we have

$$\begin{aligned} \Psi &= \frac{1}{\sqrt{\pi \tau}} \int_1^r e^{-\frac{(x-1)^2}{4\tau}} dx - 1 \\ &= \frac{2}{\sqrt{\pi}} \int_0^{\frac{r-1}{2\sqrt{\tau}}} e^{-y^2} dy - 1 \\ &= \operatorname{erf}\left(\frac{r-1}{2\sqrt{\tau}}\right) - 1. \end{aligned}$$

Substituting this into equation (B.23) gives the solution for system (B.22),

$$C(r, \tau) = 1 - \frac{1}{r} + \frac{1}{r} \operatorname{erf}\left(\frac{r-1}{2\sqrt{\tau}}\right). \tag{B.30}$$

APPENDIX C
FORMULAE AND CALCULATION DETAILS

In this Appendix, we provide evaluation of two integrals that were required in Chapter 5. Calculation details of the functions $G(u)$ on page 68 and $g(\theta)$ on page 68 are presented. A list of relations of Legendre polynomials, associated Legendre polynomials and Gegenbauer polynomials that we used in Chapter 5 and Appendix A is given at the end, followed by some useful integral formulae.

C.1 Calculation Details

C.1.1 Evaluation of Integrals

1. This integral is used for calculating $H(v)$ in equation (5.29) on page 65 in Chapter 5.

$$\int_v^\pi \frac{\sin\theta\cos^2\frac{\theta}{2}}{\sqrt{\cos v-\cos\theta}}\,d\theta = \frac{1}{2}\int_v^\pi \frac{\sin\theta(1+\cos\theta)}{\sqrt{\cos v-\cos\theta}}\,d\theta.$$

We make the change of variable $x=\cos\theta$, it follows then,

$$\begin{aligned}
&\int_v^\pi \frac{\sin\theta\cos^2\frac{\theta}{2}}{\sqrt{\cos v-\cos\theta}}\,d\theta \\
&= -\frac{1}{2}\int_{\cos v}^{-1}\frac{1+x}{\sqrt{\cos v-x}}\,dx \\
&= \int_{\cos v}^{-1}(1+x)\,d\sqrt{\cos v-x} \\
&= (1+x)\sqrt{\cos v-x}\Big|_{\cos v}^{-1} - \int_{\cos v}^{-1}\sqrt{\cos v-x}\,dx \\
&= \frac{2}{3}(\cos v-x)^{\frac{3}{2}}\Big|_{\cos v}^{-1} \\
&= \frac{2}{3}(1+\cos v)^{\frac{3}{2}}.
\end{aligned} \tag{C.1}$$

2. In what follows, we provide the calculation of the result (5.33) on page 66 in Chapter 5.

$$\begin{aligned}
&\int_{\pi-\varphi}^{v} \frac{\sin^3\frac{u}{2}\sin u}{\sqrt{\cos u-\cos v}}\,du \\
&\quad=-2\int_{\pi-\varphi}^{v}\sin^3\frac{u}{2}\,d\sqrt{\cos u-\cos v} \\
&\quad=-2\sin^3\frac{u}{2}\sqrt{\cos u-\cos v}\Big|_{\pi-\varphi}^{v}+3\int_{\pi-\varphi}^{v}\cos\frac{u}{2}\sin^2\frac{u}{2}\sqrt{\cos u-\cos v}\,du. \\
=\quad&2\cos^3\frac{\varphi}{2}\sqrt{\cos(\pi-\varphi)-\cos v}+3\int_{\pi-\varphi}^{v}\cos\frac{u}{2}\sin^2\frac{u}{2}\sqrt{\cos u-\cos v}\,du.
\end{aligned}$$

We now make the change of variable $x=\cos u$, substitute this into the above expression to find

$$\begin{aligned}
&\int_{\pi-\varphi}^{v} \frac{\sin^3\frac{u}{2}\sin u}{\sqrt{\cos u-\cos v}}\,du \\
&\quad=2\cos^3\frac{\varphi}{2}\sqrt{\cos(\pi-\varphi)-\cos v}-\frac{3}{2\sqrt{2}}\int_{\cos(\pi-\varphi)}^{\cos v}\sqrt{(1-x)(x-\cos v)}\,dx \\
&\quad=2\cos^3\frac{\varphi}{2}\sqrt{\cos(\pi-\varphi)-\cos v} \\
&\qquad-\frac{3}{2\sqrt{2}}\left[\frac{2x-1-\cos v}{4}\sqrt{(1-x)(x-\cos v)}\Big|_{\cos(\pi-\varphi)}^{\cos v}\right. \\
&\qquad\left.+\frac{(1-\cos v)^2}{8}\int_{\cos(\pi-\varphi)}^{\cos v}\frac{dx}{\sqrt{(1-x)(x-\cos v)}}\right] \\
&\quad=2\cos^3\frac{\varphi}{2}\sqrt{\cos(\pi-\varphi)-\cos v} \\
&\qquad-\frac{3}{2\sqrt{2}}\left[\frac{\sqrt{2}}{4}\cos\frac{\varphi}{2}(1+2\cos\varphi+\cos v)\sqrt{\cos(\pi-\varphi)-\cos v}\right. \\
&\qquad\left.+\frac{(1-\cos v)^2}{4}\sin^{-1}\sqrt{\frac{x-\cos v}{1-\cos v}}\Big|_{\cos(\pi-\varphi)}^{\cos v}\right] \\
&=\frac{3}{2\sqrt{2}}\sin^4\frac{v}{2}\sin^{-1}\sqrt{\frac{\cos(\pi-\varphi)-\cos v}{1-\cos v}} \\
&\qquad+\frac{1}{8}\cos\frac{\varphi}{2}(5+2\cos\varphi-3\cos v)\sqrt{\cos(\pi-\varphi)-\cos v}.
\end{aligned}$$

(C.2)

C.1.2 Calculation for $G(u)$

Here we show the result (5.40) for $G(u)$ on page 68 in Chapter 5. The expression of $G(u)$ in integral form is given by

$$G(u) = -\frac{\sqrt{2}}{\pi}\int_{\pi-\varphi}^{\pi} \frac{\cos^2\frac{\zeta}{2}}{\sqrt{\cos u - \cos\zeta}}\left[\frac{3\sin\zeta}{2\sqrt{2}}\sin^{-1}\sqrt{\frac{\cos(\pi-\varphi)-\cos\zeta}{1-\cos\zeta}}\right. \\ \left. + \frac{\cos\frac{\varphi}{2}\sin\zeta}{\sqrt{\cos(\pi-\varphi)-\cos\zeta}} + \frac{1}{2}\cos\frac{\varphi}{2}\cot\frac{\zeta}{2}\sqrt{\cos(\pi-\varphi)-\cos\zeta}\right] d\zeta. \tag{C.3}$$

We make the change of variable $x = \cos\zeta$. Also, we write $a = \cos u$ and $b = \cos(\pi-\varphi)$ for simplicity. Multiply both sides of the above equation by $-\frac{\pi}{\sqrt{2}}$. It follows that

$$\begin{aligned}
-\frac{\pi}{\sqrt{2}}G(u) &= -\frac{3}{4\sqrt{2}}\int_b^{-1}\frac{1+x}{\sqrt{a-x}}\sin^{-1}\sqrt{\frac{b-x}{1-x}}\,dx - \frac{\cos\frac{\varphi}{2}}{2}\int_b^{-1}\frac{(1+x)\,dx}{\sqrt{(a-x)(b-x)}} \\
&\quad - \frac{\cos\frac{\varphi}{2}}{4}\int_b^{-1}\frac{1+x}{1-x}\sqrt{\frac{b-x}{a-x}}\,dx \\
&= \frac{3}{2\sqrt{2}}\left[(1+x)\sqrt{a-x}\sin^{-1}\sqrt{\frac{b-x}{1-x}}\Big|_b^{-1} - \int_b^{-1}\sqrt{a-x}\sin^{-1}\sqrt{\frac{b-x}{1-x}}\,dx\right. \\
&\quad \left. + \frac{\sqrt{1-b}}{2}\int_b^{-1}\frac{1+x}{1-x}\sqrt{\frac{a-x}{b-x}}\,dx\right] \\
&\quad - \frac{\cos\frac{\varphi}{2}}{2}\int_b^{-1}\frac{(1+x)\,dx}{\sqrt{(a-x)(b-x)}} - \frac{\cos\frac{\varphi}{2}}{4}\int_b^{-1}\frac{1+x}{1-x}\sqrt{\frac{b-x}{a-x}}\,dx \\
&= -\frac{3}{2\sqrt{2}}\int_b^{-1}\sqrt{a-x}\sin^{-1}\sqrt{\frac{b-x}{1-x}}\,dx + \frac{3}{4}\cos\frac{\varphi}{2}\int_b^{-1}\frac{1+x}{1-x}\sqrt{\frac{a-x}{b-x}}\,dx \\
&\quad - \frac{\cos\frac{\varphi}{2}}{2}\int_b^{-1}\frac{1+x}{\sqrt{(a-x)(b-x)}}\,dx - \frac{\cos\frac{\varphi}{2}}{4}\int_b^{-1}\frac{1+x}{1-x}\sqrt{\frac{b-x}{a-x}}\,dx \\
&= \frac{\sqrt{2}}{2}\left[(a-x)^{\frac{3}{2}}\sin^{-1}\sqrt{\frac{b-x}{1-x}}\Big|_b^{-1} + \frac{\sqrt{1-b}}{2}\int_b^{-1}\frac{(a-x)^{\frac{3}{2}}}{(1-x)\sqrt{b-x}}\,dx\right] \\
&\quad + \frac{3}{4}\cos\frac{\varphi}{2}\int_b^{-1}\frac{1+x}{1-x}\sqrt{\frac{a-x}{b-x}}\,dx - \frac{\cos\frac{\varphi}{2}}{2}\int_b^{-1}\frac{(1+x)\,dx}{\sqrt{(a-x)(b-x)}} \\
&\quad - \frac{\cos\frac{\varphi}{2}}{4}\int_b^{-1}\frac{1+x}{1-x}\sqrt{\frac{b-x}{a-x}}\,dx
\end{aligned}$$

(continued on next page)

$$
\begin{aligned}
&= \frac{\sqrt{2}\varphi}{4}(1+a)^{\frac{3}{2}} + \frac{\cos\frac{\varphi}{2}}{2}\int_b^{-1} \frac{(a-x)^{\frac{3}{2}}}{(1-x)\sqrt{b-x}}\,dx \\
&\quad + \frac{3}{4}\cos\frac{\varphi}{2}\int_b^{-1} \frac{1+x}{1-x}\sqrt{\frac{a-x}{b-x}}\,dx - \frac{\cos\frac{\varphi}{2}}{2}\int_b^{-1} \frac{(1+x)\,dx}{\sqrt{(a-x)(b-x)}} \\
&\quad - \frac{\cos\frac{\varphi}{2}}{4}\int_b^{-1} \frac{1+x}{1-x}\sqrt{\frac{b-x}{a-x}}\,dx \\
&= \frac{\sqrt{2}\varphi}{4}(1+a)^{\frac{3}{2}} + \frac{\cos\frac{\varphi}{2}}{4}\int_b^{-1} \left[\frac{2(a-x)^2}{1-x} + \frac{3(1+x)(a-x)}{1-x} - 2(1+x)\right. \\
&\quad \left. - \frac{(1+x)(b-x)}{1-x}\right] \frac{dx}{\sqrt{(a-x)(b-x)}} \\
&= \frac{\sqrt{2}\varphi}{4}(1+a)^{\frac{3}{2}} + \frac{\cos\frac{\varphi}{2}}{4}\int_b^{-1} \frac{2x^2 - (a+b+2)x + 2a^2 + 3a - b - 2}{(1-x)\sqrt{(a-x)(b-x)}}\,dx \\
&= \frac{\sqrt{2}\varphi}{4}(1+a)^{\frac{3}{2}} + \frac{\cos\frac{\varphi}{2}}{4}\int_b^{-1} \frac{-(2x-a-b)(1-x) + 2(a^2+a-b-1)}{(1-x)\sqrt{(a-x)(b-x)}}\,dx \\
&= \frac{\sqrt{2}\varphi}{4}(1+a)^{\frac{3}{2}} \\
&\quad + \frac{\cos\frac{\varphi}{2}}{4}\int_b^{-1} \left[\frac{a+b-2x}{\sqrt{(a-x)(b-x)}} + \frac{2(a^2+a-b-1)}{(1-x)\sqrt{(a-x)(b-x)}}\right] dx \\
&= \frac{\sqrt{2}\varphi}{4}(1+a)^{\frac{3}{2}} \\
&\quad + \frac{\cos\frac{\varphi}{2}}{4}\left[-2\sqrt{(a-x)(b-x)}\Big|_b^{-1} + 2(a^2+a-b-1)\int_b^{-1} \frac{dx}{(1-x)\sqrt{(a-x)(b-x)}}\right] \\
&= \frac{\sqrt{2}\varphi}{4}(1+a)^{\frac{3}{2}} - \frac{\cos\frac{\varphi}{2}}{2}\sqrt{(1+a)(1+b)} \\
&\quad + \frac{\cos\frac{\varphi}{2}}{2}\frac{(a^2+a-b-1)}{\sqrt{(1-a)(1-b)}}\ln\left|\frac{\sqrt{(a-x)(b-x)} + \sqrt{(1-a)(1-b)}}{1-x} + \frac{a+b-2}{2\sqrt{(1-a)(1-b)}}\right| \\
&= \frac{\sqrt{2}\varphi}{4}(1+a)^{\frac{3}{2}} - \frac{\cos\frac{\varphi}{2}}{2}\sqrt{(1+a)(1+b)} \\
&\quad + \frac{\cos\frac{\varphi}{2}}{2}\frac{(a^2+a-b-1)}{\sqrt{(1-a)(1-b)}}\ln\left|\frac{\sqrt{(1-a^2)(1-b^2)} + ab - 1}{a-b}\right|.
\end{aligned}
$$

(C.4)

Substitute $a = \cos u$, $b = \cos(\pi - \varphi)$ back into equation, we obtain

$$\begin{aligned}
-\frac{\pi}{\sqrt{2}}G(u) &= \frac{\sqrt{2}\varphi}{4}(1+a)^{\frac{3}{2}} - \frac{\cos\frac{\varphi}{2}}{2}\sqrt{(1+\cos u)(1-\cos\varphi)} \\
&\quad + \frac{\cos\frac{\varphi}{2}}{2}\frac{(\cos^2 u + \cos u + \cos\varphi - 1)}{\sqrt{(1-\cos u)(1+\cos\varphi)}}\ln\left|\frac{\sin u\sin\varphi - \cos u\cos\varphi - 1}{\cos u - \cos(\pi-\varphi)}\right| \\
&= \varphi\cos^3\frac{u}{2} - \frac{\sqrt{2}}{4}\sin\varphi\sqrt{1+\cos u} \\
&\quad + \frac{\sqrt{2}}{4}\frac{(1-\cos u - \cos^2 u - \cos\varphi)}{\sqrt{1-\cos u}}\ln\left|\frac{1+\cos u\cos\varphi + \sin u\sin\varphi}{\cos u + \cos\varphi}\right| \\
&= \varphi\cos^3\frac{u}{2} - \frac{\sin\varphi}{2}\cos\frac{u}{2} \\
&\quad + \frac{\sin^2 u - \cos u - \cos\varphi}{4\sin\frac{u}{2}}\ln\left|\frac{\cos\frac{u-\varphi}{2}}{\cos\frac{u+\varphi}{2}}\right|.
\end{aligned} \tag{C.5}$$

The result (5.40) follows by multiplying equation (C.5) by $-\frac{\sqrt{2}}{\pi}$.

C.1.3 Calculation for $g(\theta)$

The calculation of result (5.41) on page 68 in Chapter 5 is given below.

$$\begin{aligned}
g(\theta) &= \frac{\cot\frac{\theta}{2}}{\pi}\int_0^\theta \frac{G(u)\tan^2\frac{u}{2}}{\sqrt{\cos u - \cos\theta}}\,du \\
&= -\frac{\sqrt{2}}{\pi^2}\cot\frac{\theta}{2}\int_0^\theta \left(\varphi\cos^3\frac{u}{2} - \frac{\sin\varphi}{2}\cos\frac{u}{2}\right. \\
&\quad \left. + \ln\left|\frac{\cos\frac{u-\varphi}{2}}{\cos\frac{u+\varphi}{2}}\right|\frac{\sin^2 u - \cos u - \cos\varphi}{4\sin\frac{u}{2}}\right)\frac{\tan^2\frac{u}{2}}{\sqrt{\cos u - \cos\theta}}\,du \\
&= \frac{\cot\frac{\theta}{2}}{\pi^2}\left[-\sqrt{2}\varphi\int_0^\theta \frac{\cos^3\frac{u}{2}\tan^2\frac{u}{2}}{\sqrt{\cos u - \cos\theta}}\,du + \frac{\sin\varphi}{2}\int_0^\theta \frac{\sqrt{1+\cos u}\tan^2\frac{u}{2}}{\sqrt{\cos u - \cos\theta}}\,du\right. \\
&\quad \left. -\frac{1}{2}\int_0^\theta \frac{(1-\cos u - \cos^2 u - \cos\varphi)\tan^2\frac{u}{2}}{\sqrt{(1-\cos u)(\cos u - \cos\theta)}}\ln\left|\frac{\cos\frac{u-\varphi}{2}}{\cos\frac{u+\varphi}{2}}\right|\right] \\
&= \frac{\cot\frac{\theta}{2}}{\pi^2}\left(-\sqrt{2}\varphi I + \frac{\sin\varphi}{2}II - \frac{1}{2}III\right),
\end{aligned} \tag{C.6}$$

where the integrals I, II and III are given by

$$
\begin{aligned}
I &= \int_0^\theta \frac{\cos^3\frac{u}{2}\tan^2\frac{u}{2}}{\sqrt{\cos u-\cos\theta}}\,du,\\
II &= \int_0^\theta \frac{\sqrt{1+\cos u}\tan^2\frac{u}{2}}{\sqrt{\cos u-\cos\theta}}\,du,\\
III &= \int_0^\theta \frac{(1-\cos u-\cos^2 u-\cos\varphi)\tan^2\frac{u}{2}}{\sqrt{(1-\cos u)(\cos u-\cos\theta)}}\ln\left|\frac{\cos\frac{u-\varphi}{2}}{\cos\frac{u+\varphi}{2}}\right|du,
\end{aligned}
$$

and are evaluated next.

1. Calculation for integral I.

$$
\begin{aligned}
I &= \int_0^\theta \frac{\cos^3\frac{u}{2}\tan^2\frac{u}{2}}{\sqrt{\cos u-\cos\theta}}\,du\\
&= \frac{1}{2\sqrt{2}}\int_0^\theta \frac{\sin u\sqrt{1-\cos u}}{\sqrt{\cos u-\cos\theta}}\,du\\
&= \frac{1}{2\sqrt{2}}\int_{\cos\theta}^1 \sqrt{\frac{1-x}{x-\cos\theta}}\,dx \qquad (x=\cos u)\\
&= \frac{1}{2\sqrt{2}}\left[\sqrt{(1-x)(x-\cos\theta)}+(1-\cos\theta)\sin^{-1}\sqrt{\frac{x-\cos\theta}{1-\cos\theta}}\right]\Bigg|_{\cos\theta}^1\\
&= \frac{\sqrt{2}\pi}{4}\sin^2\frac{\theta}{2}.
\end{aligned}
\tag{C.7}
$$

2. Calculation for integral II.

$$
\begin{aligned}
II &= \int_0^\theta \frac{\sqrt{1+\cos u}\tan^2\frac{u}{2}}{\sqrt{\cos u-\cos\theta}}\,du\\
&= \int_0^\theta \frac{1-\cos u}{\sqrt{(1+\cos u)(\cos u-\cos\theta)}}\,du\\
&= \int_{\cos\theta}^1 \frac{\sqrt{1-x}}{(1+x)\sqrt{x-\cos\theta}}\,dx \qquad (x=\cos u)\\
&= \sec\frac{\theta}{2}\sin^{-1}\left[\frac{(3+\cos\theta)x-1-3\cos\theta}{(1+x)(1-\cos\theta)}-2\sin^{-1}\sqrt{\frac{x-\cos\theta}{1-\cos\theta}}\Bigg|_{\cos\theta}^1\right]\\
&= \pi(\sec\frac{\theta}{2}-1).
\end{aligned}
\tag{C.8}
$$

3. Calculation for integral III.

$$III = \int_0^\theta \frac{(1-\cos u-\cos^2 u-\cos\varphi)\tan^2\frac{u}{2}}{\sqrt{(1-\cos u)(\cos u-\cos\theta)}} \ln\left|\frac{\cos\frac{u-\varphi}{2}}{\cos\frac{u+\varphi}{2}}\right| du$$
$$= \int_0^\theta \frac{\sin u(1-\cos u-\cos^2 u-\cos\varphi)}{(1+\cos u)^{\frac{3}{2}}\sqrt{\cos u-\cos\theta}} \ln\left|\frac{1+\cos u\cos\varphi+\sin u\sin\varphi}{\cos u+\cos\varphi}\right| du.$$

We make the change of variable $x=\cos u$, then the integral III becomes

$$III = \int_{\cos\theta}^1 \frac{1-x-x^2-\cos\varphi}{(1+x)^{\frac{3}{2}}\sqrt{x-\cos\theta}} \ln\left|\frac{1+x\cos\varphi+\sin\varphi\sqrt{1-x^2}}{x+\cos\varphi}\right| dx$$
$$= \int_{\cos\theta}^1 \left[\frac{1-\cos\varphi}{(1+x)^{\frac{3}{2}}\sqrt{x-\cos\theta}} - \frac{2x+(1-\cos)\theta}{2\sqrt{(1+x)(x-\cos\theta)}}\right.$$
$$\left. + \frac{1-\cos\theta}{2\sqrt{(1+x)(x-\cos\theta)}}\right] \ln\left|\frac{1+x\cos\varphi+\sin\varphi\sqrt{1-x^2}}{x+\cos\varphi}\right| dx$$
$$= \int_{\cos\theta}^1 \frac{(1-\cos\varphi)}{(1+x)^{\frac{3}{2}}\sqrt{x-\cos\theta}} \ln\left|\frac{1+x\cos\varphi+\sin\varphi\sqrt{1-x^2}}{x+\cos\varphi}\right| dx$$
$$- \int_{\cos\theta}^1 \frac{(2x+1-\cos\theta)\,dx}{2\sqrt{(1+x)(x-\cos\theta)}} \ln\left|\frac{1+x\cos\varphi+\sin\varphi\sqrt{1-x^2}}{x+\cos\varphi}\right| dx$$
$$+ \frac{(1-\cos\theta)}{2\sqrt{(1+x)(x-\cos\theta)}} \ln\left|\frac{1+x\cos\varphi+\sin\varphi\sqrt{1-x^2}}{x+\cos\varphi}\right| dx$$
$$= \frac{2(1-\cos\varphi)}{1+\cos\theta}\sqrt{\frac{x-\cos\theta}{1+x}} \ln\left|\frac{1+x\cos\varphi+\sin\varphi\sqrt{1-x^2}}{x+\cos\varphi}\right|\Bigg|_{\cos\theta}^1$$
$$- \frac{2(1-\cos\varphi)}{1+\cos\theta}\int_{\cos\theta}^1 \sqrt{\frac{x-\cos\theta}{1+x}}\frac{-\sin\varphi\,dx}{(x+\cos\varphi)\sqrt{1-x^2}}$$
$$-\sqrt{(1+x)(x-\cos\theta)} \ln\left|\frac{1+x\cos\varphi+\sin\varphi\sqrt{1-x^2}}{x+\cos\varphi}\right|\Bigg|_{\cos\theta}^1$$
$$- \sin\varphi\int_{\cos\theta}^1 \frac{\sqrt{(1+x)(x-\cos\theta)}}{(x+\cos\varphi)\sqrt{1-x^2}}\,dx$$
$$+ \frac{1-\cos\theta}{2}\int_{\cos\theta}^1 \ln\left|\frac{1+x\cos\varphi+\sin\varphi\sqrt{1-x^2}}{x+\cos\varphi}\right| \frac{dx}{\sqrt{(1+x)(x-\cos\theta)}}$$

(continued on next page)

$$
\begin{aligned}
&= \frac{2\sin\varphi(1-\cos\varphi)}{1+\cos\theta}\int_{\cos\theta}^{1}\sqrt{\frac{x-\cos\theta}{1-x}}\,\frac{dx}{(1+x)(x+\cos\varphi)} \\
&\quad - \sin\varphi\int_{\cos\theta}^{1}\sqrt{\frac{x-\cos\theta}{1-x}}\,\frac{dx}{x+\cos\varphi} \\
&\quad + \frac{1-\cos\theta}{2}\int_{\cos\theta}^{1}\ln\left|\frac{1+x\cos\varphi+\sin\varphi\sqrt{1-x^2}}{x+\cos\varphi}\right|\frac{dx}{\sqrt{(1+x)(x-\cos\theta)}} \\
&= \tan^2\frac{\theta}{2}\sin\varphi\int_{\cos\theta}^{1}\sqrt{\frac{x-\cos\theta}{1-x}}\,\frac{dx}{x+\cos\varphi} - \frac{2\sin\varphi}{1+\cos\theta}\int_{\cos\theta}^{1}\sqrt{\frac{x-\cos\theta}{1-x}}\,\frac{dx}{1+x} \\
&\quad + \frac{1-\cos\theta}{2}\int_{\cos\theta}^{1}\ln\left|\frac{1+x\cos\varphi+\sin\varphi\sqrt{1-x^2}}{x+\cos\varphi}\right|\frac{dx}{\sqrt{(1+x)(x-\cos\theta)}} \\
&= \tan^2\frac{\theta}{2}\sin\varphi\left[2\sin^{-1}\sqrt{\frac{x-\cos\theta}{1-\cos\theta}}\right. \\
&\quad \left. - \sqrt{\frac{\cos\varphi+\cos\theta}{1+\cos\varphi}}\sin^{-1}\frac{(1+2\cos\varphi+\cos\theta)x-(\cos\varphi+\cos\varphi\cos\theta+2\cos\theta)}{(x+\cos\varphi)(1-\cos\theta)}\right]_{\cos\theta}^{1} \\
&\quad - \frac{2\sin\varphi}{1+\cos\theta}\left[2\sin^{-1}\sqrt{\frac{x-\cos\theta}{1-\cos\theta}} - \cos^2\frac{\theta}{2}\sin^{-1}\frac{(3+\cos\theta)x-(1+3\cos\theta)}{(1+x)(1-\cos\theta)}\right]_{\cos\theta}^{1} \\
&\quad + \frac{1-\cos\theta}{2}\int_{\cos\theta}^{1}\ln\left|\frac{1+x\cos\varphi+\sin\varphi\sqrt{1-x^2}}{x+\cos\varphi}\right|\frac{dx}{\sqrt{(1+x)(x-\cos\theta)}} \\
&= -\pi\sin\varphi\left(1+\tan^2\frac{\theta}{2}\sqrt{\frac{\cos\varphi+\cos\theta}{1+\cos\varphi}} - \sec\frac{\theta}{2}\right) \\
&\quad + \frac{1-\cos\theta}{2}\int_{\cos\theta}^{1}\ln\left|\frac{1+x\cos\varphi+\sin\varphi\sqrt{1-x^2}}{x+\cos\varphi}\right|\frac{dx}{\sqrt{(1+x)(x-\cos\theta)}} \\
&= -\pi\sin\varphi\left(1+\tan^2\frac{\theta}{2}\sqrt{\frac{\cos\varphi+\cos\theta}{1+\cos\varphi}} - \sec\frac{\theta}{2}\right) \\
&\quad + \frac{1-\cos\theta}{2}\int_{0}^{\theta}\ln\left|\frac{\cos\frac{u-\varphi}{2}}{\cos\frac{u+\varphi}{2}}\right|\frac{\sin u\,du}{\sqrt{(1+\cos u)(\cos u-\cos\theta)}}.
\end{aligned}
\tag{C.9}
$$

Substitute equations (C.7), (C.8) and (C.9) into equation (C.6), to obtain the expression for $g(\theta)$.

$$
\begin{aligned}
g(\theta) = &-\frac{\varphi}{4\pi}\sin\theta + \frac{\sqrt{2}\sin\frac{\varphi}{2}}{2\pi}\tan\frac{\theta}{2}\sqrt{\cos\varphi+\cos\theta} \\
&- \frac{\sin\theta}{4\pi^2}\int_{0}^{\theta}\ln\left|\frac{\cos\frac{u-\varphi}{2}}{\cos\frac{u+\varphi}{2}}\right|\frac{\sin u\,du}{\sqrt{(1+\cos u)(\cos u-\cos\theta)}}.
\end{aligned}
\tag{C.10}
$$

C.2 Some Useful Formulae

C.2.1 Relations between Gegenbauer and Legendre Polynomials

$$C_n^{-\frac{1}{2}}(\cos\theta) = -\sin\theta P_{n-1}^{-1}(\cos\theta) \tag{C.11}$$

$$C_n^{-\frac{1}{2}}(\cos\theta) = \frac{1}{2n-1}[P_{n-2}(\cos\theta) - P_n(\cos\theta)] \tag{C.12}$$

$$\frac{dP_{n-1}(\cos\theta)}{d\theta} = -n(n-1)\frac{C_n^{-\frac{1}{2}}(\cos\theta)}{\sin\theta} \tag{C.13}$$

$$\frac{dC_n^{-\frac{1}{2}}(\cos\theta)}{d\theta} = \sin\theta P_{n-1}(\cos\theta) \tag{C.14}$$

$$P_n^{-1}(\cos\theta) = -\frac{P_n^1(\cos\theta)}{n(n+1)} \tag{C.15}$$

$$C_2^{-\frac{1}{2}}(\cos\theta) = \frac{\sin^2\theta}{2} \tag{C.16}$$

$$P_1(\cos\theta) = \cos\theta \tag{C.17}$$

$$P_2(\cos\theta) = 1 - \frac{3}{2}\sin^2\theta \tag{C.18}$$

$$\int_0^\pi P_n^m(\cos\theta)P_k^m(\cos\theta)\sin\theta = \begin{cases} 0 & \text{if} \quad n \neq k \\ \frac{2n(n+1)}{2n+1} & \text{if} \quad n = k \end{cases} \tag{C.19}$$

C.2.2 Integral Formulae

$$\int \frac{\sin\theta\, d\theta}{\sqrt{(\cos\theta - \cos u)(\cos v - \cos\theta)}} = -2\sin^{-1}\sqrt{\frac{\cos\theta - \cos u}{\cos v - \cos u}} \tag{C.20}$$

$$\int \frac{dx}{x\sqrt{ax^2+bx+c}} = -\frac{1}{\sqrt{c}}\ln\left(\frac{\sqrt{ax^2+bx+c}+\sqrt{c}}{x} + \frac{b}{2\sqrt{c}}\right) \quad (c>0) \tag{C.21}$$

$$\int \frac{dx}{x\sqrt{ax^2+bx+c}} = \frac{1}{\sqrt{-c}}\sin^{-1}\frac{bx+2c}{x\sqrt{b^2-4ac}} \quad (c<0) \tag{C.22}$$

$$\int \frac{dx}{\sqrt{ax^2+bx+c}} = \frac{1}{\sqrt{a}}\ln[2ax+b+2\sqrt{a(ax^2+bx+c)}] \quad (a>0) \tag{C.23}$$

$$\int \sqrt{ax^2+bx+c}\, dx = \frac{2ax+b}{4a}\sqrt{ax^2+bx+c} + \frac{4ac-b^2}{8a}\int \frac{dx}{\sqrt{ax^2+bx+c}} \tag{C.24}$$

$$\int \frac{dx}{\sqrt{ax^2+bx+c}} = \frac{1}{\sqrt{-a}}\sin^{-1}\frac{-2ax-b}{\sqrt{b^2-4ac}} \quad (a<0) \tag{C.25}$$

$$\int \frac{dx}{\sqrt{x-p}\sqrt{q-x}} = 2\sin^{-1}\sqrt{\frac{x-p}{q-p}} \tag{C.26}$$

$$\int \sqrt{\frac{p-x}{x+q}}\, dx = \sqrt{(p-x)(x+q)} + (p+q)\sin^{-1}\sqrt{\frac{x+q}{p+q}} \tag{C.27}$$

REFERENCES

[Acrivos & Goddard (1965)] ACRIVOS, A & GODDARD, J. D. 1965 Asymptotic expansions for laminar forced-convection heat and mass transfer. *J.Fluid Mech.,* **23**, 273–291.

[Andrews, Fike & Wong (1988)] ANDREWS, G.F., FIKE, R. & WONG, S. 1988 Bubble hydrodynamics and mass transfer at high Reynolds number and surfactant concentration *Chem. Engng. Sci.*, **43**, 1467–1477.

[Barton & Subramanian (1989)] BARTON, K. D. & SUBRAMANIAN, R. S. 1989 The Migration of Liquid Drops in a Vertical Temperature Gradient. *J. Colloid and Interface Sci.,* **133**, 211–222.

[Beitel & Heideger (1971)] BEITEL, A. & HEIDEGER,W.J. 1971 Surfactant Effects on Mass Transfer from Drops Subject to Interfacial Instability. *Chem. Engng. Sci.,* **26**, 711–717.

[Bel Fdhila & Duineveld (1996)] BEL FDHILA, R. & DUINEVELD, P. C. 1996 The effect of surfactants on the rise of a spherical bubble at high Reynolds and Peclet numbers. *Phys. Fluids,* **8**, 310–321.

[Chen & Stebe (1996)] CHEN, J. & STEBE, K. 1996 Marangoni retardation of the terminal velocity of a settling droplet: The role of surfactant physico-chemistry. *J. Colloid and Int. Sci.,* **178**, 144–155.

[Chen & Stebe (1997)] CHEN, J. & STEBE, K. 1997 Surfactant-induced retardation of the thermocapillary migration of a droplet. *J. Fluid Mech.* **340**, 35–60.

[Chang & Franses (1995)] CHANG, C. H. & FRANSES, E.I. 1995 Adsorption dynamics of surfactants at the air/water interface: a critical review of mathematical models, data, and mechanisms. *Colloids and Surfaces*, **100**, 1–45.

[Collins (1961)] COLLINS, W. D. 1961 On some dual series equations and their application to electrostatic problems for spheroidal caps. *Proc. Camb. Phil. Soc.* **57**, 367–384

[Copson (8)] COPSON, E. T. On the problem of the electrified disc *Proc. Edinb. Math. Soc. (2)* **8** (1947-50), 14–19

[Cuenot, Magnaudet & Spennato (1997)] CUENOT, B., MAGNAUDET, J. & SPENNATO, B. 1997 The effects of slightly soluble surfactants on the flow around a spherical bubble. *J. Fluid Mech.* **339**, 25–53

[Davis & Acrivos (1966)] DAVIS, R. E. & ACRIVOS, A. 1966 The influence of surfactants on the creeping motion of bubbles. *Chem. Engng. Sci.,* **21**, 681–685.

[Deryagin, Dukhin & Lisichenko (1959)] DERYAGIN, B.V., DUKHIN, S.S. & LISICHENKO, V.A. 1959 The kinetics of the attachment of mineral particles to bubbles during flotation. I. The electric field of a moving bubble *Russ. J. Phys. Chem.*, **33**, 389–393.

[Edge & Grant (1972)] EDGE, R. M. & GRANT, C. D. 1972 The motion of drops in water contaminated with a surface active agent *Chem. Engng. Sci.*, **27**, 1709-1721

[Edwards, Brenner & Wasan (1991)] EDWARDS, D.A., BRENNER, H. & WASAN, D.T. 1991 *Interfacial Transport Processes and Rheology.* Butterworth-Heinemann, Boston, MA.

[Elzinga & Banchero (1961)] ELZINGA, E.R. & BANCHERO, J.T. 1961 Some observations on the mechanics of drops in liquid-liquid systems. *AIChE J.*, **7**, 394–399.

[Frumkin & Levich (1947)] FRUMKIN, A. & LEVICH, V. 1947 On surfactants and interfacial motion. *Zhur. Fiz. Khim.* **21**, 1183 (in Russian).

[Garner & Skelland (1955)] GARNER, F.H. & SKELLAND, H.P. 1955 Some factors affecting droplet behaior in liquid-liquid systems. *Chem.Engng. Sci.* **4**, 149–158.

[Griffith (1962)] GRIFFITH, R.M. 1962 The effect of surfactants on the terminal velocity of drops and bubbles. *Chem. Engng. Sci.* **17**, 1057–1070.

[Haberman & Morton (1954)] HABERMAN, W. L. & MORTON, R. K. 1954 An experimental study of bubbles moving in liquids. *Proc. ASCE,* **387**, 1.

[Happel & Brenner (1973)] HAPPEL & BRENNER 1973 *Low Reynolds Number Hydrodynamics.* Prentice Hall, Englewood Cliffs, NJ.

[Harper (1973)] HARPER, J. F. 1973 On bubbles with small immobile adsorbed films rising in liquids at Low Reynolds numbers *J. Fluid Mech.*, **58**, 539–545.

[Harper (1974)] HARPER, J. F. 1974 On spherical bubbles rising steadily in dilute surfactant solutions *Q. Jl Mech. Appl. Math.*, **XXVII**, 87–100.

[Harper (1982)] HARPER, J. F. 1982 Surface activity and bubble motion *Appl. Sci. Res.* **38**, 343–351.

[He, Maldarelli & Dagan (1991a)] HE, Z., MALDARELLI, C. & DAGAN, Z. 1991a The size of stagnant caps of bulk soluble surfactant on the interfaces of translating fluid droplets. *J. Colloid and Interface Sci.*, **146**, 442–451.

[He, Dagan & Maldarelli (1991b)] HE, Z., DAGAN, Z. & MALDARELLI, C. 1991b The size of stagnant caps of bulk soluble surfactant adsorption on the motion of a fluid sphere in a tube. Part 1. Uniform retardation controlled by sorption kinetics. *J. Fluid Mech.*, **222**, 1–31.

[Holbrook & Levan (1983a)] HOLBROOK, J. A. & LEVAN, M. D. 1983a Retardation of Droplet Motion by Surfactant. Part I. Theoretical development and asymptotic solutions. *Chem. Eng. Commun.*, **20**, 191–207.

[Holbrook & Levan (1983b)] HOLBROOK, J. A. & LEVAN, M. D. 1983b Retardation of Droplet Motion by Surfactant. Part II. Numerical solutions for exterior diffusion, surface diffusion, and adsorption kinetics. *Chem. Eng. Commun.*, **20**, 273–290.

[Horton Fritsch & Kintner (1965)] HORTON, T.J., FRITSCH, T.R. & KINTNER, R.C. 1965 Experimental determination of circulation velocities inside drops. *Can. J. Chem. Eng.*, **43**, 143–146.

[Huang & Kintner (1969)] HUANG, W.S. & KINTNER,R.C. 1969 Effects of Surfactants on Mass Transfer Inside Drops. *AIChEJ.*, **15**, 735–744.

[Kim & Subramanian (1989a)] KIM, H & SUBRAMANIAN, R. 1989a Thermocapillary Migration of a Droplet with Insoluble Surfactant, I. Surfacant Cap. *J. Colloid and Int. Sci.*, **127**, 417–430.

[Kim & Subramanian (1989b)] KIM, H. & SUBRAMANIAN,R. 1989b Thermocapillary Migration of a Droplet with Insoluble Surfactant, II. General Case *J. Colloid and Int. Sci.*, **130**, 112–125 .

[Leal (1992)] LEAL, L. 1992 *The Effect of Surfactant on the Terminal and Interfacial Velocities of a Bubble or Drop.* Butterworth-Heinemann, Boston, MA.

[Levan & Newman (1976)] LEVAN, M. & NEWMAN, J. 1976 The effect of surfactant on the terminal and interfacial velocities of a bubble or drop. *AICHE J.*, **22**, 695–701.

[Leppinen, Renksizbulut & Haywood (1996a)] LEPPINEN, D.M., RENKSIZBULUT, M. & HAYWOOD, R.J. 1996a The effects of surfactants on droplet behaviour at intermediate Reynolds numbers - I. The numerical model and steady-state results. *Chem. Engng. Sci.* **51**, 479–489.

[Leppinen, Renksizbulut & Haywood (1996b)] LEPPINEN, D.M., RENKSIZBULUT, M. & HAYWOOD, R.J. 1996b The effects of surfactants on droplet behaviour at intermediate Reynolds numbers - II. Transient deformation and evaporation. *Chem. Engng. Sci.* **51**, 491–501.

[Levich (1962)] LEVICH 1962 *Physicochemical Hydrodynamics.* Prentic Hall, Englewood Cliffs, NJ.

[Masliyah & Epstein (1971)] MASLIYAH, J.H. & EPSTEIN, N. 1971 Numerical solution of heat and mass transfer from spheroids in steady axisymmetric flow. *Progress in Heat and Mass Transfer, Proceedings of the International Symposium on TWO-PHASE SYSTEMS* **6**, 613–632.

[McLaughlin (1997)] McLaughlin, J.B. 1997 Numerical simulation of bubble motion in water. *J. Colloid Int. Sci.* (in press).

[Nadim & Borhan (1989)] Nadim, A. & Borhan, A. 1989 The Effects of Surfactant on The Motion and Deformation of a Droplet in Thermocapillary Migration. *PhysicoChemical Hydrodynamics,* **11**, 753–764

[Peyret & Taylor (1983)] Peyret, R. & Taylor, T. D. 1983 *Computational Methods for Fluid Flow.* Springer-Verlag, New York, NY.

[Probstein (1994)] Probstein, R. F. 1994 *Physico-Chemical Hydrodynamics.* Wiley, New York, NY.

[Ryskin & Leal (1982)] G. Ryskin, G. & Leal, L. G. 1982 Numerical solution of free-boundary problems in fluid mechanics. *J. Fluid Mech.,* **148**, 1–17

[Sadhal & Johnson (1983)] Sadhal, S. & Johnson, R. 1983 Stokes flow past bubbles and drops partially coated with thin films. Part1. Stagnant cap of surfactant film - exact solution *J. Fluid Mech.,* **126**, 237–250

[Savic (1953)] Savic,P. 1953 Circulation and distortion of liquid drops falling through a viscous medium. *Nat. Res. Counc. Can., Div. Mech. Eng. Rep.* **MT-22**,

[Saville (1973)] Saville, D. 1973 The effects of interfacial tension on the motion of drops and bubbles. *Chem. Eng. J.,* **5**, 251–259.

[Schechter & Fairley (1963)] Schechter, R.S. & Fairley, R.W. 1963 Interfacial tension gradients and droplet behavior. *Cn. J. Chem. Eng,* **41**, 103–117.

[Stebe, Lin & Maldarelli (1991)] Stebe, K.J., Lin, S.-Y. & Maldarelli, C. 1991 Remobilizing surfactant retarded fluid particle interfaces. I Stress-free conditions at the interfaces of micellar solutions of surfactants with fast sorption kinetics. *Phys. Fluids A,* **3**, 3–20.

[Subramanian (1992)] Subramanian, R. S. 1992 *in The Motion of Bubbles and Drops in Reduced Gravity, in Transport Processes in Bubbles, Drops and Particles.* Hemisphere Publishing, New York, NY.

[Tsai & Miksis (1997)] Tsai, T.M. & Miksis, M.J. 1997 The effects of surfactant on the dynamics of bubble snap-off. *J. Fluid Mech.,* **337**, 381–405.

[Yamamoto & Ishii (1987)] Yamamoto, T. & Ishii, T. 1987 Effect of surface active materials on the drag coefficients and shapes of single large gas bubbles. *Chem. Engng. Sci.,* **42**, 1297–1303.